

INFORMATION TO USERS

This manuscript has been reproduced from the microfilm master. UMI films the text directly from the original or copy submitted. Thus, some thesis and dissertation copies are in typewriter face, while others may be from any type of computer printer.

The quality of this reproduction is dependent upon the quality of the copy submitted. Broken or indistinct print, colored or poor quality illustrations and photographs, print bleedthrough, substandard margins, and improper alignment can adversely affect reproduction.

In the unlikely event that the author did not send UMI a complete manuscript and there are missing pages, these will be noted. Also, if unauthorized copyright material had to be removed, a note will indicate the deletion.

Oversize materials (e.g., maps, drawings, charts) are reproduced by sectioning the original, beginning at the upper left-hand corner and continuing from left to right in equal sections with small overlaps.

Photographs included in the original manuscript have been reproduced xerographically in this copy. Higher quality 6" x 9" black and white photographic prints are available for any photographs or illustrations appearing in this copy for an additional charge. Contact UMI directly to order.

Bell & Howell Information and Learning
300 North Zeeb Road, Ann Arbor, MI 48106-1346 USA

UMI[®]
800-521-0600

**THERMAL EXPANSION STUDY OF PARTICULATE REINFORCED
ALUMINUM MATRIX COMPOSITE MATERIALS**

**Stéphane Lemieux
Department of Mechanical Engineering
McGill University, Montreal**

November, 1997

**A thesis submitted to the Faculty of Graduate Studies and
Research in partial fulfilment of the requirements of
the degree of Master of Engineering**

©Stéphane Lemieux, 1997.



**National Library
of Canada**

**Acquisitions and
Bibliographic Services**

395 Wellington Street
Ottawa ON K1A 0N4
Canada

**Bibliothèque nationale
du Canada**

**Acquisitions et
services bibliographiques**

395, rue Wellington
Ottawa ON K1A 0N4
Canada

Your file Votre référence

Our file Notre référence

The author has granted a non-exclusive licence allowing the National Library of Canada to reproduce, loan, distribute or sell copies of this thesis in microform, paper or electronic formats.

The author retains ownership of the copyright in this thesis. Neither the thesis nor substantial extracts from it may be printed or otherwise reproduced without the author's permission.

L'auteur a accordé une licence non exclusive permettant à la Bibliothèque nationale du Canada de reproduire, prêter, distribuer ou vendre des copies de cette thèse sous la forme de microfiche/film, de reproduction sur papier ou sur format électronique.

L'auteur conserve la propriété du droit d'auteur qui protège cette thèse. Ni la thèse ni des extraits substantiels de celle-ci ne doivent être imprimés ou autrement reproduits sans son autorisation.

0-612-44021-4

Canada

Acknowledgments

I would first like to thank Dr. James A. Nemes of the Department of Mechanical Engineering at McGill University who accepted, without hesitation, to supervise this research project. His support, understanding and guidance were very important in achieving this work.

I would like to affirm my sincere gratefulness to Dr. Samir Elomari, Material Scientist at the Canadian Space Agency, for giving me the incredible opportunity of doing my Master's degree in collaboration with the aerospace industry. Working at the Canadian Space Agency has been a very enriching experience for myself. I am also very grateful for the continuous help he gave me during my research work. This thesis would not have been possible without his precious comments and help.

Not to be forgotten are Dr. M. Skibo from MC-21, San Diego, Dr. S. Suresh from MIT and Dr. M. Chibani from 2CI Technologies, Ontario, for their insightful comments concerning the scientific papers. Also, a particular thank to Dr. Paul Lagacé from MIT for first pointing out the importance of this study. Besides, I want to thank Dr. George Vukovich, Director of Spacecraft Engineering at the Canadian Space Agency for supporting this research project.

In addition, a very special thank you to my girlfriend, Geneviève Gagné, for supporting me during the difficult periods I encountered while pursuing my Master's degree, as well as for her assistance in expressing and explaining the research that has been done.

I would also like to thank my friend, Christopher Hossie, for his valuable help in revising this thesis.

Finally, I want to thank the institutions that financially contributed to the realization of this work such as the Canadian Space Agency and the Natural Sciences and Engineering Research Council of Canada.

Abstract

The thermal expansion behavior of Duralcan particle reinforced composite materials was investigated. Initially, the temperature dependence of the CTE of Al-Si alloy containing SiC reinforcement particles ranging from 10 to 40% in volume was experimentally examined and compared with standard theoretical model predictions. In addition, the effects of reinforcement volume fraction and nature of the composite constituents during thermal cycling between 25 and 350°C were determined for Al-Si alloy containing between 10 and 40% SiC particles and Al alloy having 40% alumina in volume. Accurate experimental CTE measurements were made using a high precision Thermomechanical Analyzer system. Silicon carbide reinforced composite average CTE values were bounded by two elastic CTE theoretical models consisting of Schapery and Kerner predictions over the 25-350°C interval for reinforcement volume fractions between 10 and 40%. The CTE mismatch between the particles and the matrix does not appear to be the only factor influencing the expansion response of the composites. Indeed, the nature of the composite constituents also plays an important role by influencing the ductility and bonding of the particle-matrix interface.

Résumé

Le principal but de cette thèse est l'étude de l'expansion thermique de matériaux composites à matrice métallique renforcés avec des particules de céramique produits par Duralcan. Dans un premier temps, l'effet de la température sur le coefficient d'expansion thermique de composites faits d'alliages Al-Si renfermant entre 10 et 40% de renforts de SiC a été expérimentalement observé et comparé aux prédictions de certains modèles théoriques. De plus, l'effet de la fraction volumique de renforts ainsi que de la nature des phases du composite pendant le cyclage thermique entre 25 et 350°C a été analysé pour des composites Al-Si/SiC avec des fractions volumiques entre 10 et 40% ainsi que pour un composite à matrice d'aluminium contenant 40% de particules d'alumine. L'utilisation d'un appareil d'analyse thermomécanique a permis d'obtenir des mesures précises du coefficient d'expansion thermique dans l'intervalle de température étudié. Il a été démontré que les coefficients d'expansion thermique moyens des composites renforcés de SiC sont délimités par les prédictions des modèles de Schapery et Kerner sur l'intervalle 25-350°C pour des fractions volumiques de renforts entre 10 et 40%. La différence de coefficient d'expansion thermique entre les particules et la matrice ne semble pas être le seul facteur influençant la réponse d'expansion des composites. En effet, la nature des éléments constitutifs des composites joue également un rôle important en influençant la ductilité ainsi que la résistance de l'interface particule-matrice.

Preface to the external examiner

Candidates have the option of including, as part of the thesis, the text of one or more papers submitted or to be submitted for publication, or the clearly-duplicated text of one or more published papers. These texts must be bound as an integral part of the thesis.

If this option is chosen, connecting texts that provide logical bridges between the different papers are mandatory. The thesis must be written in such a way that it is more than a mere collection of manuscripts; in other words, results of a series of papers must be integrated.

The thesis must still conform to all other requirements of the “Guidelines for Thesis Preparation”. The thesis must include: A table of contents, an abstract in English and French, an introduction which clearly states the rationale and objectives of the study, a review of the literature, a final conclusion and summary, and a thorough bibliography or reference list.

Additional material must be provided where appropriate (e.g. in appendices) and in sufficient detail to allow a clear and precise judgment to be made of the importance and originality of the research reported in the thesis.

In the case of manuscripts co-authored by the candidate and others, the candidate is required to make an explicit statement in the thesis as to who contributed to such work and to what extent. Supervisors must attest to the accuracy of such statements at the doctoral oral defense. Since the task of the examiners is made more difficult in these cases, it is in the candidate’s interest to make perfectly clear the responsibilities of all the authors of the co-authored papers.

Myself, Stéphane Lemieux, am the first author of two scientific papers. My contribution has been to find the experimental setup needed to measure the experimental data given in this thesis. In addition, I have been analyzing the experimental results and writing the first draft of the papers. I have also been incorporating the co-authors’ comments in the papers. Dr. S. Elomari and Dr. J. A. Nemes have acted as my thesis supervisors and have provided me precious help in writing the papers. Dr. M. D. Skibo contributed to the completeness of the analysis of the experimental results. Dr. S. Suresh is the co-author of a paper on thermal cycling of particle reinforced MMCs and added comments concerning previous theoretical models used to describe the observed thermal expansion behavior.

Dr. M. Chibani helped in processing the 30% silicon carbide aluminum matrix composite material and helped establish the link between the coefficient of thermal expansion and the particle-matrix interface bonding.

Table of Contents

Acknowledgments	II
Abstract	III
Résumé	IV
Preface to the external examiner	V
Table of Contents	VII
List of Tables	XII
List of Figures	XIII
List of Abbreviations	XVI
General introduction	1
Chapter 1. Fabrication processes	3
1.1 Powder metallurgy	3
1.2 Liquid phase casting	4
1.2.1 Mixing process	4
1.2.1.1 Interfacial reactions	5
1.2.1.2 Duralcan process	6
1.2.1.2.1 Example of MMC fabrication by the Duralcan process	7
1.2.2 In-situ formation	8
1.2.3 Squeeze casting	9
1.2.4 Pressureless infiltration (Lanxide™)	9
1.3 Spraying technique	10

Conclusion	12
References	13
Chapter 2. Mechanical properties	19
2.1 Nomenclature	19
2.2 Elastic modulus	19
2.3 Strength	20
2.4 Ultimate strain	21
2.5 Fracture toughness	21
References	22
Chapter 3. Thermal expansion of MMCs	27
3.1 Turner model	27
3.2 Kerner model	28
3.3 Schapery model	29
3.4 Rule of mixtures	29
3.5 Plot of the theoretical models	30
References	31
Introduction to Chapter 4	36
Chapter 4. Thermal Expansion of Isotropic Duralcan Metal-Matrix Composites	37
Abstract	37
4.1 INTRODUCTION	38

4.2 EXPERIMENTAL PROCEDURES	39
4.2.1 Composite materials	39
4.2.2 TMA Test	40
4.3 RESULTS	41
4.4 DISCUSSION	42
4.4.1 Theoretical models	42
4.4.1.1 Turner's model	42
4.4.1.2 Kerner's model	43
4.4.1.3 Schapery's model	43
4.4.2 Comparison between the experimental and theoretical results	44
4.5 CONCLUSIONS	47
References	48
Chapter 5. Thermal cycling of MMCs	56
5.1 Elastoplastic model	56
5.1.1 Characteristic temperatures	58
5.1.2 Strain during thermal cycling	60
5.1.2.1 Total macroscopic strain	60
5.1.2.2 Effective plastic strain within the representative volume	61
5.1.2.3 Interfacial decohesion	62
5.1.3 Conclusion	64
5.2 Numerical analysis of the effect of thermal cycling	64
5.2.1 Mathematic tool	65
5.2.2 Instructions for using the Maple V sheet	65
5.2.3 Description of the Maple sheet sections	66
5.2.3.1 Material selection	66
5.2.3.2 Material properties	67
5.2.3.3 Stress state model	67

5.2.3.4 Characteristic temperatures	68
5.2.3.5 Characteristic volume fraction	68
5.2.3.6 Temperature history	68
5.2.3.7 Strain on first thermal loading	68
5.2.3.8 Plastic strain accumulation during thermal cycling	68
5.2.3.9 Coefficient of thermal expansion	69
5.2.3.10 Number of cycles to decohesion	69
5.2.3.11 Numerical results	69
5.2.4 Restrictions concerning the Maple V sheet	70
5.2.5 Analysis of the results	70
5.2.6 Conclusions	72
5.2.7 Aspects to improve modeling the elastoplastic behavior of MMCs under thermal cycling	73
References	75
Introduction to chapter 6	80
Chapter 6. Effect of Thermal Cycling on Thermal Expansion Behavior of Isotropic Duralcan Metal-Matrix Composites	81
Abstract	81
6.1 INTRODUCTION	82
6.2 EXPERIMENTAL PROCEDURES	83
6.2.1 Composite materials	83
6.2.2 TMA Test	84
6.3 RESULTS	85
6.3.1 Al/SiC composites	85
6.3.2 Al/Al ₂ O ₃ composite	86

6.4 DISCUSSION	86
6.4.1 CTE theoretical models	87
6.4.1.1 Kerner's model	87
6.4.1.2 Schapery's model	87
6.4.1.3 Elastoplastic theoretical analysis of thermal cycling	88
6.4.2 Comparison between the experimental and theoretical results	91
6.4.2.1 Al/SiC composites	91
6.4.2.2 Al/Al ₂ O ₃ composite	94
6.5 CONCLUSIONS	95
References	97
General conclusion	111
Recommendations	112
Appendix 1	113
Appendix 2	117
Appendix 3	129

List of Tables

Chapter 2

Table 1. Typical mechanical properties for some particle reinforced metal matrix composites available in the industry. _____	23
Table 2. Typical mechanical properties of commonly used aluminum alloys. _____	24
Table 3. Typical fracture toughness values for 2014 and 6061 aluminum alloys containing Al ₂ O ₃ particles with theoretical predictions. _____	24

Chapter 3

Table 1. Temperature-dependence of the properties of the composite matrix constituents. _____	33
Table 2. Temperature-dependence of the properties of the composite reinforcement constituents. _____	33
Table 3. Theoretical percent change and average CTEs between 25 and 350°C for a typical 6061/Al ₂ O ₃ /40p composite material. _____	34

Chapter 4

Table 1. Chemical composition of aluminum alloy matrices. _____	50
Table 2. Properties of reinforcement particles and aluminum matrices. _____	50
Table 3. Temperature-dependence of the properties of the composite constituents. _____	51

Chapter 5

Table 1. Summary of the most important results obtained with the elastoplastic model. _____	77
---	----

Chapter 6

Table 1. Chemical composition of aluminum alloy matrices. _____	99
Table 2. Properties of reinforcement particles and aluminum matrices. _____	99
Table 3. Characteristic temperatures of five composite materials. _____	100
Table 4. Temperature-dependence of the properties of the matrix constituents. _____	100
Table 5. Comparison between experimental and theoretical mean CTE values. _____	101
Table 6. Comparison between experimental and theoretical normalized mean CTE values. _____	101

List of Figures

Chapter 1

- Figure 1. Main steps for MMC processing using the powder metallurgy technique. 15
- Figure 2. Recommended silicon content in an aluminum alloy to prevent carbide formation. _____ 16
- Figure 3. Apparatus used for the Duralcan process. _____ 16
- Figure 4. Pressure casting head used in the Duralcan process. _____ 17
- Figure 5. Apparatus used for squeeze casting. _____ 17
- Figure 6. Pressureless infiltration technique by Lanxide. _____ 18
- Figure 7. Spraying technique developed by Osprey. _____ 18

Chapter 2

- Figure 1. Typical elastic modulus curve of a 6061/ Al_2O_3 composite material as a function of reinforcement volume fraction with the Rule of Mixtures and Tsai-Halpin theoretical predictions. _____ 25
- Figure 2. Typical yield stress curves of A356/SiC and 6061/SiC composite materials as a function of reinforcement volume fraction. _____ 26
- Figure 3. Typical maximum ductility of 6061/SiC and 6061/ Al_2O_3 composite materials as a function of reinforcement volume fraction. _____ 26

Chapter 3

- Figure 1. Theoretical CTE predictions obtained with the Kerner, Turner, Schapery and Rule of Mixtures models for a 6061/ Al_2O_3 /40p composite material. _ 35
- Figure 2. Average theoretical CTE values obtained with the Kerner, Turner, Schapery and Rule of Mixtures models as a function of reinforcement volume fraction. _____ 35

Chapter 4

- Figure 1. Microstructures of Duralcan SiC/Al metal-matrix composites: (a) 10% SiC, (b) 20% SiC, (c) 30% SiC, and (d) 40% SiC. _____ 52
- Figure 2. Aspect ratio histograms of SiC particulate for Duralcan composites. _____ 53

Figure 3. Thermal expansion behaviour of SiC composites: (a) Dimensional change versus Temperature, and (b) CTE versus Temperature. _____	53
Figure 4. Comparison of the measured CTE of Duralcan SiC/Al composites with the theoretical predictions. _____	54
Figure 5. Comparison of the mean CTE of Duralcan SiC/Al composites with theory for the 25-350°C temperature range. _____	55

Chapter 5

Figure 1. Geometry of the representative volume element of the composite. _____	78
Figure 2. Typical thermal history. _____	78
Figure 3. Composite thermal strains as a function of the temperature change. _____	79
Figure 4. Plastic strain accumulation throughout the matrix with the number of temperature reversals. _____	79

Chapter 6

Figure 1. Microstructures of Duralcan SiC/Al metal-matrix composites: (a) 10% SiC, (b) 20% SiC, (c) 30% SiC, and (d) 40% SiC. _____	102
Figure 2. Microstructure of Duralcan 6061/Al ₂ O ₃ /40p metal-matrix composite. _____	103
Figure 3. Aspect ratio histograms of SiC particles for Duralcan composites. _____	104
Figure 4. Comparison of the initial and last dimensional change with temperature curves for 20 complete temperature reversals between 25 and 350°C for SiC/Al Duralcan composites: (a) 10% SiC, (b) 20% SiC, (c) 30% SiC, and (d) 40% SiC. _____	105
Figure 5. CTE variation with the number of complete temperature reversals for SiC/Al Duralcan composites: (a) 10% SiC, (b) 20% SiC, (c) 30% SiC, and (d) 40% SiC. _____	106
Figure 6. Comparison of the initial and last dimensional change with temperature curves for 20 complete temperature reversals between 25 and 350°C for 6061/Al ₂ O ₃ /40p Duralcan composite material. _____	107
Figure 7. CTE variation with the number of complete temperature reversals for 6061/Al ₂ O ₃ /40p Duralcan composite material. _____	107

Figure 8. Geometry of the representative volume element for the elastoplastic model. _____	108
Figure 9. Typical thermal load history during thermal cycling. _____	108
Figure 10. Typical thermal strain with temperature change curve during thermal cycling of a particle reinforced composite. _____	109
Figure 11. Comparison of the measured mean CTE during thermal cycling of Duralcan SiC/Al composites with theory for the 25-350°C temperature range. _____	109
Figure 12. Comparison of the experimental normalized mean CTE values of SiC/Al composites with the theoretical predictions. _____	110
Figure 13. Comparison of the experimental and theoretical CTE change with reinforcement volume fraction during thermal cycling. _____	110

Appendix 1

Figure 1. Typical dimensional change versus temperature curve for A359/SiC/10p.	114
Figure 2. Typical dimensional change versus temperature curve for A359/SiC/20p.	115
Figure 3. Typical dimensional change versus temperature curve for A359/SiC/40p.	116

List of Abbreviations

<u>Symbol</u>	<u>Description</u>
m	Matrix constituent / Mismatch parameter
p	Particle constituent / Particle-matrix interface pressure
c	Composite / Particle concentration
Al	Aluminum alloy
Si	Silicon
Li	Lithium
Ti	Titanium
Mg	Magnesium
SiC	Silicon carbide
CTE	Coefficient of thermal expansion
Al ₂ O ₃	Alumina
MMC	Metal matrix composites
TMA	Thermomechanical analyzer
μm	Micrometer
E	Elastic modulus
V	Volume fraction
s	Particle shape factor
K _{th}	Theoretical fracture toughness
K _{exp}	Experimental fracture toughness
K	Bulk modulus of the matrix
ΔT	Temperature difference
ΔT ₁	Temperature amplitude for the onset of plasticity in the matrix
ΔT ₂	Temperature amplitude for the onset of reversed plasticity
ΔT ₃	Temperature amplitude for full plasticity in the matrix
ΔT ₄	Temperature amplitude for full reversed plasticity in the matrix
ΔT _a	Temperature amplitude
r _p	Radius of plasticity
r _{rp}	Radius of reversed plasticity

ϵ_T	Thermal strain
N_f	Number of cycles to failure of the interface
D	Ductility of the particle-matrix interface
σ_d	decohesion strength
v/o	Volume fraction
β	Volumetric coefficient of thermal expansion / Linear strain hardening coefficient
ppm	10^{-6}
σ	Normal stress component
α	Coefficient of thermal expansion
G	Shear modulus
ν	Poisson's ratio
σ_r	Radial stress component
σ_θ	Tangential stress component
a	Radius of the particle
b	Radius of the matrix

General introduction

The development of metal-matrix composites has been one of the most important innovations of the past 20 years in the field of material science. Initially, fiber reinforced composites received most of the research attention but it soon became apparent that their complex fabrication and the high cost of the fibers would restrict their usefulness [1]. This lack of commercial opportunities prompted researchers to investigate discontinuously reinforced composites. Nowadays, particle reinforced MMCs are widely used in many industrial applications such as piston cylinders for diesel and gas engines, brake discs, bicycle frames and missile components [2,3,4]. Comprehension of the factors influencing the mechanical and physical properties of MMCs is challenging because they are very sensitive to the reinforcement volume fraction, fabrication process and the nature of the composite constituents. The addition of ceramic particles in an unreinforced aluminum alloy influences the physical and mechanical properties by increasing the stiffness, decreasing the coefficient of thermal expansion and improving creep properties. Indeed, MMCs represent a 10 to 50% increase in elastic modulus, a decrease in the CTE up to 70% and a significant reduction of weight (density) in comparison to pure aluminum alloys. In addition, the superiority of discontinuous metal matrix composites in the area of thermal stability when compared to unreinforced alloys makes them an excellent choice for structural components in variable temperature environments. However, it has been demonstrated that large stress concentration factors appear at the sharp corners of particles [5]. Indeed, repeated temperature changes can induce large thermal stresses causing plastic deformation around the particles in the matrix which, in turn, can cause CTE changes in the composite material. For this reason, modeling the expansion behavior of particle reinforced MMCs under thermal cycling is difficult which is confirmed by a lack of literature on the subject.

The primary objective of this thesis is the characterization of different metal-matrix composite materials using a high precision TMA (Thermomechanical Analyzer) system. More specifically, the thermal expansion behavior of particle reinforced aluminum matrix composites in terms of temperature, reinforcement volume fraction and fabrication process will be experimentally investigated.

The specific objectives of this work are:

1. Describe and analyze the effect of reinforcement volume fraction on the expansion behavior of Al/SiC Duralcan composite materials.
2. Determine and analyze the effect of thermal cycling on the expansion behavior of Al/SiC and Al/Al₂O₃ Duralcan composite materials.

This thesis consists of a collection of scientific papers submitted or to be submitted to scientific journals. Two papers directly related to the specific goals of this thesis are presented in chapters 4 and 6. A brief presentation preceding each paper is included which describes the scientific contribution of the research to the composite material area. Each paper includes an introduction with a literature review, which is followed by the experimental procedures, results, discussions and a concise conclusion. Since each paper is submitted for publication independently of each other, some repetition between the papers is inevitable. In addition to these scientific papers, a complete literature review on fabrication processes and mechanical properties is presented in chapters 1 and 2. In chapter 3, theoretical models for predicting the coefficient of thermal expansion are discussed. Chapter 5 is divided into two distinct sections. The first section introduces the effect of thermal cycling on the expansion behavior of MMCs while the second section consists of computer modeling of the CTE of composites subjected to different thermal histories. To facilitate reading, figures, tables and references appear at the end of each chapter. This was done because of the independent nature of each chapter.

Chapter 1. Fabrication processes

Generally, the nature of the constituents and their interfacial bonding control the mechanical and physical properties of particle reinforced composite materials. However, the material's fabrication process can also have a significant effect on the properties and, therefore, a better understanding of the controlling parameters is essential. In order to gain widespread commercial acceptance, a fabrication process must possess several important characteristics, such as reproducibility, volume of production and process automation [6].

The different fabrication processes for making MMCs can be classified into five major groups: powder metallurgy, liquid phase casting, spray deposition, semisolid and solid state casting. Although a lot of money has been spent developing the two last techniques, they are not used yet for large volume production due to the high production cost, and long processing times and will, therefore, not be discussed in this chapter.

This following section offers a review of the widely used industrial fabrication processes for making particle reinforced metal-matrix composites. For each of the techniques described below, a brief description accompanied by sketches of the apparatus are provided to clearly illustrate the process. As well, a list of the main characteristics of each process is included for future reference.

1.1 Powder metallurgy

Incorporation of ceramic particles into molten aluminum is difficult because molten metals do not generally wet the particles. This is one of the main reasons why the powder metallurgy fabrication process was one of the first techniques to receive industrial consideration. The principal steps involved in this technique are shown in Figure 1. The first step consists of blending aluminum powders and ceramic particles. The most commonly used reinforcements are SiC and Si₃N₄, which generally have a diameter between 20 and 40 μm. This first step is followed by a cold isostatic compaction usually combined with a degassing process. The mixture is then hot pressed and the final shape is usually obtained using a direct extrusion process. An extrusion

ratio of 20:1 or higher must be used to eliminate the oxide layer between the metallic grains. This also increases the mechanical and physical properties of the material. In addition, it allows a uniform distribution of the particles throughout the matrix.

The main characteristics of the powder metallurgy process are:

- Any aluminum alloy can be used.
- Interfacial reactions between the alloy and the ceramic particles can be minimized.
- Non-equilibrium alloys can be used to fabricate the composites [7].
- High reinforcement volume fractions can be achieved.
- Slow process.
- High porosity.
- High production cost (100\$/kg) which restrains its use for high performance and small dimension components.

1.2 Liquid phase casting

When MMCs were first being examined, several techniques that incorporated ceramic particles into a molten aluminum alloy were tried without much success because the molten aluminum alloys would not wet the ceramic particles. The reinforcing particles are actually rejected from the melt [8]. Recently, various new techniques that consist of adding ceramic particles to a molten aluminum alloy have been developed. The following section offers a review of the most important ones.

1.2.1 Mixing process

The production of MMCs by the process of incorporating ceramic particles into a molten alloy has received the most attention because of the low number of controlling parameters. In addition, standard industrial casting techniques which are widely used, inexpensive and well suited to large scale production can be easily used or adapted for MMC production. The technique consists of incorporating the particles into a molten alloy while it is being vigorously agitated. The mixing temperature is not a crucial parameter, whereas the quality of the atmosphere is very important. Indeed, the mixing

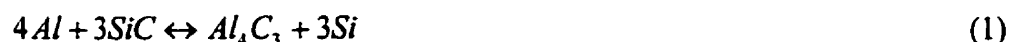
process can last over a long period of time and reactions between the mixture and the atmosphere must be avoided, due to the possible formation of unwanted chemical products which would have a negative effect on the mechanical properties of the composite. As a final step, once the mixture is considered homogeneous, ingots are cast which are then used in shape forming processes.

The mixing process must possess the following attributes:

- Avoid particle sedimentation.
- Avoid particle agglomerates. For particles having a dimension below 20 μm , dispersion is difficult and requires a high shear rate.
- Control of the reactivity between ceramic particles and molten alloy. In order to improve wettability of the particles, alloying elements such as Mg, Ti or Li are added to the molten aluminum to decrease the surface tension. These alloying elements also increase the reactivity of the alloy and therefore a compromise must be made to ensure a good wettability and a low reactivity.
- Control of the mixture viscosity. For a reinforcement volume fraction above 20%, viscosity increases drastically and the mixture is difficult to cast. Generally, for higher volume fractions, infiltration techniques using preforms are preferred.

1.2.1.1 Interfacial reactions

Interfacial reactions can have significant effects on the interface strength [9]. A summary of the thermodynamic stability of several reinforcement phases in aluminum and magnesium alloys has been made by Lloyd *et al* [10]. In an Al/SiC composite, silicon carbide particles are unstable above the melting temperature of the aluminum alloy and the following reaction can occur to form aluminum carbides:



As Al_4C_3 forms, Si concentration increases in the alloy which, in turn, decreases the melting point of the composite. Formation of Al_4C_3 must be avoided because it decreases the strength of the matrix-particle interface. In addition, aluminum carbides have a negative effect on fluidity, corrosion and mechanical properties. In order to prevent

aluminum carbide formation, a high Si concentration is needed. Generally, a concentration exceeding 7% is normally recommended [11] as illustrated in Figure 2. Similarly, alumina is stable in pure aluminum but reacts with magnesium according to the two following reactions:



MgO will form according to reaction (2) if the Mg concentration is high and the temperature is low, whereas MgAl₂O₄ will form according to reaction (3) at lower magnesium concentrations. It is worth mentioning that SiC is stable at temperatures below the solidus line. Adversely, reactions for Al₂O₃ can occur in the solid phase [12].

1.2.1.2 Duralcan process

The most well known mixing process was developed by Duralcan in the late eighties. In 1995, the volume of production was approximately 12 000 tons per year. In general, MMCs with reinforcement volume fraction ranging from 5 to 40% can be made with this technique. Most of the composites fabricated by this process possess a 6061, A35X or A38X matrix reinforced with SiC or Al₂O₃ particles. Schematics of the apparatus used by Duralcan for MMC fabrication are shown in Figures 3 and 4. The shape of the rotating impeller allows a strong agitation vortex which is necessary for wetting the particles. The process consists mainly of adding ceramic particles to a molten aluminum alloy followed by strong agitation of the mixture under vacuum conditions until there is a uniform distribution of the reinforcement phase. In general, for standard casting techniques, casting temperatures are chosen such that a low viscosity of the molten metal is achieved. However, for MMCs other considerations have to be taken into account such as the chemical reactions between the matrix and the reinforcement phase. Therefore, the casting temperature is selected such that there is little or no reaction between the particles and the matrix. As a general rule, for the Duralcan process, the casting temperature is 20°C above the liquidus temperature for alloys containing volatile products, 70°C above the liquidus for conventional alloys and from 100 to 125°C above the liquidus line temperature for alloys containing alloying elements that decrease interfacial reactions.

The mixing period varies from 30 to 40 minutes depending on the combination of alloy/reinforcement. The production cost of MMCs with the Duralcan process is about 1/3 to 1/2 that of competing processes. Analysts predict that prices could be as low as 1/10 of the production cost of the other processes for very large volumes of production.

In summary, the Duralcan process has the following characteristics:

- Uniform distribution of the reinforcement phase.
- High interfacial strength due to strong agitation.
- No oxide layer at particle surface.
- Secondary transformation process such as extrusion and rolling can be used.
- Excellent mechanical properties obtained (stiffness, strength, fracture toughness and ductility).
- Volume fractions between 5% and 40%.
- Low production cost.
- No treatment of the reinforcement prior to fabrication

1.2.1.2.1 Example of MMC fabrication by the Duralcan process

This example demonstrates the fabrication of a composite composed of an aluminum 6061 matrix and silicon carbide particles. Before mixing, the following steps are taken [13]. The impeller (made of graphite), which has been previously bead blasted clean, is given three coating layers of Aremco 552 adhesive ceramic. The coating layers are cured and the impeller is kept at 200°C to drive off any absorbed water. The 6061 aluminum alloy is cut into a convenient size and weight. A measured quantity of alloy is put in the crucible which had previously been heated to 300°C. The mixing furnace is started and the temperature is set to 850-870°C. Argon is blown in the melt at the rate of 10 cc/min for 15 minutes, displacing any absorbed hydrogen and bringing oxide particles to the surface which are subsequently skimmed off. As the alloy begins melting, the temperature is reduced to 680°C. Then, silicon carbide particles are added to the mixture. Simultaneously, the mixing assembly is put in place and a vacuum pulled on the crucible to 15-20 torr or lower. The mixing motor is then turned on and the impeller set to rotate at 750 rpm. After 5 minutes of mixing, the chamber is brought to atmospheric pressure with argon and any excess silicon carbide powder coating the walls is scraped back into

the melt. The cleaning is repeated two or three times at 5 minute intervals. The total mixing time is 50 minutes. As the mixing motor is turned off, the pressure casting head, shown in Figure 4, is clamped into place. The fill tube is immersed in the molten aluminum composite to nearly the bottom of the crucible. The inside of the chamber is then slowly pressurized to 1.5 psi. This low pressure forces the composite in the fill tube into the mold. When the aluminum composite seeps out of the small vent hole and seals it, the pressure is raised to 9 psi until final solidification. MMCs obtained with this technique show a relatively homogenous particle distribution.

1.2.2 In-situ formation

This process consists of forming a composite by precipitating the reinforcing phase directly into the molten alloy [14]. Production volumes are relatively small compared to those of the Duralcan process. However, a great deal of research has been undertaken in an effort to further develop the process and ultimately, improve its efficiency. For instance, one particular technique, that has been proposed, sprays a metal in a reactive atmosphere to precipitate the silicon carbide reinforcements according to the following reaction [15]:



The necessary elements for the reaction to occur are introduced in a liquid bath which is composed mainly of the molten aluminum alloy. The precipitates have an average diameter of between a couple of hundredth's of a micron and four microns. As well, they possess a MgO coating on their surface with an average thickness of a couple of tenth's of an angstrom. Controlling the reactive atmosphere is the key factor which determines the potential of successful MMC fabrication with this technique.

The main characteristics of this technique are:

- MMCs produced can be recycled because they are produced at equilibrium.
- Very low volume fraction composites (< 1%).
- Interesting process for reactive metals such as magnesium.
- Problems with agglomeration of precipitates.

- Avoids the formation of oxide layer.

Considering that only very low reinforcement volume fractions have been achieved, the in-situ formation technique has received little attention from manufacturers.

1.2.3 Squeeze casting

This technique consists of infiltrating a molten aluminum alloy into a ceramic powder preform to make a composite containing up to 50% reinforcement volume fraction [16]. Preforms are made of fibers, whiskers or particles and are preheated at the casting temperature. The molten alloy infiltrates the preform with a pressure varying from 10 to 200 MPa. Infiltration of the preform can also take place under vacuum conditions to facilitate infiltration. The apparatus used for infiltrating preforms is shown in Figure 5. The main characteristics of the process are:

- Fabrication time: 40 to 90 seconds.
- Presence of interfacial reactions between particles and matrix.
- High volume fraction composites can be made.

1.2.4 Pressureless infiltration (Lanxide™)

A new technique, developed by Lanxide Corp. Primex™ by Dr. Schiroky, consists of infiltrating without pressure, in a nitrogen atmosphere, an aluminum-magnesium alloy into a ceramic powder preform. The main steps for fabricating particle reinforced MMCs are:

1. Make ceramic preform with CERASET™ type binder.
2. Preheat preform in a furnace.
3. Apply barrier and release coating to the preform.
4. Make infiltration lay-up.
5. Infiltrate preform in furnace.
6. Solidify composite and remove coatings.

Preforms are usually made of SiC or Al₂O₃ particles held together with a CERASET™ type binder. This binder is an organic polymer and is the basis of the pressureless infiltration process. Preheating the preform is necessary to remove H₂O molecules and to

increase the strength prior to infiltration. As shown in Figure 6, a barrier coating must be applied on the surface of the preform that is not in contact with the molten alloy. This thin layer decreases the surface roughness of the final product and prevents spilling during the infiltration stage. In addition, a release film on the surface of the preform, in contact with the molten alloy, helps the infiltration of the preform. This layer also acts as a wear interface for shear stress because the contraction of the alloy is more severe than that of the MMC on cooling.

The infiltration process is made at 800°C in a nitrogen atmosphere. An aluminum-magnesium alloy must be used because the evaporation of the magnesium is a very important element of the process. At elevated temperatures, magnesium evaporates and reacts with nitrogen to form a thin nitrate layer on the surface of the particles according to the following reaction:



Finally, the magnesium nitrate reacts with the molten aluminum according to the following reaction to form aluminum nitrate which produces an excellent interfacial strength between the particles and the matrix:



The main characteristics of the process are:

- Volume fractions up to 70%.
- Variety of mechanical properties possible.
- Any component dimension.
- Low cost.

1.3 Spraying technique

This technique consists of projecting fine droplets of molten metal on a substrate where there is solidification [17,18]. The main advantages of this technique are the low temperature of the substrate and the rapid solidification which minimizes grain growth and surface oxidation. Osprey [19] developed the most well known technique. Figure 7

shows the apparatus needed for the fabrication process. The process consists of atomizing a stream of molten metal to form a spray of hot metal particles by subjecting the stream to relatively cold gas. This generates a fluidised bed of fine solid particles of mean size (diameter) less than 20 μm . The ceramic particles are injected at room temperature or higher temperature in the atomising zone immediately after the molten metal begins to break up into spray. The atomizing gas may be argon or nitrogen. The spray is directed onto a rotating collecting surface to form a tubular spray deposit. Subsequently, the tubular deposit can be further processed.

Another spraying technique consists of melting the alloy in a plasma flame. This flame is generally produced by passing a high velocity gas stream through an electric arc. The main advantage of this technique as compared to the atomising method is the higher velocity of the molten metal particle stream. The composites obtained with this technique almost have a maximum compactness.

The main characteristics of these processes are:

- Volume fractions up to 50%.
- Particle dimension below 20 μm for atomising and below 2 μm for plasma spraying.
- High density composites (95% to 100%).
- Rapid solidification which minimizes interfacial reactions and oxidation.

Conclusion

Currently, a wide variety of MMCs are commercially available. Depending on the fabrication process, there exists an almost infinite number of matrix/particles combinations. Although fiber reinforced composites offer better directional mechanical properties, particle composites have isotropic properties and are far more cost effective. Particle reinforced composites can be made from the standard fabrication processes which greatly decrease their production cost. The most widely used fabrication process for making MMCs is, by far, the Duralcan mixing process for its low cost/volume ratio. However, for large reinforcement volume fractions, the powder metallurgy and squeeze casting techniques are preferred. Finally, even if the pressureless infiltration and spraying techniques are very promising, they are not yet used on a large production scale.

In order to be commercially successful, MMCs need to be used in applications requiring large production volumes like those in the transportation industry and particularly in the automotive industry. For the moment, MMCs are being used for sporting goods, spacecraft and aircraft components and a few specialized automotive parts [20]. The use of particle reinforced MMCs will increase during the next years since reproducibility of the components is good and mechanical property requirements can be satisfied at a relatively low production cost.

References

1. T. W. Chou, A. Kelly and A. Okura. Fibre-Reinforced Metal-Matrix Composites, *Composites*, vol. 16, no. 3, p. 187-206 (1985)
2. S. Elomari, R. Boukhili, C. San Marchi, A. Mortensen and D. J. Lloyd, Thermal expansion responses of pressure infiltrated SiC/Al metal-matrix composites, *Journal of Materials Science*, vol. 32, no. 8, p. 2131-2140 (1996)
3. S. Elomari, H. Richards, C. San Marchi, M. D. Skibo and G. Vokovich, Advanced composite materials in space structures, *37th Israel Annual Conference on Aerospace Sciences*, Technion-Israel Institute of Technology, Haifa, p. 287-297 (1997)
4. M. K. Premkumar, W. H. Hunt and R. R. Sawtell, Aluminum Composite Materials for Multichip Modules, *Journal of Metals*, vol. 44, no. 7, p. 24-28 (1992)
5. T. Nakamura, S. Suresh, Effects of Thermal Residual Stresses and Fiber Packing on Deformation of Metal-Matrix Composites, *Acta Metallurgica et Materialia*, vol. 41, no. 6, p. 1665-1681 (1993)
6. D. M. Schuster, M. D. Skibo, R. S. Bruski, R. Provencher and G. Riverin, The Recycling and Reclamation of Metal-Matrix Composites, *Journal of Metals*, vol. 45, no. 5, p. 26-30 (1993)
7. R. Angers, Nouveaux matériaux métalliques et nouveaux procédés de fabrication, CNRC, chapter 6 (1987)
8. A. M. Patton, Foundry Trials of Graphite-Containing Aluminum Alloys, *Journal Institute of Metals*, vol. 100, p. 197-201 (1972)
9. A. Mortenson, Mechanical and physical behavior of metallic and ceramic composites, *9th Riso International Symposium on Metallurgy and Materials Science*, p. 141-155 (1991)
10. D. J. Lloyd, H. P. Lagacé and A. D. McLeod, Interfacial phenomena in metal matrix composites, *Controlled interphases in composite materials*, Proceedings of the 3rd International Conference on Composite Interfaces, Cleveland, New York, p. 359-376 (1990)

11. D. J. Lloyd, Comp. The solidification microstructure of particulate reinforced aluminum/SiC composites, *Composites Science and Technology*, vol. 35, no. 2, p. 159-179 (1989)
12. D. J. Lloyd, Particle reinforced aluminum and magnesium matrix composites, *International Materials Reviews.*, vol. 39, no. 1, p. 1-23 (1994)
13. M. D. Skibo and D. M. Schuster, US Patent 4 786 467, Dural Aluminum Composites Corp., San Diego, California (1988)
14. M. J. Koczak and K. S. Kumar, US Patent, 4 808 372, Drexel University, Philadelphia, Pa. (1986)
15. H. Miura, H. Sutou, T. Natsume and H. Katagiri, US Patent, 4 508 682, Toyota, Japan (1985)
16. S. Elomari, Analyses mécanique et thermomécanique des composites à matrices d'aluminium, Phd Thesis, Ecole Polytechnique of Montreal, December (1995)
17. E. A. Feest, P. F. Chesney and J. S. Coombs. US Patent, 4 928 745, United Kingdom Atomic Energy, London, England (1990)
18. D. J. Lloyd, Metal Matrix Composites – An Overview, *Advanced Structural Materials*, Proceedings Oxford, vol. 9, p. 1-21 (1989)
19. A. Leatham, R. G. Brooks and J. Coomes, UK Patent, GB2172827A, Osprey Metals (1986)
20. P. Morris and C. Baker, Production, refining and recycling of light metals, *CIM*, vol. 19, p. 190-209 (1990)

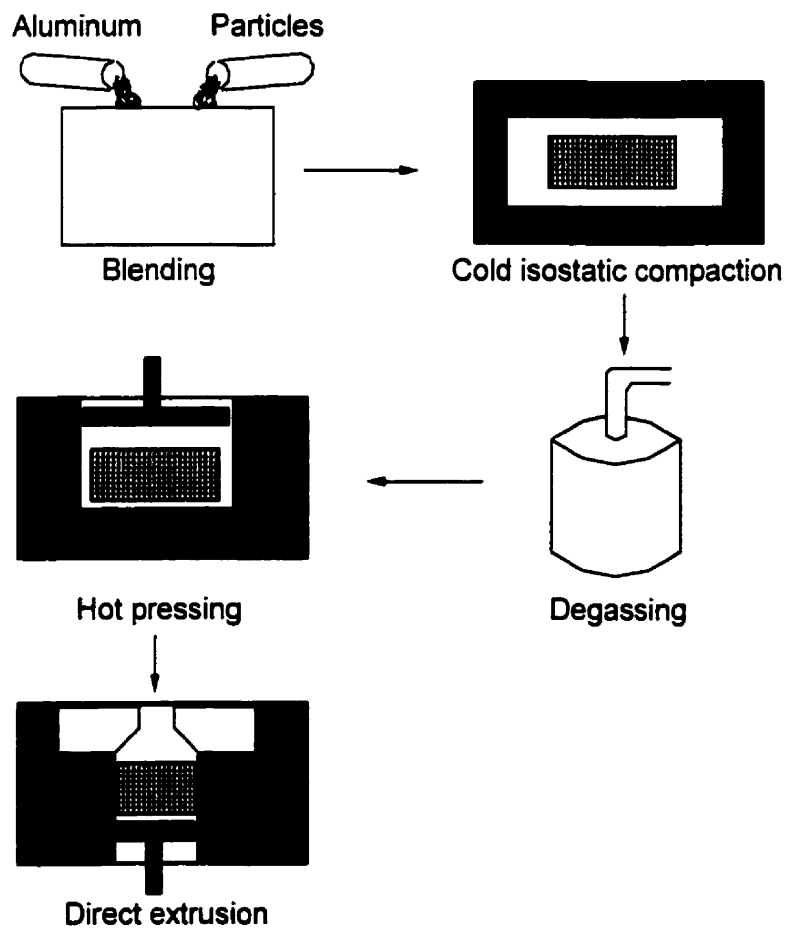


Figure 1. Main steps for MMC processing using the powder metallurgy technique.

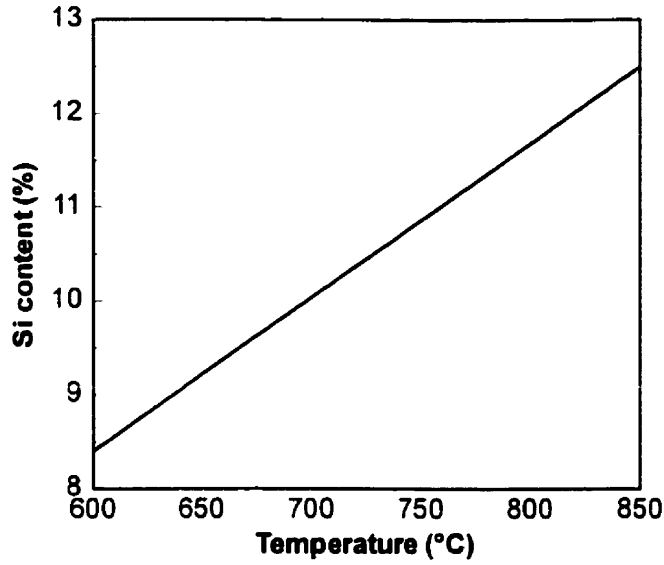


Figure 2. Recommended silicon content in an aluminum alloy to prevent carbide formation.

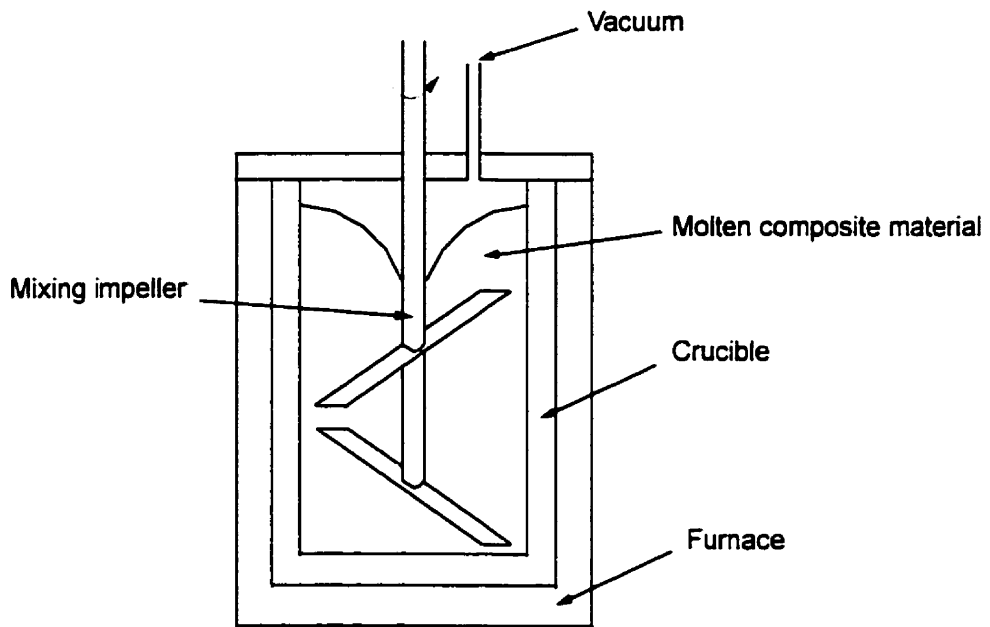


Figure 3. Apparatus used for the Duralcan process.

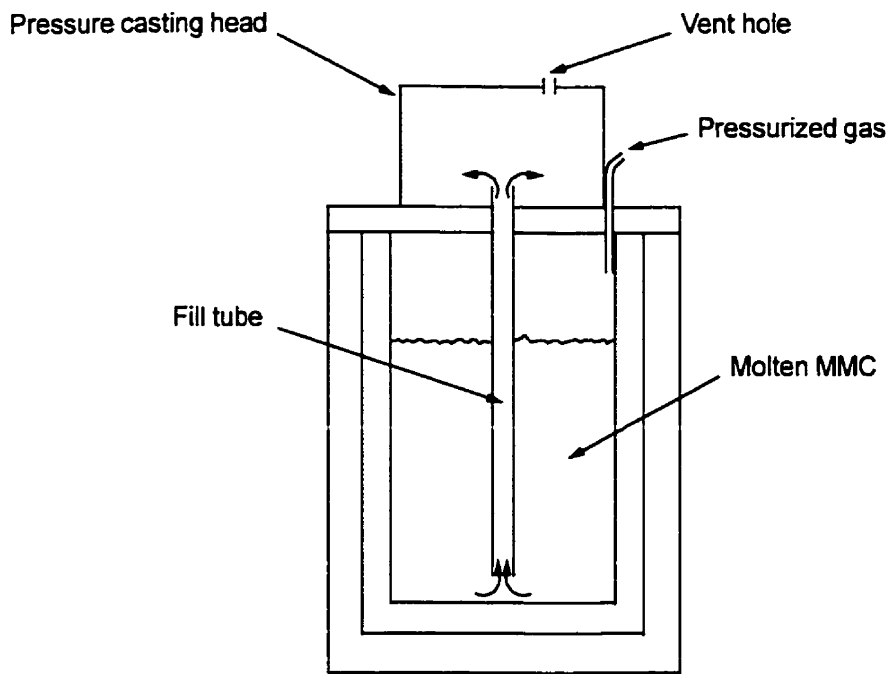


Figure 4. Pressure casting head used in the Duralcan process.

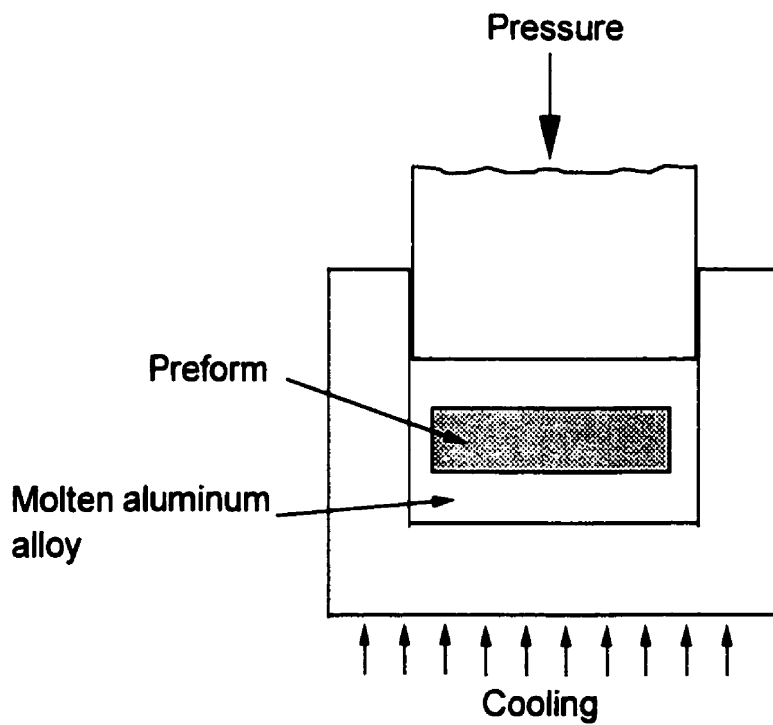


Figure 5. Apparatus used for squeeze casting.

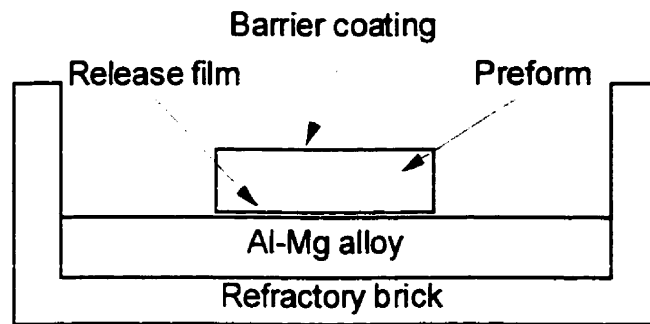


Figure 6. Pressureless infiltration technique by Lanxide.

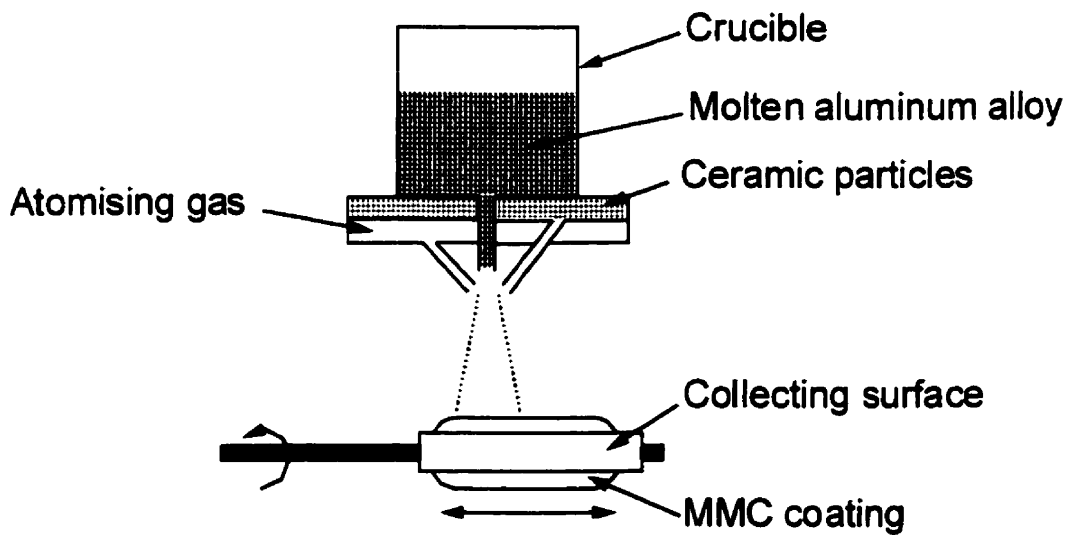


Figure 7. Spraying technique developed by Osprey.

Chapter 2. Mechanical properties

2.1 Nomenclature

The ANSI H35.5-1992 nomenclature [1] provides a simple and comprehensive notation to describe a composite material:

“alloy type”/“reinforcement type”/“reinforcement volume fraction”/“reinforcement shape”-“heat treatment”

For example, a 6061/Al₂O₃/40p-T4 composite is composed of a 6061 aluminum matrix reinforced with 40% Al₂O₃ particles in volume. This composite has also been heat treated to T4 (solutionized at 550°C for 1 hour then quenched in water followed by room temperature aging for a minimum of 2 days).

2.2 Elastic modulus

The mechanical property that always significantly increases with addition of ceramic particles into an aluminum alloy is the elastic modulus. Although the elastic modulus can be experimentally obtained for unreinforced alloys, it is difficult to accurately measure it for a particle reinforced composite. These difficulties are due to the residual stresses present in the composite which are caused by the CTE mismatch between the matrix and the particles. For MMCs containing SiC or Al₂O₃ particles, the CTE mismatch ratio can reach 6:1 causing the aluminum matrix to be in tension. This implies that the composite will plastically deform sooner in tension than in compression [2]. Measuring the elastic modulus is even more difficult when the particle distribution is non-uniform within the composite. However, in general, the addition of particles increases the elastic modulus, as shown in Figure 1. Several theoretical models have attempted at predicting the elastic modulus of particle reinforced MMCs. The simplest of these models is the rule of mixtures, and it is written as follows:

$$E_c = V_p E_p + V_m E_m \quad (1)$$

where E_c , E_m and E_p are the elastic modulus of the composite, the matrix and the particles respectively, and V_m and V_p , the volume fraction of the matrix and the particles. This model frequently overestimates the elastic modulus. However, the rule of mixtures has been modified by Halpin-Tsai [3] in an effort to make better predictions of the experimental modulus:

$$E_c = \frac{E_m(1 + 2sqV_p)}{1 - qV_p} \quad (2)$$

where

$$q = \frac{\left(\frac{E_p}{E_m} - 1\right)}{\frac{E_p}{E_m} + 2s} \quad (3)$$

and s is the shape factor which represents the aspect ratio of the average dimensions of the reinforcement particles. This relation usually gives an accurate representation of the experimental values of the elastic modulus as shown in Figure 1. Indeed, the experimental elastic modulus of particle reinforced metal-matrix composites can be bounded by Equation 2 using upper and lower values of the elastic modulus of the reinforcement particles.

2.3 Strength

Most of the papers published in this area show that the main factor influencing strength is the addition of reinforcing particles as shown in Figure 2. Indeed, adding particles can increase the strength of a pure alloy by more than 60%. However, due to the different fabrication processes there exists a great deal of uncertainty in the experimental data. Despite these variations, several particle reinforced MMCs, which are commercially available, meet the strength requirements as shown in Table 1 [4]. As well, typical mechanical properties of the unreinforced alloys are given for comparison purpose in Table 2. In addition to reinforcement volume fractions and fabrication processes, particle shape factors also seem to have an effect on strength. However, the effect is minimized

for MMCs containing particles with a shape factor of less than 2:1 and it becomes an insignificant parameter [5].

2.4 Ultimate strain

The chief shortcoming of MMCs is their poor ductility. Ultimate strain rapidly decreases with the addition of reinforcing particles as shown in Figure 3. Studies revealed that the failure of MMCs was associated with cracking of the reinforcing phase and the formation of microscopic voids in the matrix, thus significantly increasing stresses above the flow stress of the matrix [6,7]. In most cases, stress concentrations are caused by the particles of larger dimensions. Indeed, the largest particles are the most susceptible to containing inherent defects. In addition, they support a larger fraction of the load which accelerates their cracking due to higher stress levels [2].

2.5 Fracture toughness

Even though the behavior of fracture toughness with the addition of ceramic particles is somewhat similar to that of the ultimate strain, it appears that the decrease in fracture toughness is more significant between levels of 0 and 10% reinforcement. Table 3 gives values of fracture toughness for different composites with comparison to some theoretical model predictions. Having a typical fracture toughness between 15 and 20 $\text{Mpa}\sqrt{\text{m}}$, particle reinforced aluminum MMCs have fracture toughness values comparable to those of other materials.

References

- 1 T. H. Hahn, Metal matrix composites: mechanisms and properties, Academic Press, Boston, p. 33 (1990)
- 2 D. J. Lloyd, Particle reinforced aluminum and magnesium matrix composites, *International Materials Reviews*, vol. 39, no. 1, p. 1-23 (1994)
- 3 J. C. Halpin, Primer on composite materials: Analysis, Technomic Publication, Lancaster, PA, p. 130 (1984)
- 4 P. D. Pitcher, A. J. Shakesheff and A. D. Tarrant, Thermal properties of SiC particulate reinforced aluminum alloys, *International Conference on Powder Metallurgy in Aerospace*, p. 181-188 (1995)
- 5 M. Taya, K. E. Lulay and D. J. Lloyd, *Morris E. Fine Symp.*, p. 153-164 (1990)
- 6 D. C. Drucker, High strength materials, Wiley, New York, p. 795-830 (1965)
- 7 D. J. Lloyd, P. L. Morris and E. Nehme, Fabrication of particles reinforced metal composites, ASM International, Materials Park, OH, p. 235-243 (1990)

Composite material	Yield stress (MPa)	Ultimate tensile stress (MPa)	Elongation (%)	Elastic modulus (GPa)	Supplier
6061/Al ₂ O ₃ /10p	296	338	7.5	81	Duralcan, Alcan
6061/Al ₂ O ₃ /15p	317	359	5.4	87	Duralcan, Alcan
6061/Al ₂ O ₃ /20p	359	379	2.1	98	Duralcan, Alcan
6061/Al ₂ O ₃ /20p	305	330	3.4	85	Comalco
6061/ Al ₂ O ₃ /25p	430	515	4.0	115	DWA
A356/SiC/10p	287	308	0.6	82	Duralcan, Alcan
A356/SiC/15p	329	336	0.3	91	Duralcan, Alcan
A356/SiC/20p	336	357	0.4	98	Duralcan, Alcan
A380/SiC/20p	308	356	0.4	114	Duralcan, Alcan
2124/SiC/25p	490	630	2.0-4.0	116	British Petroleum
8090/SiC/13p	310	450	4.0-7.0	103	British Petroleum
8090/SiC/17p	450	540	3.0-4.0	103	British Petroleum
7075/SiC/15p	556	601	3.0	95	Cospray, Alcan
A356/SiC/50p	360	401	0.6	165	DWA

Table 1. Typical mechanical properties for some particle reinforced metal-matrix composites available in the industry [2].

Aluminum alloy	Yield stress (MPa)	Ultimate tensile stress (MPa)	Elongation (%)	Elastic modulus (GPa)
6061	275	310	20.0	69
A356	205	280	6.0	76
A380	160	320	3.5	72
2124	325	470	12	72
8090	415	485	7.0	80
7075	505	570	10.0	72

Table 2. Typical mechanical properties of commonly used aluminum alloys [2].

Composite material	K_{exp} (MPa/ \sqrt{m})	K_{th} (MPa/ \sqrt{m})
2014/Al ₂ O ₃ /15p		
3 h, 160°C	24.2	25.4
48 h, 160°C	18.1	15.6
6061/Al ₂ O ₃ /15p		
3 h, 160°C	24.7	21.5
48 h, 160°C	21.2	18.0

Table 3. Typical fracture toughness values for 2014 and 6061 aluminum alloys containing Al₂O₃ particles compared with theoretical predictions [2].

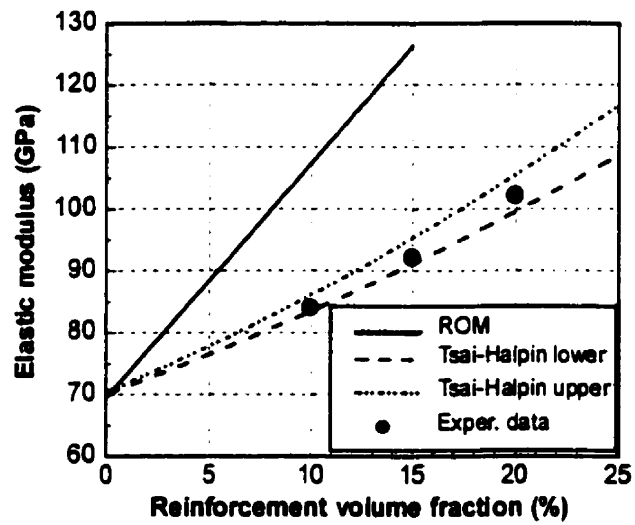


Figure 1. Typical elastic modulus curve of 6061/ Al_2O_3 composite material as a function of reinforcement volume fraction with the Rule of Mixtures and Tsai-Halpin lower and upper bound theoretical predictions.

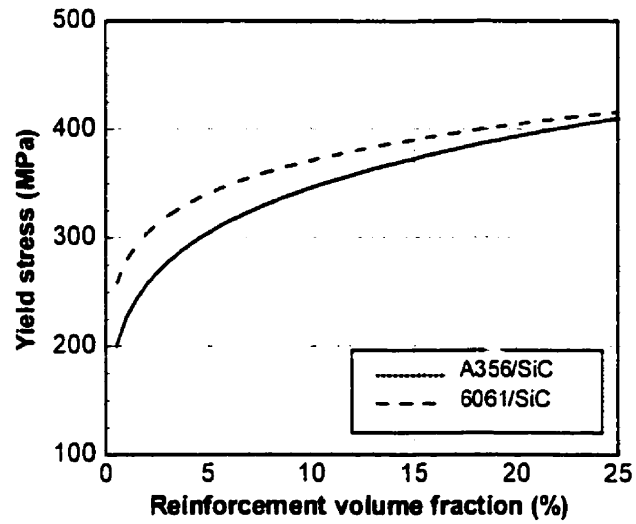


Figure 2. Typical yield stress curves of A356/SiC and 6061/SiC composite materials as a function of reinforcement volume fraction.

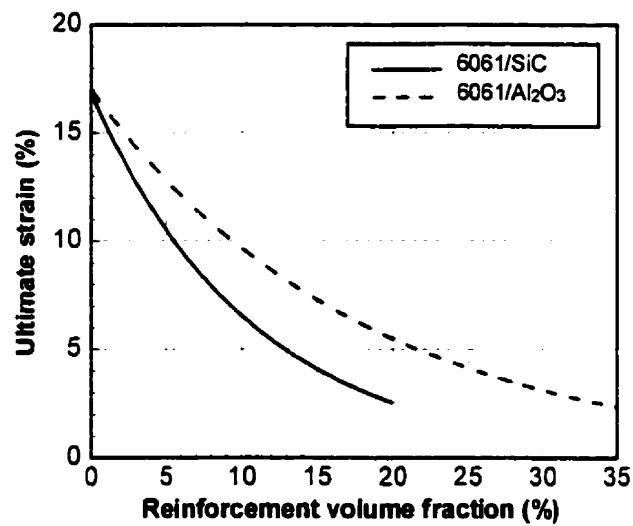


Figure 3. Typical maximum ductility of 6061/SiC and 6061/Al₂O₃ composite materials as a function of reinforcement volume fraction.

Chapter 3. Thermal expansion of MMCs

The CTE of MMCs is difficult to predict because it is influenced by several factors, including, the matrix plasticity and the internal structure of the composite. The matrix and particles often have different CTEs and different expansion behaviours. In the theoretical models that will be described, it is assumed that the interface bond is strong enough to resist the stresses developed on heating or cooling of the material due to CTE mismatch.

There exists a variety of theoretical models available in the literature which attempt to predict the CTE of particle reinforced aluminum composites [1,2]. Among those, four models are particularly interesting: Turner, Kerner, Schapery and the Rule of Mixtures.

3.1 Turner model

The Turner model [3] assumes homogeneous strain throughout the composite and uses a balance of internal average stresses to derive the thermal expansion of the composite. In this model, it is assumed that each component is constrained to change dimensions with temperature changes at the same rate as the composite. Neglecting shear deformation, we can write the stress acting on each phase of the composite (the matrix and the particles) with the volume strain and bulk modulus, as:

$$\sigma_i = (\beta_c - \beta_i)K_i\Delta T \quad i = p, m \quad (1)$$

where β is the volumetric coefficient of thermal expansion, K is the bulk modulus and the subscripts c , p and m refer to the composite, particle and matrix respectively. The resultant force acting on any cross-section of the composite must sum to zero such that:

$$\sigma_p A_p + \sigma_m A_m = 0 \quad (2)$$

where A_p and A_m are the cross sectional areas of the particles and the matrix respectively. For a homogeneous distribution of the reinforcing particles, the cross sectional areas become proportional to the volume fractions of each constituent such that Equation 2 becomes:

$$\sigma_p V_p + \sigma_m V_m = 0 \quad (3)$$

Substituting this last equation into (1) and knowing that the volumetric coefficient of thermal expansion is related to the linear CTE by $\alpha = \beta / 3$, the composite coefficient of thermal expansion is:

$$\alpha_c = \frac{\alpha_p V_p K_p + \alpha_m V_m K_m}{V_p K_p + V_m K_m} \quad (4)$$

3.2 Kerner model

The Kerner model [4] assumes that the composite can be represented by two concentric spheres of different materials. The outer (hollow) sphere is the matrix and the inner sphere is the particle. Each constituent is assumed to be homogeneous and isotropic. In addition, the interface between the matrix and the particle is assumed to be mechanically bonded. The size of the spheres represents the volume fraction of each phase. The CTE of this two element sphere is, thus, the CTE of the composite and can be written as follows:

$$\alpha_c = V_p \alpha_p + V_m \alpha_m + \left[\frac{4G_m}{K_c} \right] \left[\frac{(K_c - K_p)(\alpha_m - \alpha_p)V_p}{4G_m + 3K_p} \right] \quad (5)$$

where G is the shear modulus and K_c , the bulk modulus of the composite derived by Hashin [5,6] which is given by:

$$K_c = \frac{\left(\frac{V_p K_p}{3K_p + 4G_m} + \frac{V_m K_m}{3K_m + 4G_m} \right)}{\left(\frac{V_p}{3K_p + 4G_m} + \frac{V_m}{3K_m + 4G_m} \right)} \quad (6)$$

The bulk modulus is related to the elastic modulus by the following standard relationship:

$$K = \frac{E}{3(3 - E/G)} \quad (7)$$

The temperature dependence of the CTE of the composite comes from the temperature dependence of the parameters: α_m , α_p , K_m , K_p and G_m . Variations of the elastic, shear and bulk moduli for aluminum alloys 6061, A359 and A360 [7] with both SiC and Al₂O₃ ceramic materials [8] are shown in Tables 1 and 2 respectively.

3.3 Schapery model

The CTE can also be modeled on the basis of a model developed by Schapery which utilizes extremum principles of thermoelasticity [5,9]. The CTE of the composite, according to the Schapery model is written as:

$$\alpha_c = \alpha_p + (\alpha_m - \alpha_p) \frac{1/K_c - 1/K_p}{1/K_m - 1/K_p} \quad (8)$$

where K_c is the bulk modulus of the composite. This equation states an exact relation between the composite CTE and the bulk modulus. Since only upper and lower bounds of K_c can be determined using Hashin's bounds [10], Equation 8 will provide bounds on the CTE. The lower bound on the bulk modulus is:

$$K_c = K_m + \frac{V_p}{\frac{1}{K_p - K_m} + \frac{V_m}{K_m + \frac{4}{3}G_m}} \quad (9)$$

The upper bound is obtained by interchanging indices m and p everywhere. Note that the upper bound of the composite CTE coincides with the CTE value determined using the Kerner's model. Although not explicitly written, the CTE of the composite is dependent on the reinforcement volume fraction through its effect on the bulk modulus of the composite.

3.4 Rule of mixtures

When there is no elastic interaction between the constituents of a composite, a simple expression which describes its CTE is the volume fraction rule of mixtures relation [2]:

$$\alpha_c = V_m \alpha_m + V_p \alpha_p \quad (10)$$

where V is the volume fraction, α is the CTE and m and p subscripts represent the matrix and the particles respectively. The Rule of Mixtures model is usually seen as an upper bound that the composite CTE should never exceed.

3.5 Plot of the theoretical models

A plot of the theoretical CTE obtained with the Kerner, Turner, Schapery and Rule of Mixtures models versus temperature is given in Figure 1 for a 6061/Al₂O₃/40p composite. The temperature-dependent values of E , G , K and α for A359 and SiC were taken from Tables 1 and 2 [11]. All four models show a relatively linear behavior between 25 and 350°C. The Turner model represents the lower bound for the elastic CTE while the Rule of Mixtures gives the upper limit. Between those models, Schapery's upper and lower bounds are found (the upper bound is the Kerner model which is a particular case of the Schapery model). All models predict an increasing CTE with temperature. The increase of the CTE from room temperature to 350°C is shown in Table 3. In the same table, the average CTEs from 25 to 350°C are also presented. All models predict a significant increase of the CTE of approximately 14%. This increase is significant and should be accounted for by engineers working with such materials. A different approach is to look at the average CTE variation with reinforcement volume fraction as shown in Figure 2 for a typical A359/SiC/40p composite. These theoretical curves are obtained by computing the average values of the constituent properties and substituting them into the theoretical model equations. The Rule of Mixtures and the Kerner models show relatively linear behavior with volume fraction while the Schapery and the Turner models do not. All models converge towards the average CTE of pure A359 aluminum alloy between 25 and 350°C as the reinforcement volume fraction approaches zero. Similar results were obtained by Balch *et al* [12].

References

- 1 R. J. Vaidya and K. K. Chawla, Thermal expansion of Metal-Matrix Composites, *Composite Science and Technology*, vol. 50, no. 1, p.13-22 (1994)
- 2 T. H. Hahn, Metal matrix composites: mechanisms and properties., Academic Press, Boston, p. 329-355 (1990)
- 3 S. Elomari, R. Boukhili, C. San Marchi, A. Mortensen and D. J. Lloyd, Thermal expansion reponses of pressure infiltrated SiC/Al metal-matrix composites. *Journal of Materials Science*, vol. 32, no. 8, p. 2131-2140 (1996)
4. E. H. Kerner, The elastic and thermo-elastic properties of composite media, *Proceedings of the Physics Society*, vol. 69B, p. 808-813 (1956)
- 5 R. A. Schapery, Thermal Expansion Coefficients of Composite Materials Based on Energy Principles, *Journal of Composite Materials*, vol. 2, no. 3, p. 380-404 (1968)
- 6 B. W. Rosen and Z. Hashin, Effective thermal expansion coefficients and specific heats of composite materials, *International Journal of Engineering Science*, vol. 8, no. 2, p. 157-174 (1970)
- 7 D. J. Lloyd, H. Burke and B. Farahbakhsh, Temperature dependence of modulus in particle reinforced composites, *Materials Science and Technology*, vol. 10, no. 3, p.257-262 (1994)
- 8 Duralcan composites casting guidelines, "Duralcan composites-mechanical and physical property, Wrought composites, SI Units", Duralcan^{USA}, San Diego, CA, USA (1992)
- 9 S. Elomari, R. Boukhili and D. J. Lloyd, Thermal expansion studies of prestrained Al₂O₃/Al metal matrix composite, *Acta metallurgica and materialia.*, vol. 44, no. 5, p. 1873-1882 (1996)
10. Z. Hashin and S. Shtrikman, A variational approach to the theory of the elastic behavior of multiphase materials, *Journal of the Mechanics and Physics of Solids*, vol. 11, p. 127-141 (1963)
11. P. K. Mallick, Fiber-reinforced composites: Materials, manufacturing and design, ed. Dekker, New York (1993)

12 D. K. Balch, T. J. Fitzgerald, V. J. Michaud, A. Mortensen, Y. -L. Shen and S. Suresh,
Thermal expansion of metals reinforced with ceramic particles and microcellular
foams, *Metallurgical and Materials Transactions A*, vol. 27A, p. 3700-3717 (1996)

T (°C)	6061				A359				A360			
	E (GPa)	G (GPa)	K (GPa)	CTE ($\mu^\circ\text{C}$)	E (GPa)	G (GPa)	K (GPa)	CTE ($\mu^\circ\text{C}$)	E (GPa)	G (GPa)	K (GPa)	CTE ($\mu^\circ\text{C}$)
25	71.3	26.5	77.8	22.3	70.4	26.9	68.4	21.1	71.4	27.2	69.4	21.2
50	71.5	26.5	78.4	22.7	70.3	26.8	68.3	21.8	71.2	26.9	69.1	21.6
150	71.3	26.4	78.4	23.9	68.7	25.2	67.5	22.7	69.4	25.4	68.2	22.9
250	69.3	25.8	74.3	24.8	66.4	23.9	63.2	24.5	67.1	24.2	63.8	24.3
350	65.4	24.5	66.3	25.4	65.3	22.1	61.6	26.2	65.9	22.9	60.7	25.9

Table 1. Temperature-dependence of the properties of the composite matrix constituents [11].

T (°C)	SiC				Al ₂ O ₃			
	E (GPa)	G (GPa)	K (GPa)	CTE ($\mu^\circ\text{C}$)	E (GPa)	G (GPa)	K (GPa)	CTE ($\mu^\circ\text{C}$)
25	450	192	227	4.5	409.3	163.8	272.5	6.0
50	450	192	227	4.5	408.1	163.3	271.7	6.1
150	450	192	227	4.5	403.2	161.3	268.5	6.7
250	450	192	227	4.5	398.2	159.3	265.3	7.1
350	450	192	227	4.5	393.3	157.3	262.1	7.3

Table 2. Temperature-dependence of the properties of the composite reinforcement constituents [11].

	Change from 25 to 350°C (%)	Mean CTE over 25-350°C (ppm/°C)
Turner model	13.42	11.91
Schapery model	13.16	13.92
Kerner model	14.00	16.09
Rule of Mixtures	14.38	17.17

Table 3. Theoretical percent change and average CTEs between 25 and 350°C for a typical 6061/Al₂O₃/40p composite material.

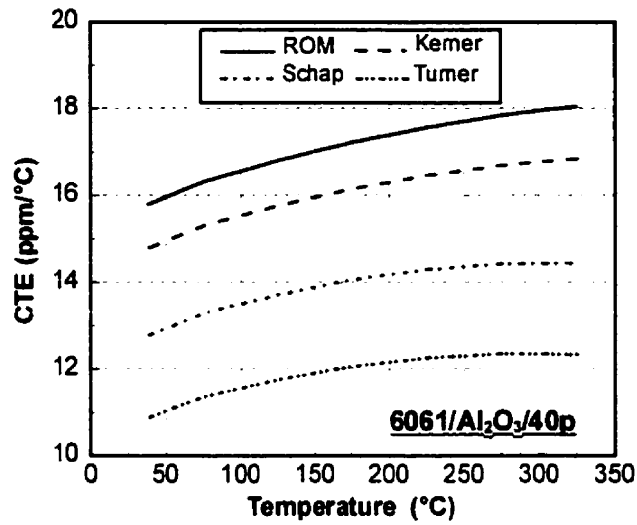


Figure 1. Theoretical CTE predictions obtained with the Kerner, Turner, Schapery and Rule of Mixtures models for a 6061/Al₂O₃/40p composite material.

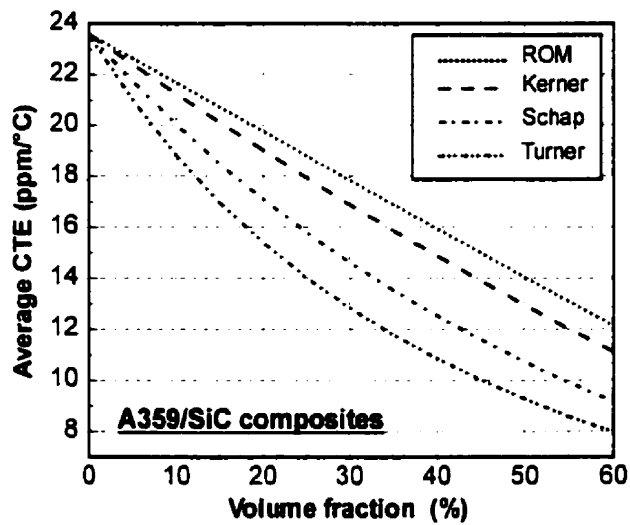


Figure 2. Average theoretical CTE values obtained with the Kerner, Turner, Schapery and Rule of Mixtures models as a function of reinforcement volume fraction.

Introduction to Chapter 4

The objective of this first paper is the characterization of the thermal expansion behavior of particle reinforced composite materials. Specifically, TMA (thermomechanical analyzer) measurements were made to determine the effect of temperature and reinforcement volume fraction on the coefficient of thermal expansion of the composites. The dimensional change from 25 to 350°C was measured on four different Al/SiC Duralcan composite materials containing between 10 and 40% volume fraction of particles. Typical TMA dimensional change versus temperature curves are given in Appendix 1. It has been shown that the CTE values increase with temperature and decrease with reinforcement volume fraction. Moreover, the instantaneous expansion behaviour of the four composites was similar. The experimental CTE values were below the theoretical predictions in the low temperature region and close to the Kerner model predictions at higher temperatures. However, mean CTE values between 25 and 350°C were found to lie between the upper and lower elastic CTE bounds defined by the Schapery theoretical model. Furthermore, in order to aid the analysis, a mean CTE with volume fraction curve was established using other authors experimental CTE data for Al/SiC composite materials. The low CTE values combined with the excellent mechanical properties of these composites make them superb choices for electronic packaging and space structure applications.

Chapter 4. Thermal Expansion of Isotropic Duralcan Metal-Matrix Composites

S. LEMIEUX*, S. ELOMARI

*Spacecraft Engineering, Canadian Space Agency, 6767 route de l'Aéroport, Saint-Hubert, J3Y 8Y9,
Canada, Fax: 514-926-4695*

**Department of Mechanical Engineering, McGill University, Montreal, Canada*

J. A. NEMES

Department of Mechanical Engineering, McGill University, Montreal, Canada

M. D. SKIBO

MC-21 Incorporated, San Diego, CA 92121, USA

(Submitted to the Journal of Materials Science)

Abstract

The thermal expansion behavior of Duralcan composites having a matrix of hypoeutectic Al-Si alloy containing SiC reinforcements ranging from 10 to 40 % in volume was investigated. The coefficient of thermal expansion (CTE) of the MMCs was measured between 25 and 350°C by a high-precision Thermomechanical Analyzer (TMA), and compared to the predictions of three theoretical models. At low temperature, the experimental CTEs show substantial deviation from the predictions of the elastic analysis derived by Schapery, while the Kerner model agrees relatively well at high temperature. The overall measured CTE, in the range of 25-350°C, as a function of the volume fraction of SiC is well predicted using Schapery's lower bound. We interpret these features as being an effect of reinforcement phase geometry and the modified microstructure derived from the Duralcan process and subsequent heat treatments.

Keywords: Metal-Matrix Composite, Ceramic Particle, Thermal Expansion.

4.1 INTRODUCTION

Metal-matrix composites have emerged as a class of materials capable of advanced structural, aerospace, automotive, electronic, thermal management, and wear applications. These alternatives to conventional materials provide the specific mechanical properties necessary for cryogenic and elevated temperature applications. In many cases, the performance of MMCs is superior in terms of improved physical, mechanical, and thermal properties. The performance advantage of aluminum alloys reinforced with various ceramics such as SiC and Al₂O₃ is their tailored mechanical, physical, and thermal properties that include low density, high specific strength, high specific modulus, good fatigue response, control of thermal expansion, high abrasion and wear resistance [1,2]. Tailorability for specific applications is one of the greatest attractions of MMCs. Thus, these composites are gaining rapid prominence in aerospace [3], automotive, electronic [4] and energy sectors. For instance, low CTE and high thermal conductivity are desirable properties for applications such as heat sink and radiator panels for satellite structures and space shuttles [5]. Furthermore, MMC material is being successfully used as diecast components, which include pistons [6,7], cylinder liners, connecting rods [8], brake drums and even engine blocks. The interest in this composite stems from its high specific strength and stiffness, low thermal expansion, high thermal conductivity and improved tribological properties.

The thermal expansion coefficient (CTE) of metal-matrix composites has been recognized as one of the important thermomechanical properties since the thermal stability can be a critical issue in the design of components subjected to temperature variations. Tailoring the CTE is an important consideration in minimizing the expansion-contraction mismatch or to maintain specific dimensional tolerances between components subjected to various temperature gradients. In addition, a thermal expansion study of MMCs is required in order for thermal stresses to be investigated for particular applications such as electronic packaging.

In recent years, extensive numerical and analytical research has been performed on thermomechanical properties, such as CTE, of Al/SiC composites and on the dependence of such properties on processing parameters [9,10]. For instance, it has been well

established from numerical investigations that geometrical variables such as the concentration, size, shape, and spatial distribution (architecture) of the ceramic particles in the aluminum matrix can substantially influence the thermal expansion behavior of particle-reinforced metal-matrix composites. However, detailed experimental studies of such geometrical effects on the CTEs of MMCs have so far not been reported.

We explore, in what follows, the effect of reinforcement volume fraction, which is known to exert a significant influence on the thermal expansion behavior of isotropic metal-matrix composites, as might be expected from a simple rule of mixtures. In this work, the thermal expansion behavior of Duralcan composites having a matrix of hypoeutectic Al-Si alloy containing SiC reinforcements ranging from 10 to 40 % in volume was investigated. The coefficient of thermal expansion (CTE) of the MMCs was measured between 25 and 350°C by a high-precision Thermomechanical Analyzer (TMA), and compared to the predictions of three theoretical models.

4.2 EXPERIMENTAL PROCEDURES

4.2.1 Composite materials

The chemical compositions of the aluminum alloy matrices used in this study are given in Table 1. The composite materials were received in the form of ingots from Duralcan Canada and MC-21 Incorporated, San Diego, California. The specifications of the reinforcement particle and aluminum alloys used in this study are shown in Table 2. The MMC materials were produced by the Duralcan[™] (Trademark, Alcan Aluminum Ltd, San Diego, U.S.A.) molten metal mixing process [11,12]. The composites were permanent mold cast and then heat treated to the T4 condition (solutionized at 550°C for 1 hour then quenched in water followed by room temperature aging for a minimum of 2 days). Fig. 1 shows SEM micrographs of polished sections of the SiC/Al composites. All composites exhibit a uniform particle distribution which seems to be responsible for the isotropic nature of mechanical and physical properties. At low volume fraction, the reinforcing particles are very effective in nucleating new grains within the aluminum matrix, and stabilizing the resulting fine grain size. Quantitative metallography analysis of the composites were examined with a light microscope interfaced with the IBAS 2000

system. Typically, 20 fields of about 100 particles per field were investigated. This system enabled the data acquisition for the SiC particles, including location of the particle centroid in the field, particle area and aspect ratio (ratio of maximum and minimum particle diameter). Aspect ratio distribution histograms of SiC particulate for all four material systems accumulated during image analysis are shown in Fig. 2. The SiC particulate is irregular in shape having an average aspect ratio of 1.4-2.2 with the rare occurrence of larger shards of much greater convexity. The average SiC particle size in the 10 v/o composite is 9.3 micrometers (600 grit), and at 20, 30 and 40 v/o, 13 micrometers (500 grit). The aluminum alloy matrix has a fine uniform grain size of the order of the interparticle spacing (5-40 μm depending on volume fraction). Energy dispersive X-ray analysis in the SEM revealed no unusual second phases other than those associated with the Al-Si-Mg matrix and the typical trace elements. No evidence of chemical reaction between the matrix and the SiC particulates was noted. No particle cracking is apparent and essentially no porosity is present in the composite material.

4.2.2 TMA Test

The average dimension of the specimens for TMA testing was 10 x 5 x 1.5 mm. Coupons were cut from the cast materials using a diamond saw and were polished using 1 μm diamond paste. More than 4 samples of each composite were tested to verify reproducibility of the experimental data. CTE measurements were performed from 25°C to 350°C at 10°C/min using a commercial thermomechanical analysis equipment (model TMA 2940, Dupont, USA). Experimental curves shown in this study represent the average values for all samples. The thicknesses of the samples were measured with increased sensitivity (0.01 μm) using the standard expansion probe. The TMA apparatus measures linear or volumetric changes in the dimensions of a specimen as a function of time, temperature and force. The dimensional change of the sample is measured with a LVDT (linear variable differential transformer) that has an output which is proportional to the linear displacement of the core caused by changes in sample dimensions. The samples were placed in a chamber where atmosphere quality can be controlled. An inert gas, helium, was blown into the chamber at a rate of 40 ml/min. A thermocouple adjacent to the sample assures accurate measurements of the sample temperature. The

final output is a plot of PLC (percent linear change) versus time, temperature or force. TMA standard data analysis software was used to evaluate instantaneous and average CTEs of the composites tested. In this study, average CTEs were determined at intervals of 50°C based on the calculated slope fit between two selected temperatures using PLC versus temperature curves.

4.3 RESULTS

The precision of the TMA measurement technique was established by repeated tests of the same composite specimen as well as various aluminum alloys. The experimental results of the dimensional change with temperature of the four silicon carbide reinforced composites are shown in Fig. 3a. For a given temperature, the dimensional change decreases with reinforcement volume fraction. In addition, the slope of the dimensional change versus temperature curves becomes shallower for the entire temperature interval as the reinforcement volume fraction increases from 10 to 40%. Note that all thermal expansion versus temperature responses of the composites are not linear.

The effect of reinforcement volume fraction on thermal expansion behavior of Duralcan composite for various temperature ranges is shown in Fig. 3b. As expected from Fig. 3a, the CTE strongly depends on volume fraction of SiC for a given temperature range. The composite reinforced with 40% SiC exhibits the lowest CTE around 10 ppm/°C at 25-50°C which is about 2.2 times that of monolithic SiC. It is evident that the measured CTE shows, for each Duralcan composite, similar variations with temperature, but with a substantial increase in the CTE value, by about 6 ppm/°C, as the temperature range increases from 25-50°C to 300-350°C. This effect of temperature is expected since the temperature dependence of CTE for each aluminum alloy [13,14], as illustrated in Table 3, clearly points to a similar increase in CTE (5.4 ppm/°C).

4.4 DISCUSSION

4.4.1 Theoretical models

The CTE of MMCs is generally difficult to predict because it is influenced by several factors such as reinforcement volume fraction, fabrication process and the nature of the composite constituents. Several models have been proposed for predicting the CTE of particle reinforced MMCs. Among those, three are worth mentioning due to their simplicity and good accuracy: Turner [15], Kerner [16], and Schapery models [17].

4.4.1.1 Turner's model

The Turner model assumes homogeneous strain throughout the composite and uses a balance of internal average stresses to derive the thermal expansion of the composite. In this model, each constituent is assumed to be constrained to change dimensions with the temperature changes at the same rate as the composite. Neglecting shear deformation, we can write the stresses acting on the matrix and the particles using the volume strain and bulk modulus:

$$\sigma_i = (\beta_c - \beta_i) K_i \Delta T \quad i = p, m \quad (1)$$

where β is the volumetric coefficient of thermal expansion, K the bulk modulus and subscripts c , p and m refer to the composite, particle and matrix respectively. The resultant force acting on any cross-section of the composite must be zero for equilibrium such that:

$$\sigma_p A_p + \sigma_m A_m = 0 \quad (2)$$

where A_p and A_m are the cross sectional areas of the particles and the matrix respectively. For a homogeneous distribution of the reinforcing particles, the cross sectional areas become proportional to the volume fraction of each constituent such that equation (2) becomes:

$$\sigma_p V_p + \sigma_m V_m = 0 \quad (3)$$

Substituting this last equation into (1) and knowing that the volumetric coefficient of thermal expansion is related to the linear CTE by $\alpha = \beta / 3$, the CTE of the composite becomes:

$$\alpha_c = \frac{\alpha_p V_p K_p + \alpha_m V_m K_m}{V_p K_p + V_m K_m} \quad (4)$$

4.4.1.2 Kerner's model

The Kerner model assumes that the reinforcement is spherical and wetted by a uniform layer of matrix; thus the CTE of the composite is stated to be identical with that of a volume element composed of a spherical reinforcement particle surrounded by a shell of matrix, both phases having the volume fractions present in the composite. This model gives the composite CTE as:

$$\alpha_c = \bar{\alpha} + V_p (1 - V_p) (\alpha_p - \alpha_m) \frac{K_p - K_m}{(1 - V_p) K_m + V_p K_p + (3K_p K_m / 4G_m)} \quad (5)$$

Where the rule of mixtures is given by $\bar{\alpha} = (1 - V_p) \alpha_m + V_p \alpha_p$. K and G are the bulk and shear moduli, V is the volume fraction, and α is the coefficient of thermal expansion. The bulk modulus is calculated using the standard relationship:

$$K = \frac{E}{3(3 - E/G)} \quad (6)$$

4.4.1.3 Schapery's model

Among the several formulae that have been suggested for the calculation of the thermal expansion coefficients of composite materials taking into account the stress interaction between components is that of Schapery who has derived the effective CTE of isotropic composites, by employing extremum principles of thermoelasticity. The CTE value can be written as

$$\alpha_c = \alpha_p + (\alpha_m - \alpha_p) \frac{(1/K_c) - (1/K_p)}{(1/K_m) - (1/K_p)} \quad (7)$$

where α_c and K_c are the CTE and bulk modulus of the composite. Note that α_c depends on the volume fraction and phase geometry only through their effect on bulk modulus. This equation states an exact relation between the composite CTE and bulk modulus. However, only upper and lower bounds of K_c are determined in a given case (Hashin's bounds [18]). Thus, this expression will provide only bounds on CTE. The lower bound on bulk modulus is

$$K_c = K_m + \frac{V_p}{\frac{1}{K_p - K_m} + \frac{V_m}{K_m + \frac{4}{3}G_m}} \quad (8)$$

The upper bound is obtained by interchanging indices m and p everywhere. The lower bound on K_c yields the upper bound on the composite CTE shown in equation (7) (and vice-versa). Note that this upper bound of the composite CTE was shown by Schapery to coincide with the CTE value determined using Kerner's model. This is not surprising since Hashin's lower bound for bulk modulus is stated to be an exact result for an elastic composite, in which the reinforcement is a sphere coated with a uniform layer of the matrix.

Numerical values of parameters, E, K, G and α , used for the computation of predicted composite CTE using Equations (4), (5) and (7) are extracted from previous experimental work [13,14,19-22]. The variation in Young's and shear moduli with temperature for pure aluminum was examined using Dynamic Mechanical Analysis (DMA) and the temperature dependence of aluminum alloys CTE was studied using TMA. A summary of the elastic constants and CTE of the composite constituents is provided in Table 3.

4.4.2 Comparison between the experimental and theoretical results

An advantage of the present theoretical calculations over the mean field theory, which consider the CTE constant over a given temperature range, is that it can take into account the temperature dependence of the CTE of Al/SiC Duralcan composites. Since we experimentally determined extensive data for the constituent phases of the composite materials [22,23], it is possible to compare quantitatively the theoretical predictions with experimental results. Therefore, the predicted effects of reinforcement volume fraction

on the CTE of composite materials do furnish some worthwhile information for better understanding the composites thermal expansion behavior.

The comparison between the theoretical calculations and experimental results of the composite CTE for the 10-40% volume fraction range is shown in Fig. 4. At low temperature, the experimental CTEs show substantial deviation from the predictions of the elastic analysis derived by Schapery, since these are significantly lower than the elastic lower bound. This trend become more prominent as reinforcement volume fraction increases, while the Kerner model agrees relatively well at high temperature. Obviously, the low-temperature CTE measured upon heating of the Duralcan composites are closer to the Turner model values than the elastic lower bound. However, the agreement with Turner and Schapery's lower bound model is still good at lower temperatures. As the temperature is increased, experimental results are seen to deviate from these predictions, presumably because of a change in the physical interaction between ceramic particles and the aluminum matrix. The Kerner's model which takes into account both the normal and shear stresses between the particles and the matrix, is a better fit at high temperature than those of Turner and Schapery. This feature was reported in previous work [17,23] on pressure infiltrated composites containing high volume fraction of reinforcement (56%). A good agreement with Kerner's model at high temperatures was found while the CTEs in the low-temperatures agreed relatively well with the values predicted by Turner's and Schapery's equations.

The average CTE between 25 and 350°C as a function of reinforcement volume fraction is given in Fig. 5. Knowing the equation of the experimental CTE as a function of temperature (second order polynomial best fit curve) from Fig. 4, we can compute the experimental average CTE using the following general relationship:

$$F_{avg} = \frac{1}{T_2 - T_1} \int_{T_1}^{T_2} F(T) dT \quad (9)$$

where T_1 and T_2 represent the limits of the temperature interval. In addition, theoretical predictions of the average CTE versus volume fraction curves were obtained using the average values of the constituent properties given in Table 3 over the same temperature interval. The average CTEs of the four composites of the present study were combined with those of Balch et al [17] and Elomari et al [23], for Al/56% SiC and Al/47% SiC

composites, respectively. This experimental average CTE curve provides an excellent approximation of the expansion behavior of SiC/Al composites over 25-350°C temperature range. The overall measured CTE as a function of the volume fraction of SiC, in the range of 0-60%, is shown in Fig. 5, as well as the predictions of Kerner, Schapery and Turner. Although the influence of ceramic concentration on the CTE is consistent, the thermal expansion behavior is well predicted using Schapery's lower bound, up to 60% of SiC phase. This trend is not surprising since particle shape has a significant effect on the CTE of Al-SiC composites. Indeed, the results of finite element analysis indicate that for spherical particles, the Kerner model provides the weakest constraint while high aspect ratio particles (>1) gives the strongest constraint on the matrix [24]. Therefore, Kerner's model, which assumed spherical particles, may underestimate the constraints actually offered in real composites. The previous argument applies to any two phase material composed of constituents with distinct properties. For example, it was reported experimentally [25], in WC-Co alloys, that the constraint imposed on the binder phase depends strongly on the aspect ratio and concentration of Co phase.

In summary, the thermal expansion behavior of Duralcan composites is the result of a complex interaction between the SiC particulate reinforcement and the aluminum matrix microstructure. The composite is not a homogeneous monolithic structure but a mixture of a continuous aluminum matrix and discontinuous particulates each having significantly different mechanical and thermal properties across a thin interface. The mismatch in CTE between the particles and the matrix results in the generation of localized stresses at the particle interfaces during the solidification of the composite as well as the solutionizing and quenching step of the heat treatment cycle. It is possible that these stresses may be in part responsible for the very low CTE measured in all composite samples at low temperatures. At higher temperatures these localized stresses (strains) relax and should have less of an effect on the thermal response of the composites. The CTE of metal-matrix composites is further influenced by its discontinuous microstructure. At a fine scale, the MMC may be viewed as having a complex defect structure. The aluminum matrix grains can be extremely small due to the limiting effect of the reinforcing phase. As a result, there is a high concentration of grain boundaries.

There is also a large number of particle-matrix interfaces, typical of particle reinforced composites. The high incidence of these planar discontinuities can result in strain and dislocation generation at the interfaces during the heating cycle due to the property mismatch. This complex defect microstructure and dislocation cells at the interfaces are thought to strongly affect the CTE of metal-matrix composites. The interplay of these effects and others, less understood and more poorly defined, result in the complex CTE response discussed above.

4.5 CONCLUSIONS

The geometry and volume fraction of the reinforcing ceramic phase in Duralcan metal-matrix composite appear to be the major factors in the determination of composite thermal expansion coefficients. SiC particle reinforced Duralcan composites show similar thermal expansion behavior over the temperature range tested and appear to be more stable in that range. At low temperature, the experimental CTEs show substantial deviation from the predictions of the elastic analysis derived by Schapery, while the Kerner model agrees relatively well at high temperature. The Duralcan composites, as demonstrated in this study, exhibit a great dimensional stability and are well suited for applications such as electronic packaging which require low and tailorable CTEs that do not noticeably increase within the usage temperature range.

References

1. F. A. GIROT, J. M. QUENISSET and R. NASLAIN, *Comp. Sci. Tech.*, **30** (1987) 155
2. A. MORTENSON, in Proc. Conf. Fabrication of Particulates Reinforced Metal Matrix Composites, Montreal, Canada, September 1990, edited by F. G. Hamel, p. 235
3. MILLER, in "Hybrid and select metal matrix composites", edited by W. J. Renton, (The American Institute of Aeronautics and Astronautics, New York, USA) p. 56.
4. D. J. LLOYD, *International Materials Reviews*, **39** (1994) 1
5. S. ELOMARI, H. RICHARDS, C. SAN MARCHI, M. D. SKIBO and G. VUKOVICH, in Proc. of the 37th Israel Annual Conference on Aerospace Sciences, Israel, Feb. 1997, Edited by Kenes Tel Aviv (Omanuth Press Ltd., Haifa), p. 287.
6. S. ELOMARI, A. SUNDARAJAN, and M. FLEMINGS, "In Situ Strengthened Metal Matrix Composite". Case Number: MIT-CSA 7185, US Patent, Serial number 60/029,321
7. H. E. DEVE and C. MCCULLOUGH, *JOM*, **47** (1995) 33
8. K. ROHATGI, US Patent 5 407 495, Board of Regents of the University of Wisconsin on behalf of the University of Wisconsin-Milwaukee, Milwaukee, WI (1995)
9. A. LEVY and J.M. PAPA ZIAN, *Journal of Engineering Materials and Technology*, **115** (1993) 129
10. W. ROSEN and Z. HASHIN, *Int. J. Eng. Sci.*, **8** (1970) 157
11. D. SKIBO and D. M. SCHUSTER, US Patent 4 786 467, Dural Aluminum Composites Corp., San Diego, California (1988)
12. D. SKIBO and D. M. SCHUSTER, US Patent 4 759 995, Dural Aluminum Composites Corp., San Diego, California (1988)
13. Duralcan composites casting guidelines, "Duralcan composites-mechanical and physical property, Foundry composites, SI Units", Duralcan^{USA}, San Diego, CA, U.S.A. (1992)

14. Duralcan composites casting guidelines, "Duralcan composites-mechanical and physical property, Wrought composites, SI Units", Duralcan^{USA}, San Diego, CA, U.S.A. (1992)
15. K. BALCH, T. J. FITZGERALD, V. J. MICHAUD, A. MORTENSEN, Y. L. SHEN and S. SURESH, *Metallurgical and Materials Transactions A*, **27A** (1996) 3700
16. H. KERNER, *Proc. Phys. Soc. B.*, **69B**, (1956) 808
17. A. SCHAPERY, *Journal of Composite Materials*, **2** (1968) 380
18. Z. HASHIN and S. SHTRIKMAN, *Journal Mech. Phys. Solids*, **11** (1963) 127
19. ASM Specialty Handbook, Aluminum and Aluminum Alloys, edited by J. R. Davis and Davis & Associates (ASM International, Materials Park, 1993) p. 718
20. J. LLOYD, H. BURKE and B. FARAHBAKHS, *Materials Science and Technology*, **10** (1994) 257
21. T. H. HAHN, in "Metal matrix composites: mechanisms and properties", edited by R. K. Everett and R. J. Arsenault (Academic Press, Boston, 1991) p. 329
22. S. ELOMARI, R. BOUKHILI and D. J. LLOYD, *Acta mater.*, **44** (1996) 1873
23. S. ELOMARI, R. BOUKHILI, C. SAN MARCHI, A. MORTENSEN and D. J. LLOYD, *Journal of Materials Science*, **31** (1996) 2131
24. L. R. DHARANI and W. HONG, in Conference on Processing, Fabrication and Application of Advanced Composites, Long Beach, August 1993 (ASM International, 1993) p.51
25. M. H. POECH and H. F. FISCHMEISTER, *Acta Metallurgica and Materialia*, **40** (1992) 487

	Si	Fe	Cu	Mn	Mg	Ti	Zn	All Other elements	Al
A359	8.50-9.50	0.20 max.	0.20 max.	0.45-0.65	0.45-0.65	0.20 max.	-	0.03 max. 0.10 total	Rem.
A360	9.50-10.50	0.80-1.20	0.20 max.	0.50-0.80	0.50-0.70	0.20 max.	0.03 max.	0.03 max. 0.10 total	Rem.

Table 1. Chemical composition of aluminum alloy matrices.

	Density (g.cm-3)	Yield stress (MPa)	Maximum plastic strain (%)	Thermal conductivity (W/m.K)
SiC	3.2	303	0	80-200
A359	2.685	207-262	3-5	138
A360	2.63	170	3.5	113

Table 2. Properties of reinforcement particles and aluminum matrices.

T°C	SiC				A359				A360			
	E (GPa)	G (GPa)	K (Gpa)	CTE ($\mu^\circ\text{C}$)	E (GPa)	G (GPa)	K (GPa)	CTE ($\mu^\circ\text{C}$)	E (GPa)	G (GPa)	K (Gpa)	CTE ($\mu^\circ\text{C}$)
25	450	192	227	4.5	70.4	26.9	68.4	21.1	71.4	27.2	69.4	21.2
50	450	192	227	4.5	70.3	26.8	68.3	21.8	71.2	26.9	69.1	21.6
100	450	192	227	4.5	69.4	25.5	68.1	22.3	70.2	26.2	68.6	22.4
150	450	192	227	4.5	68.7	25.2	67.5	22.7	69.4	25.4	68.2	22.9
200	450	192	227	4.5	68.2	24.7	66.3	23.6	68.4	25.1	67.2	23.2
250	450	192	227	4.5	66.4	23.9	63.2	24.5	67.1	24.2	63.8	24.3
300	450	192	227	4.5	65.9	23.1	59.2	25.3	66.4	23.6	60.4	25.4
350	450	192	227	4.5	65.3	22.1	61.6	26.2	65.9	22.9	60.7	25.9

Table 3. Temperature-dependence of the properties of the composite constituents.

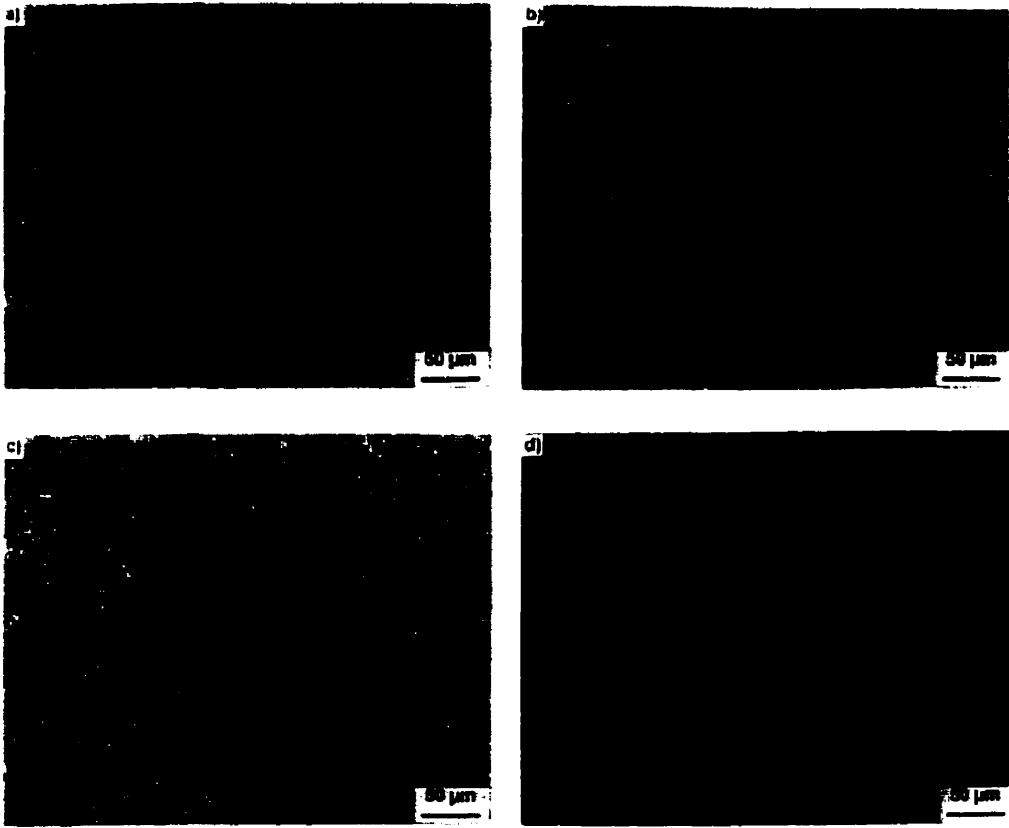


Figure 1. Microstructures of Duralcan SiC/Al metal-matrix composites: (a) 10% SiC, (b) 20% SiC, (c) 30% SiC, and (d) 40% SiC

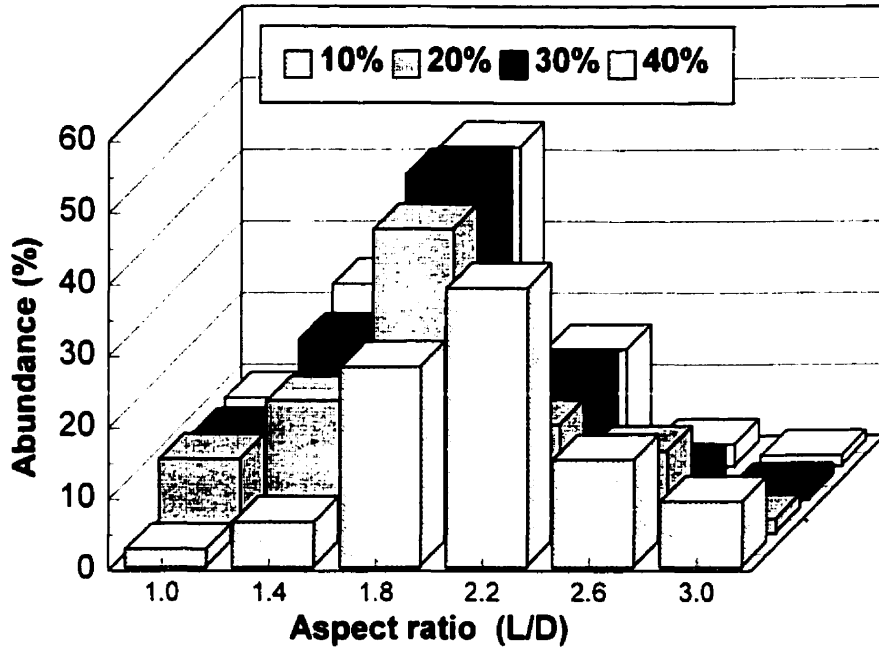


Figure 2. Aspect ratio histograms of SiC particulate for Duralcan composites.

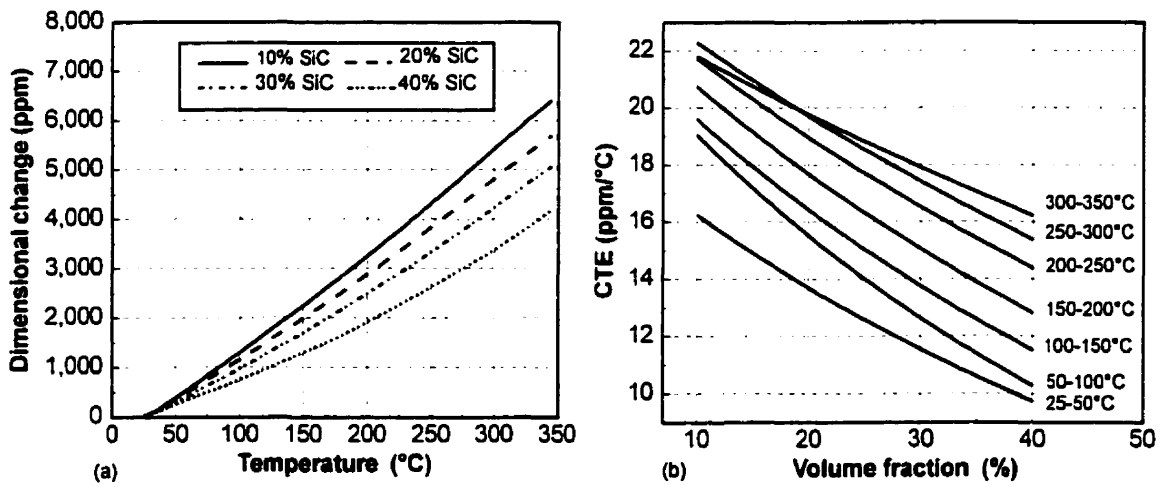


Figure 3. Thermal expansion behavior of SiC composites: (a) Dimensional change vs. Temperature, and (b) CTE vs. temperature.

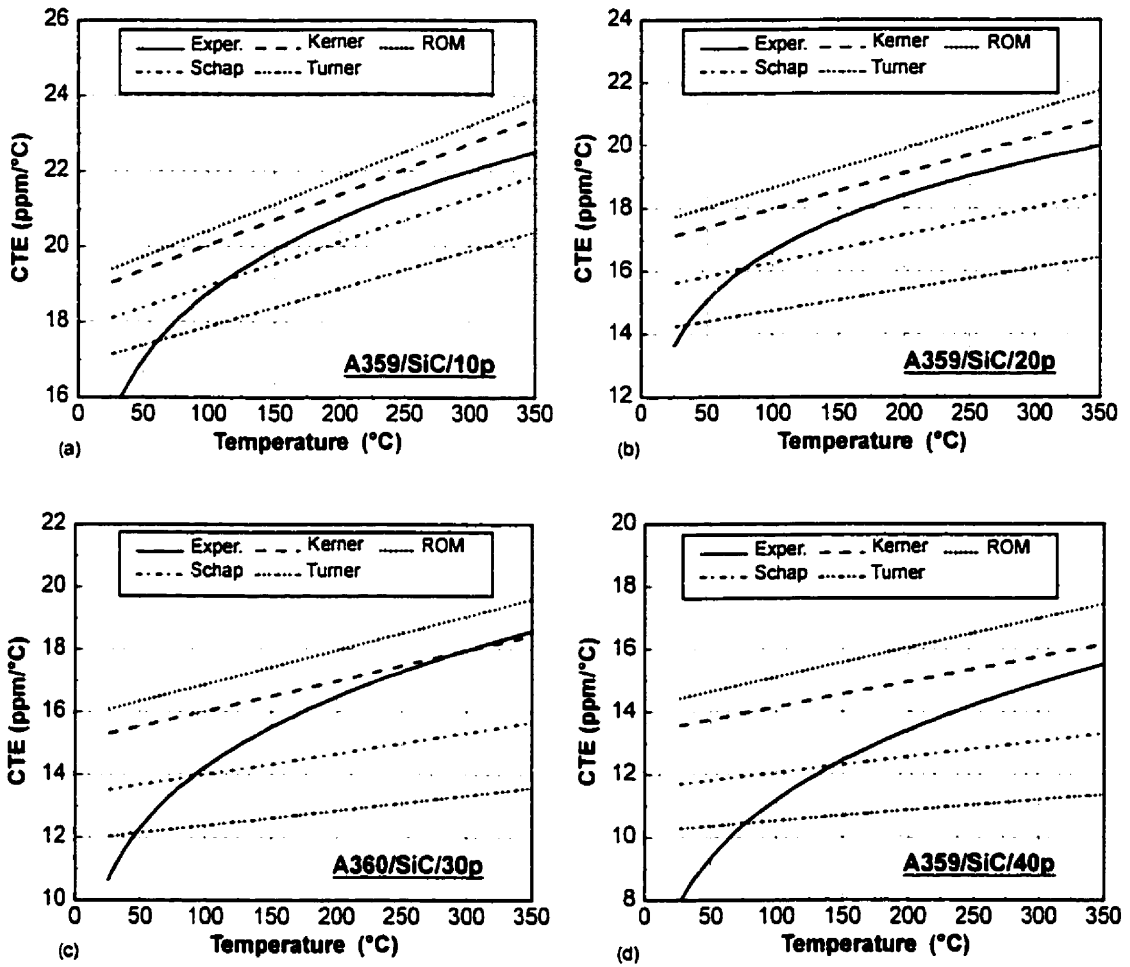


Figure 4. Comparison of the measured CTE of Duralcan SiC/Al composites with the theoretical predictions.

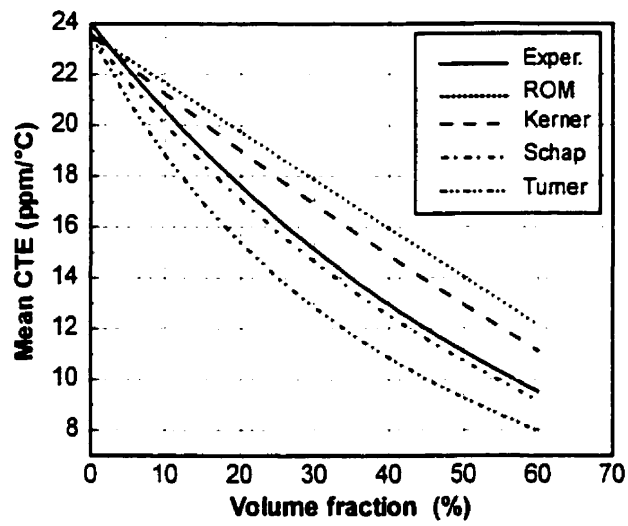


Figure 5. Comparison of the mean CTE of Duralcan SiC/Al composites with theory for 25-350°C temperature range.

Chapter 5. Thermal cycling of MMCs

Thermal cyclic loading is a phenomenon that any material must be characterized for before it can be used extensively in a high performance application. For example, particle reinforced composites are now being used in the spacecraft industry and are subjected to repeated high temperature gradients which cause damage within the microstructure of the composite. Actually, the temperature of space components can go up to 150°C when exposed to direct sunlight and can reach -150°C in the shadow of the earth. Since dimensional stability is of the utmost importance for spacecraft components, it is essential to have models that can describe the expansion behavior of these composites. Most of the research papers dealing with CTE of MMCs do not take into account repeated thermal loading. However, several authors have shown that thermal cycling leads to residual strain and, thus, changes the CTE of composites [1,2]. Consequently, a model is required to study the evolution of the residual stresses and strains evolving around spherical inclusions embedded in an elastic matrix or an elastic-ideally plastic matrix in response to monotonic temperature changes.

Olsson *et al* [3] developed a theoretical model to analyze the elastoplastic deformation due to thermal cycling of a MMC reinforced with ceramic particles. Following is a summary of this analysis.

5.1 Elastoplastic model

The expansion behavior of a particle reinforced MMC is assumed to be similar to that of two concentric spheres made of different materials each occupying the average volume fraction of its constituent as shown in Figure 1. The outer shell of radius, b , is the matrix (aluminum alloy) and the inner sphere of radius, a , represents the ceramic particle. It is assumed that both constituents are homogeneous and isotropic and that the interface between the matrix and the particle is mechanically bonded. Heating and cooling rates are assumed to be fast enough to avoid creep and diffusion and slow enough to avoid thermal shock. In addition, heat distribution is assumed to be constant throughout the spheres at the different stages of thermal cycling. The material is also assumed to be in a

stress-free state at the beginning of the thermal loading. The analysis is divided into two stages: a monotonic temperature change from the stress-free state followed by an analysis of thermal cycling.

Assuming that the particle is in a hydrostatic stress state, that the radial stresses are equal on both sides of the interface and that the normal stress at the outer boundary is zero, we can derive an expression to evaluate the interface pressure:

$$p = \frac{\frac{2E_m}{3(1-\nu_m)}(\alpha_p - \alpha_m)(1-c)\Delta T}{\left[1 - \frac{2m}{3}(1-c)\right]} \quad c = \left(\frac{a}{b}\right)^3 \quad (1)$$

where c represents the reinforcement volume fraction. The parameter m is an elastic mismatch parameter which is given by:

$$m = \frac{E_m}{(1-\nu_m)} \left[\frac{(1-2\nu_m)}{E_m} - \frac{(1-2\nu_p)}{E_p} \right] \quad (2)$$

Note that the interface pressure can be negative depending on the sign of ΔT . A negative pressure means that the interface is under tensile stress. Using the assumption that the spherical particle is in a hydrostatic stress state, we can also derive the radial and tangential stresses in the particle:

$$\sigma_r = -p \quad \sigma_{\theta p} = -p \quad (3)$$

The stresses in the matrix are functions of the radial position in the matrix. Therefore, for $a \leq r \leq b$, the stresses are:

$$\sigma_m = \frac{cp}{(1-c)} \left[1 - \left(\frac{b}{r}\right)^3 \right] \quad \sigma_{\theta m} = \frac{cp}{(1-c)} \left[1 + \frac{1}{2} \left(\frac{b}{r}\right)^3 \right] \quad (4)$$

It is important to note that for a small concentration, i.e. as c approaches 0, the stresses in the matrix vanish except in the region close to the particle representing an isolated inclusion. The following results will therefore be applicable for isolated inclusions by allowing c to approach 0.

5.1.1 Characteristic temperatures

According to the model, there exist four characteristic temperatures which clearly distinguish the transition in plastic response during thermal cycling. The effective stress in the matrix is given by the following equation:

$$\sigma_{em} = |\sigma_{\theta m} - \sigma_{rm}| = \frac{3}{2} \frac{c}{(1-c)} P \left(\frac{b}{r} \right)^3 \quad (5)$$

for $a < r < b$. This effective stress is maximum for $r = a$ meaning that plasticity will spread outward from the interface. It is important to note that the particle remains in a hydrostatic stress state, and therefore does not plastically deform. Knowing that the matrix will yield for a certain temperature change, the temperature amplitude, ΔT_1 , needed to initiate plastic deformation at $r = a$, can be derived by equating the effective stress with the mean yield stress of the matrix, σ_y , within the studied temperature interval:

$$|(\alpha_p - \alpha_m) \Delta T_1| = \frac{\sigma_y (1 - \nu_m)}{E_m} \left[1 - \frac{2m}{3} (1-c) \right] \quad (6)$$

By substituting $\sigma_{em} = \sigma_y$ and $r = r_p$ in Equation 5, we can get the radius of plasticity, r_p , for any $\Delta T < \Delta T_1$:

$$|(\alpha_p - \alpha_m) \Delta T| = \frac{\sigma_y (1 - \nu_m)}{E_m} \left[\left(\frac{r_p}{a} \right)^3 - m \left(2 \ln \left(\frac{r_p}{a} \right) + \frac{2}{3} \left(1 - \left(\frac{r_p}{b} \right)^3 \right) \right) \right] \quad (7)$$

Equation 7 cannot be solved explicitly but the value of r_p as a function of ΔT can be found numerically using an iterative process. If $r_p = a$, the result from equation 6 is obtained. After the initiation of plasticity, there exist three distinct regions within the representative volume:

- The particle in a hydrostatic stress state.
- An elastic-plastic region for $a \leq r \leq r_p$ where the effective stress is the yield stress of the matrix.
- An elastic region for $r \geq r_p$ with a stress-free outer boundary.

In the same manner we got ΔT_1 , we can find the temperature change, ΔT_3 , at which the matrix becomes fully plastic, i.e. when $r_p = b$:

$$|(\alpha_p - \alpha_m)\Delta T_3| = \frac{\sigma_y(1-\nu_m)}{E_m} \left[\frac{1}{c} + \frac{2m}{3} \ln(c) \right] \quad (8)$$

The two characteristic temperatures found are valid for a monotonic temperature change assuming an elastic perfectly plastic deformation behaviour of the matrix. The thermal cycling issue is now discussed using the same methodology considering the thermal loading shown in Figure 2. The temperature difference between the starting point and the first peak represents the thermal amplitude, ΔT_a . Both the thermal amplitude and the temperature change are measured from an initially stress-free state. For the next calculations, point A will be considered as the starting point for measuring the temperature changes. Knowing that the material has an elastic response up to ΔT_1 on heating and assuming that the yield stress of the matrix in compression is the same as in tension, it can be shown that the temperature change, ΔT_2 , at which reversed plasticity appear on cooling is:

$$\Delta T_2 = 2\Delta T_1 \quad (9)$$

Therefore, if $\Delta T_a < \Delta T_2$, there will be no accumulation of plastic deformation during thermal cycling. However, if ΔT_a exceeds ΔT_2 , a reversed plastic region of radius r_{rp} will spread outward from the interface. Using the same procedure, the temperature change, ΔT_4 , at which the matrix becomes fully reversed plastic can be calculated by:

$$\Delta T_4 = 2\Delta T_3 \quad (10)$$

For particle reinforced MMCs, the relationships $\Delta T_1 < \Delta T_2$ and $\Delta T_3 < \Delta T_4$ are always true but $\Delta T_2 < \Delta T_3$ may not always be true. In other words, the first thermal load can cause full plasticity with no reversed plasticity at unloading, i.e. no plastic strain accumulation.

The extent of the reversed plasticity in the matrix can be found by computing the radius of reversed plasticity using an approach similar to the one used for finding the radius of plasticity given by Equation (7):

$$|(\alpha_p - \alpha_m)(\Delta T_a - \Delta T)| = \frac{2\sigma_y(1-\nu_m)}{E_m} \left[\left(\frac{r_{rp}}{a} \right)^3 - m \left(2 \ln \left(\frac{r_{rp}}{a} \right) + \frac{2}{3} \left(1 - \left(\frac{r_{rp}}{b} \right)^3 \right) \right) \right] \quad (11)$$

Again, the values for r_p must be obtained numerically. Note that the expression $r_p \geq r_{rp}$ is always true, no matter if $\Delta T_2 \geq \Delta T_3$ or conversely.

5.1.2 Strain during thermal cycling

5.1.2.1 Total macroscopic strain

In order to properly model the CTE of a MMC, it is important to have an expression for the thermal strain of the representative volume of the composite. Expressions of the total macroscopic strain for the different temperature ranges delimited by the four characteristic temperatures can be derived. For the purely elastic response on the first thermal load, i.e., when $|\Delta T| < \Delta T_1$, we have:

$$\varepsilon_T = \left[\alpha_m + \frac{(\alpha_p - \alpha_m)c}{\left(1 - \frac{2m}{3}(1-c)\right)} \right] \Delta T \quad (12)$$

The term in square brackets represents α_{EL} , the elastic coefficient of thermal expansion for the spherical particle composite. For temperature changes above ΔT_1 , plastic deformation of the matrix has to be taken into account. For $\Delta T_1 < |\Delta T| < \Delta T_3$ on the first temperature change, the thermal strain is:

$$\varepsilon_T = \alpha_m \Delta T + c \left(\frac{r_p}{a} \right)^3 \frac{\sigma_y (1 - \nu_m)}{E_m} \Phi \quad \Phi = \text{Sign}\{(\alpha_p - \alpha_m) \Delta T\} \quad (13)$$

where r_p is found from Equation (7) and $\text{Sign}(x)$ is defined as $x / |x|$ for $x \neq 0$ and 0 for $x = 0$. As plastic deformation appears in the matrix, thermal strain becomes a complicated function of temperature. Furthermore, for a fully plastic deformation on the first thermal loading, i.e. for $|\Delta T| > \Delta T_3$, we have:

$$\varepsilon_T = [c\alpha_p + (1-c)\alpha_m] \Delta T - \frac{2}{3} \sigma_y c \ln(c) \left[\frac{(1-2\nu_m)}{E_m} - \frac{(1-2\nu_p)}{E_p} \right] \Phi \quad (14)$$

For repeated thermal loading and unloading in the elastic-plastic region, returning the composite to its initial temperature leads to residual strains in the matrix. Figure 3 shows

the different thermal strain paths that can be imposed by the thermal history of the composite. Figure 3 is not to scale but is intended to display the principal features of the deformation for the thermal history described in Figure 2. The starting point of the composite thermal loading is located at the origin of the initially stress-free state of the composite. During the first stage of heating for $|\Delta T| < \Delta T_1$, the strain is linear. Once ΔT_1 is reached at point A, non-linearity of the strain begins to appear as plastic deformation begins accumulating at the interface. As shown in Figure 3, unloading occurs in the regions of $\Delta T = \Delta T_a$, $\Delta T_1 < \Delta T_a < \Delta T_3$, at point B. Thermal strain on unloading follows the linear elastic solution up to point C which corresponds to $\Delta T = \Delta T_a - \Delta T_2$. At that point, a region of reversed plasticity begins to appear according to equation 11. Complete unloading of the composite leads to residual strain at point D. Repeated thermal loading of the composite will result in the hysteresis loop represented by the region DEBCD in Figure 3. If ΔT_a is such that no reversed plasticity appears during unloading, the following linear relationship represented by line FG holds:

$$\varepsilon_T = (\alpha_m - \alpha_{EL})\Delta T_a + c\left(\frac{r_p}{a}\right)^3 \frac{\sigma(1-\nu_m)}{E_m} \Phi + \alpha_{EL}\Delta T \quad (15)$$

However, if $\Delta T_2 < \Delta T_a < \Delta T_3$, then reversed plastic zones will be generated for each load reversal. Passing a line through point D and B gives an approximate relationship between thermal strain and temperature for the subsequent cycles, which can be written as:

$$\varepsilon_T = \frac{(1-\nu_m)\sigma_y c}{E_m} \Phi \left[\left(\frac{r_p}{a}\right)^3 - 2\left(\frac{r_p}{a}\right)^3 \right] + \left[\alpha_m + \frac{2(1-\nu_m)\sigma_y c}{E_m \Delta T_a} \Phi \left(\frac{r_p}{a}\right)^3 \right] \Delta T \quad (16)$$

5.1.2.2 Effective plastic strain within the representative volume

The plastic strain during the first thermal loading, as a function of the radius of the representative element, can be expressed as:

$$\varepsilon_{eff}^{pl}(r) = \frac{2\sigma_y(1-\nu_m)}{E_m} \left[\left(\frac{r_p}{r}\right)^3 - 1 \right] \quad a \leq r \leq r_p \quad (17)$$

For continued thermal cycling, the plastic strains are affected only in the reversed plastic zone, therefore, the region of the representative element $r > r_p$ will not accumulate plastic deformation. The total accumulation of effective plastic strain after n temperature reversals for $\Delta T_a < \Delta T_3$ becomes:

$$\varepsilon_{eff}^{pl,n}(r) = \frac{2\sigma_y(1-\nu_m)}{E_m} \left\{ \left[\left(\frac{r_p}{r} \right)^3 - 1 \right] + 2(n-1) \left[\left(\frac{r_p}{r} \right)^3 - 1 \right] \right\} \quad a \leq r \leq r_p \quad (18)$$

Note that $n=1$ at B, $n=2$ at D in Figure 2, etc. On the other hand, if $\Delta T_3 < \Delta T_a < \Delta T_4$, the effective plastic strain relationship becomes:

$$\varepsilon_{eff}^{pl,n}(r) = \frac{2\sigma_y(1-\nu_m)}{E_m} \left\{ \left[\left(\frac{b}{r} \right)^3 \left(1 + \frac{cE_m|\alpha_p - \alpha_m|(|\Delta T_a| - \Delta T_3)}{\sigma_y(1-\nu_m)} \right) - 1 \right] + \right. \\ \left. 2(n-1) \left[\left(\frac{r_p}{r} \right)^3 - 1 \right] \right\} \quad (19)$$

In equations 18 and 19, the temperature dependence of the effective plastic strain is determined by equations 7 and 11, which define the radius of plasticity and reversed plasticity, respectively. The first term of the previous equation represents the plastic strain during the first temperature change and the second term represents the following $(n-1)$ temperature reversals. Figure 4 illustrates the results of equations 18 and 19. The maximum plastic strain occurs at the interface. It is interesting to note that the rate of plastic strain accumulation is highest during the first cycle. Therefore, if the plastic strain rate of the first cycle is used for predictions of thermal fatigue life, it is likely to lead to conservative estimates.

5.1.2.3 Interfacial decohesion

The author [3] considered that decohesion of the particle can be a result of two possible mechanisms:

1. The tensile stress across the interface reaches the strength of the interface, i.e. brittle decohesion occurs.
2. The accumulated effective plastic strain at the interface reaches the ductility of the material, i.e. ductile decohesion.

According to Olsson *et al*, if brittle decohesion occurs, it will be during the initial loading. Let σ_d be the decohesion strength of the interface and ΔT_d , the temperature change corresponding to σ_d . According to equations 18 and 19, if $\sigma_d < 2\sigma_y(1-c)/3$, decohesion will occur without any plastic deformation of the matrix (equality means $\Delta T_d = \Delta T_1$). Another limiting case is when $\sigma_d > 2\sigma_y \ln(1/c)/3$ where brittle decohesion will never occur (equality means $\Delta T_d = \Delta T_3$). In this case, the plasticity at the interface will contribute in reducing the stress concentrations around the reinforcement particles during thermal loading.

Let us now consider decohesion due to the accumulation of plastic strain at the interface of the representative volume. Let D be the ductility of the interface between the matrix and the particle. Knowing that the maximum plastic deformation occurs at the interface, we can easily compute the number of cycles to failure of the interface, N_f , by using equations 17 and 18:

$$N_f = \frac{E_m D}{4\sigma_y(1-\nu_m)} \frac{1}{\left[\left(\frac{r_p}{a} \right)^3 - 1 \right]} \quad (20)$$

The simplifications of $N_f \gg 1$ and temperature-independent properties reduce the complexity of the relation. If linear strain hardening, β , is accounted for, the equation can be rewritten as:

$$N_f = \frac{\ln \left[1 - \frac{H}{\sigma_y} \frac{D}{\left[\left(\frac{r_p}{a} \right)^3 - 1 \right]} \right]}{\ln \left[\frac{1-\beta}{1+\beta} \right]} \quad (21)$$

Indeed, for a composite with a strain-hardening matrix, the four characteristic temperatures described previously will no longer be constant and will depend on the accumulated plastic strains. For a given plastic strain distribution, these temperatures can be obtained using an approach similar to the one described previously but will not be shown here. Obviously, the first characteristic temperature, ΔT_1 , will not be affected by

strain hardening. However, the other characteristic temperatures will increase with the degree of strain-hardening in the matrix.

5.1.3 Conclusion

The previous analysis only takes into account the reinforcement volume fraction. Consequently, the elastoplastic model is not valid for interconnected reinforcement phases as well as for reinforcements not having a spherical geometry. However, if a spherical representative volume can be identified in the composite material, the elastoplastic analysis can be used as a good approximation of the expansion behavior. Indeed, the authors showed, by comparing the results of this analysis to those of a finite element model, that the influence of sharp corners and matrix hardening on the effective thermal expansion coefficient is very small [3, 4].

Four characteristic temperatures are found defining the different stress states within the ductile matrix. These temperature amplitudes determine the resistivity of the composite to undergo repeated thermal loading without decohesion. The model also estimates the plastic strain accumulation at the interface and throughout the matrix. It was found that the rate and amount of plastic strain accumulation is more important during the first cycle of the thermal history.

Finally, the analysis also estimates the number of cycles to failure of the interface which, most often, is caused by the accumulation of the plastic deformation at the interface reaching its maximum ductility [5].

5.2 Numerical analysis of the effect of thermal cycling

The effect of thermal cycling on the coefficient of thermal expansion is an area of research which historically has not received a great deal of attention. The variation of the CTE with temperature for particle reinforced MMCs is well documented but conversely, it is much more difficult to find accurate data concerning variation of mechanical properties with thermal cycling. Several authors [6-13] have noted changes in the microstructure of whisker and fiber reinforced MMCs under changing temperature conditions. Indeed, the dimensional change and the CTE of particle reinforced MMCs can be significantly affected by repeated temperature changes (temperature cycles).

Accurate models are thus needed in order to predict the changes in strain that can appear in a composite material under thermal cycling. Olsson *et al* [3] developed an analytical tool, that was previously explained in this chapter, for modeling the elastoplastic behavior of ceramic particle reinforced MMCs under thermal cycling. This analytical model is very unique and is one of the only existing theories for predicting plastic deformation under thermal cycling. This section presents the results of this analysis for five specific metal matrix composites: A359/SiC/10-20-40p, A360/SiC/30p and 6061/Al₂O₃/40p. Four SiC composites were selected in order to determine the effect of reinforcement volume fraction on CTE and the Al₂O₃ reinforced composite was chosen to observe the effect of the reinforcement type on the expansion behavior according to the model.

The first sub-section concerns computer modeling of the elastoplastic analysis of thermal cycling; a program was written to compute and plot the equations describing the CTE behavior of the composites. The second sub-section deals with the analysis of the results obtained with the model. Finally, the last sub-section concerns certain aspects of the model that might be improved.

5.2.1 Mathematic tool

Maple V, Waterloo Maple Advancing Mathematics, is a powerful mathematical software package that has the ability to manage symbolic information. Maple V allows one to work with complete algebraic representations of mathematical expressions and gives exact solutions to systems of equations. The software includes a complete and flexible procedural programming language that lets the user define his or her own specialized library. The creation of a Maple sheet (mathematical program that is executed within Maple V) was essential for computing the results from the elastoplastic analytical model of thermal cycling. The complete listing of the program is given in Appendix 2.

5.2.2 Instructions for using the Maple V sheet

The primary objective for creating a mathematical sheet was to facilitate the acquisition of the theoretical data discussed earlier in this thesis (section 5.1). The Maple sheet was built as simply as possible and is intended to be used with the Maple V release 4 software or a newer release. The sheet is composed of 11 sections which are listed below:

1. Material selection
2. Material properties
3. Stress state model
4. Characteristic temperatures
5. Characteristic volume fraction
6. Temperature history
7. Strain on first thermal loading
8. Plastic strain accumulation during cycling
9. Coefficient of thermal expansion
10. Number of cycles to decohesion
11. Numerical results

5.2.3 Description of the Maple sheet sections

5.2.3.1 Material selection

This is the section where material selection is done. The information provided by the user is essential for the program to run correctly. It lets the user choose the matrix and particle materials independently as well as the reinforcement volume fraction and the average particle dimension. The available matrix materials are:

- Aluminum alloy 6061
- Aluminum alloy A359

The particle materials are:

- Silicon carbide, SiC
- Alumina, Al₂O₃

The diameter of the sphere composed by the matrix material is automatically obtained from the reinforcement volume fraction and the average particle diameter, which have previously been defined. The physical and mechanical properties of the composite constituents are read from two files called matdata.dat and pardata.dat for matrix and particle materials respectively and can easily be modified to change or add new materials.

For greater accuracy, the property mean values should be calculated over the studied temperature interval. The format of the matrix material file is given as follows:

Elastic modulus (Pa)
Poisson's ratio
CTE (ppm/°C)
Yield strength (Pa)
Maximum ductility
Linear strain hardening parameter H

and the format of the particle material file is:

Elastic modulus (Pa)
Poisson's ratio
CTE (ppm/°C)

Each column represents a different material. Thus, to add a new material to the list, simply add a new column separated by a blank space. To verify the validity of the entered properties, the user can refer to the section called Material Properties. For a more accurate representation of the actual expansion behaviour of the composites, the temperature-dependent property best fit equations can be entered as a function of temperature in the Material Properties section, thus ignoring the values provided in the files described above. The temperature-dependence of the coefficient of thermal expansion, elastic, bulk and shear moduli, was previously described in Chapter 4.

5.2.3.2 Material properties

In this section, the properties of the selected materials in the Material Selection section are listed. The material properties are read from two files located in the current file directory.

5.2.3.3 Stress state model

This section contains all the necessary equations (Equations 1 to 5) for calculating the pressure and stresses in the particle and the matrix as described in the previous pages.

5.2.3.4 Characteristic temperatures

All the equations needed for determining the characteristic temperatures (Equations 6 to 11) can be found in this segment of the Maple sheet. The determination of the four characteristic temperatures is essential because they are needed to calculate the strain versus temperature relationships.

5.2.3.5 Characteristic volume fraction

The characteristic concentration represents the reinforcement volume fraction at which full plasticity of the matrix is achieved on the first cycle with no reversed plasticity at unloading, i.e., $\Delta T_2 = \Delta T_3$. This characteristic concentration is computed in this section and is given as a reference point but is not used anywhere else in the calculations.

5.2.3.6 Temperature history

This section specifies the thermal history of the material in question. Two parameters have to be specified: the thermal amplitude and the number of complete cycles. The thermal amplitude, ΔT_a , is taken from a stress-free state at room temperature and has a positive value for heating on the first half cycle and negative for cooling. The number of complete cycles, n , represents the number of times the composite will be thermally loaded and unloaded.

5.2.3.7 Strain on first thermal loading

The strain and plastic deformation radii during the first thermal load, i.e. first half cycle, given by equations 12 through 19 are computed in this section.

5.2.3.8 Plastic strain accumulation during thermal cycling

In this section are performed the calculations needed to derive the effective plastic strain as a function of temperature and position within the representative volume. In addition, the data for plotting strain versus temperature and strain versus position curves is

calculated and assembled. It is important to note that the strain versus temperature curves were obtained in three steps:

1. Elastic behavior using equation 12.
2. Elastic-plastic behavior during first thermal load using equation 13.
3. Elastic-plastic behavior during thermal cycling using the approximate relationship given by equation 16.

The resulting graphs are shown in the Numerical results section.

5.2.3.9 Coefficient of thermal expansion

The numerical values of the CTE are taken from the calculated slopes of the strain versus temperature curves, i.e. $\Delta\epsilon / \Delta T$. The elastic CTE is obtained using equation 12 and acts as a reference point for calculating the damage parameter which is defined as the CTE change over the elastic CTE. Note that the damage parameter can be negative or positive but it is expected to be positive for particle reinforced metal-matrix composites. The changing CTE with thermal cycling is obtained using the approximate relationship given by Equation 16.

5.2.3.10 Number of cycles to decohesion

In this section, the number of cycles to decohesion of the interface between the matrix and the particle is calculated. As mentioned earlier, decohesion occurs when plastic deformation at the interface reaches its maximum ductility, D . When strain hardening effects are not accounted for, the number of cycles to decohesion is given by the equation 20. On the other hand, for a matrix having a certain degree of linear strain hardening, the number of cycles to decohesion is given by equation 21. Both values are always listed in the numerical results section in order to allow the user the opportunity to see the influence of matrix strain hardening.

5.2.3.11 Numerical results

All the results of the analysis are presented in this section. This analysis is well documented and explained in the program, and hence there is no real need to duplicate it

here. Numerical results are frequently accompanied by their equations as well as a short description of the variables implied in the computation. A typical result sheet is shown in Appendix 3 and the results are summarized in section 5.2.5.

5.2.4 Restrictions concerning the Maple V sheet

Although the numerical results were verified using the data provided in the paper from Olsson *et al* [3], it is possible that some computational problems might occur during execution of the mathematical sheet. For instance, for temperature amplitudes below ΔT_1 and above ΔT_4 , the analysis is not reliable. In addition, for reinforcement volume fractions exceeding 50%, the user should refer to the paper written by Olsson *et al* [3] to ensure that the model remains valid as described in the previous pages. Indeed, if reinforcement concentration is important, particle interactions become significant and reinforcements may then be in contact which is not considered in the analysis.

Even though the equations can sometimes give a radius of reversed plasticity exceeding that of the representative volume, one should be aware that this can never happen in the composite materials and such a result does not have any physical meaning. In such cases, full reversed plasticity was achieved and the radius of reversed plasticity should be taken as the radius of the representative volume element. Full reversed plasticity generally occurs when composite materials are subjected to very large temperature changes (often exceeding the melting point of the matrix) and this situation never occurred in this study.

5.2.5 Analysis of the results

The behavior of five different composite materials was analyzed using the model. All composites were subjected to identical thermal histories: 20 complete cycles with a thermal amplitude of 325 degrees representing heating and cooling between 25°C and 350°C. The composites were also assumed to be in a stress-free state at room temperature. The reinforcing particles were modeled by concentric spheres having an inner diameter of 10 μm , which represents the reinforcement, while the matrix was represented by a hollow sphere around the particle having an external diameter varying from 13.6 to 21.5 μm depending on reinforcement volume fraction. The linear strain

hardening parameter was chosen as 10% of the yield stress of the matrix, i.e. 24.1 MPa and 27.6 MPa for A359 and 6061 aluminum alloys respectively. The interface was assumed to be mechanically bonded, i.e. no brittle decohesion can occur, and its maximum ductility was arbitrary taken as 20%. This value, although close to the maximum ductility of the matrix, is independent of the matrix constituent. It represents the plastic deformation that the interface can withstand without damage and is closely related to the interaction between the reinforcement phase and the matrix. It is important to note that this value will only affect the number of cycles to decohesion of the interface. The number of cycles to decohesion is directly proportional to the maximum ductility of the interface (equation 20), and therefore, it is easy to interpolate for different values of the interface ductility. A summary of the results from the analysis is given in Table 1.

The four characteristic temperatures are given in the first four rows of the table. By looking at the results for A359/SiC/40p and 6061/Al₂O₃/40p composites, it is clear that the Al₂O₃ reinforced composite has a better resistance to temperature changes than the SiC composite. Indeed, the alumina composite shows a 6% increase in the characteristic temperatures as compared to the SiC composite. For a given thermal amplitude of 325°C, we can see that both composites undergo full plasticity of the matrix during the first loading. Reversed plasticity is also present in both composites under thermal cycling but represents only 22% and 17% of the matrix volume for SiC and Al₂O₃ composites respectively. As a result, for the same thermal history, the SiC composite has a larger change in the CTE than the Al₂O₃ composite that can be seen by the values of the damage parameter of both composites which are 1.04 and 0.33% respectively. In other words, the CTE of the SiC composite goes from 14.70 ppm/°C in the elastic region to 14.85 ppm/°C due to plastic strain accumulation in the matrix and the Al₂O₃ composite CTE changes from 16.00 to 16.05 ppm/°C. It should be noted that these changes are very small and it might be difficult to observe them experimentally. However these values represent average CTEs over the temperature interval (325 degrees in our study) and significantly different results might arise for the lower and upper regions of the temperature interval. Although equation 16 gives the approximate strain versus temperature curve during thermal cycling, a more complete form of this equation would result in a better model of the instantaneous CTE change with both the temperature and the number of cycles.

However, one conclusion that can be drawn from the results is that the most significant change in the CTE will occur during the first half temperature cycle. This is because greater plastic deformation accumulation occurs at the particle-matrix interface during the first thermal load as compared to the smaller plastic deformation during subsequent cycles.

Now looking at the results for A359/SiC/10-20-40p and A360/SiC/30p, it is interesting to note the effect of the reinforcement volume fraction. Volume fraction has a minor effect on ΔT_1 and ΔT_2 but can considerably affect ΔT_3 and ΔT_4 . Indeed, ΔT_1 and ΔT_2 increased by 8% while ΔT_3 and ΔT_4 decreased by a significant 76% with increasing reinforcement volume fraction. The four composites do not experience the same plastic deformation during the first load; the 40% SiC composite undergoes full plasticity while the 10% SiC composite undergoes a slight plastic deformation representing 19% of the volume of the matrix. None of the four composites experience full reversed plasticity during cycling. However, they all undergo different degrees of reversed plastic deformation; from 5% of the matrix volume for the 10% SiC composite to 22% for the 40% SiC composite. Following the same trend, the damage parameter increases with the reinforcement volume fraction from 0.29 to 1.04%. Although the number of cycles to decohesion of the interface is based on an arbitrary maximum ductility, this value increases with volume fraction by more than 22%.

5.2.6 Conclusions

- An increase of the average CTE over a given temperature interval during thermal cycling is predicted by the model. The CTE change becomes more important as the reinforcement volume fraction increases in the matrix. However, instantaneous CTE changes during thermal cycling cannot be accurately predicted by the model due to the use of an approximate relationship between strain and temperature.
- The number of cycles to decohesion of the interface increases with increasing reinforcement volume fraction. However, this value is based on an arbitrary maximum ductility of the interface which is often difficult to determine.
- All the SiC reinforced composites studied in this analysis have a ΔT_4 , which corresponds to the temperature change for reversed plasticity to spread entirely in the

matrix, greater than or close to the melting point of the matrix which means that full reversed plasticity can never be obtained experimentally. Moreover, for the same reason, ΔT_3 for the 10 and 20% SiC reinforced composites can also never be reached meaning that the matrix will never completely plastically deform during the first loading.

- Subjecting the composites to identical thermal histories leads to an increasing damage parameter with reinforcement volume fraction.
- Reinforcement volume fraction does not significantly affect ΔT_1 and ΔT_2 but substantially affects ΔT_3 and ΔT_4 . In addition, the model predicts increasing ΔT_1 and ΔT_2 (9% increase) and decreasing ΔT_3 and ΔT_4 (76% decrease) with increasing volume fraction from 10% to 40%.
- The CTE of SiC reinforced composite materials is more affected (approximately 3 times more) by repeated temperature changes than the CTE of Al_2O_3 reinforced composites.

5.2.7 Aspects to improve modeling the elastoplastic behavior of MMCs under thermal cycling

Although this model has yet to be verified experimentally, it gives a good representation of the elastoplastic behavior of particle reinforced MMCs under thermal cycling. However, some aspects of the analysis could be improved to increase the reliability and accuracy of the model.

- The strain during thermal cycling is given by an approximate relationship which consists of a straight line giving the strain as a function of temperature for a given number of cycles. Calculating the slope of this curve gives the average CTE during thermal cycling for the temperature interval corresponding to ΔT_a . A relationship that would give the instantaneous variation of the CTE as a function of the number of cycles would be very useful.
- Analytical equations for temperature-dependent mechanical and physical properties were not derived in the analysis. The temperature-dependent constituent properties were experimentally determined and included in the model but a more general

representation would be to include theoretical variations of the properties as functions of temperature.

- The number of cycles to decohesion of the interface between the particles and the matrix is based on an arbitrary maximum ductility which is relatively difficult to estimate. A simpler approach to the problem would be to determine the ductility of the interface as a function of the ductility of the matrix, the fabrication process and the reactivity of the constituents. Another way of approaching the problem would be to experimentally determine the maximum ductility of the interface and try to find an empirical relationship describing its variation as a function of the nature of the constituents. As well, the variation of the ductility of the interface with temperature should also be taken into account.
- The heating and cooling rates are not accounted for in this analysis. The only mention of their effect is that the heating and cooling rates must be slow enough to avoid thermal shock and fast enough to avoid diffusion. Although the experimental heating and cooling rates of 10°C/min were representative of the actual heating and cooling rates for space components, it might be important to determine if these rates induce additional stresses other than those already determined in the analysis.
- Dwelling periods during thermal cycling are not accounted for in the model. Although dwelling periods at low temperature might not change the stress state within the composite, at high temperature, they might cause the stresses to relax and influence the elastoplastic expansion behavior predicted by the analysis.

References

- 1 L. Boniface, S. L. Ogin and P. A. Smith, The change in thermal expansion coefficient as a damage parameter during thermal cycling of crossply laminates, *Composite Materials: Fatigue and Fracture*, vol. 4, p. 139-160 (1993)
- 2 T. Chandra and Y. Dake, High-temperature deformation behavior and microstructural investigation of silicon carbide particulate reinforced aluminum composite, *International conference on composite materials*, p. 21F1-21F12 (1991)
- 3 M. Olsson, A. E. Giannakopoulos and S. Suresh, Elastoplastic Analysis of Thermal cycling: Ceramic Particles in a Metallic Matrix, *Journal of the Mechanics and Physics of Solids*, vol. 43, no. 10, p. 1639-1671 (1995)
- 4 Y. -I. Shen, A. Needleman and S. Suresh, Coefficients of thermal expansion of metal-matrix composites for electronic packaging, *Metallurgical and Materials Transactions A*, vol. 25A, p. 839-850 (1994)
- 5 S. Suresh, Fatigue of materials, Cambridge University Press, Cambridge, p. 586 (1991)
- 6 G. S. Daehn and G. Gonzalez-Doncel, Deformation of whisker-reinforced metal-matrix composites under changing temperature conditions, *Metallurgical Transactions A*, vol. 20A, no. 11, p. 2355-2368 (1989)
- 7 W. G. Patterson and M. Taya, Thermal cycling damage of SiC whisker/2124 aluminum, *International Conference on Composite Materials*, p. 53-66 (1985)
- 8 M. L. Dunn and M. Taya, Modeling of Thermal Cycling creep Damage of Short Fiber Metal Matrix Composites, *Materials Science and Engineering A*, vol. 176A, no. 1-2, p. 349-355 (1994)
- 9 L. Boniface, S. L. Ogin and P. A. Smith, The change in thermal expansion coefficient as a damage parameter during thermal cycling of crossply laminates, *Composite Materials: Fatigue and Fracture*, p. 139-160 (1993)
- 10 M. Taya, W. D. Armstrong and M. Dunn, Analytical study on dimensional changes in thermally cycled metal matrix composites, *Materials Science and Engineering*, vol. A143, p. 143-154 (1991)

- 11 C. M. Warwick and T. W. Clyne, The micromechanisms of strain ratchetting during thermal cycling of fibrous MMCs, *Fundamental relationships between microstructures and mechanical properties of metal matrix composites*, Proceedings of the symposium, p. 209-223 (1989)
- 12 G. S. Daehn, H. Zhang, Y. -C Chen and R. H. Wagoner, Approaches to modeling the plastic deformation of metal matrix composites under thermal cycling conditions, *Modeling the deformation of crystalline solids presented at the annual meeting of the minerals, Metals and materials society conference*, p.665-678 (1991)
- 13 H. Zhang, G. S. Daehn and R. H. Wagoner, Simulation of the plastic response of whisker reinforced metal matrix composites under thermal cycling, *Scripta metallurgica et Materialia*, vol, 25, no. 10, p. 2285-2290 (1991)

MMCs → Parameters ↓	A359/SiC/ 10p	A359/SiC/ 20p	A360/SiC/ 30p	A359/SiC/ 40p	6061/Al ₂ O ₃ / 40p
ΔT_1 (°C)	98	101	104	107	129
ΔT_2 (°C)	196	202	208	214	258
ΔT_3 (°C)	1178	575	380	284	344
ΔT_4 (°C)	2355	1150	759	568	389
N_f w/o strain hard. effects	34	37	39	42	75
N_f with strain hard. effects	35	38	40	43	78
Damage parameter (%)	0.29	0.56	0.81	1.04	0.33
Elastic CTE (ppm/°C)	21.1	18.9	16.7	14.7	16.0
r_p ($m \cdot 10^{-3}$)	0.72	0.72	0.71	full plasticity	full plasticity
r_{rp} ($m \cdot 10^{-3}$)	0.59	0.58	0.58	0.57	0.54

Table 1. Summary of the most important results obtained with the elastoplastic model.

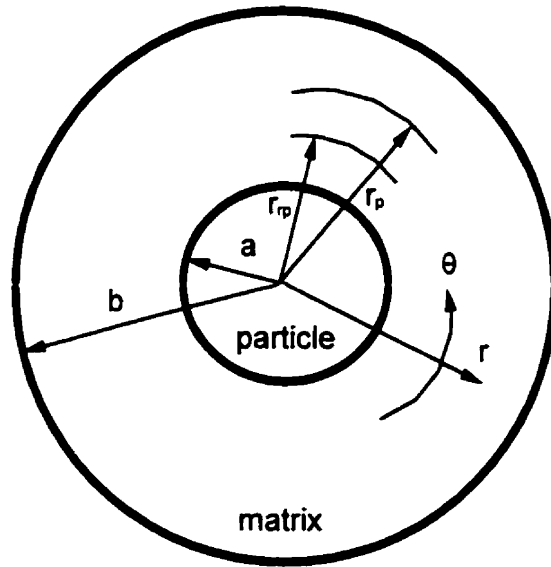


Figure 1. Geometry of the representative volume element of the composite.

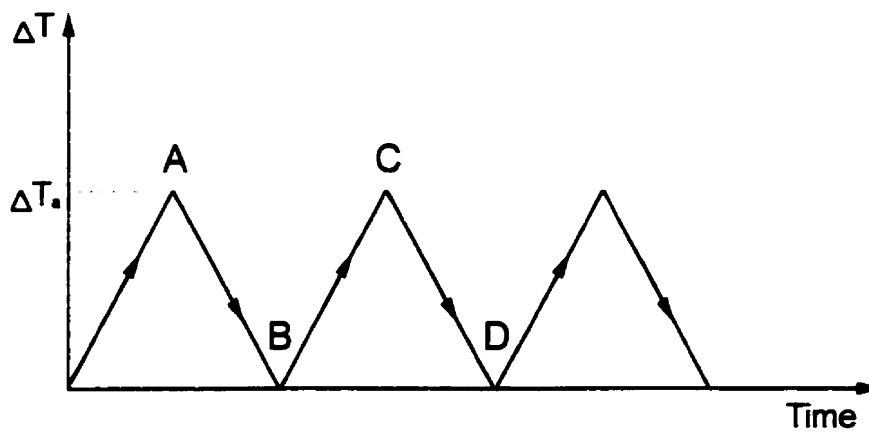


Figure 2. Typical thermal history.

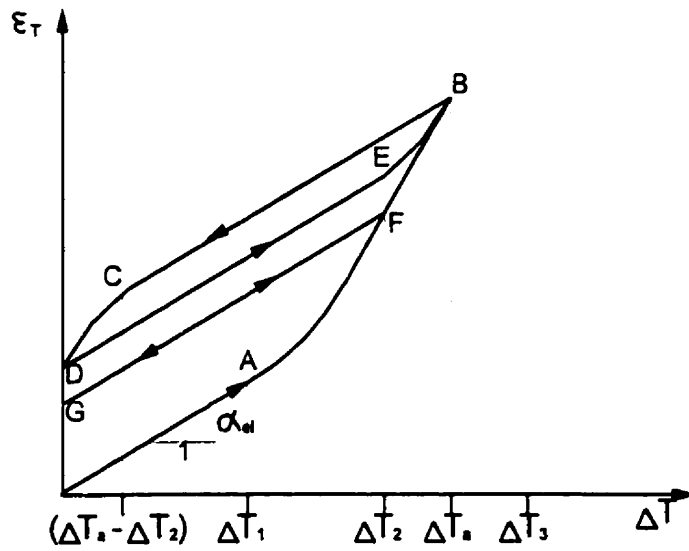


Figure 3. Composite thermal strains as a function of the temperature change.

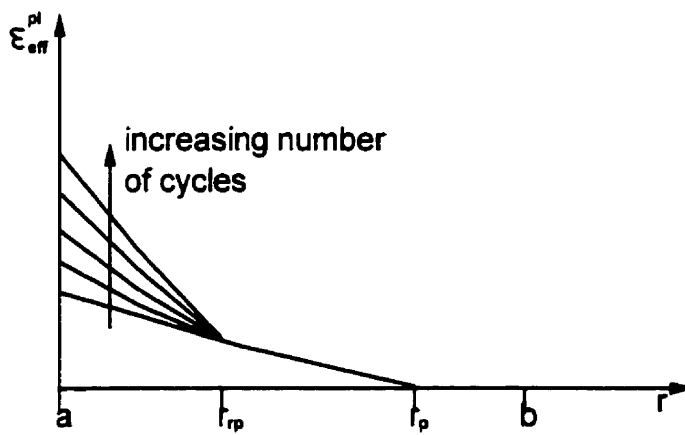


Figure 4. Plastic strain accumulation throughout the matrix with the number of temperature reversals.

Introduction to chapter 6

In the first paper (Chapter 4), the effect of both reinforcement volume fraction and temperature on the expansion behavior of Al/SiC composite materials was determined. In this second paper, the thermal cycling issue is investigated. It has been demonstrated that thermal cycling can induce large stresses within the composite, which often lead to plastic strain accumulation at the particle-matrix interface. This plastic deformation frequently results in a CTE change with the number of temperature reversals within the composite due to changes of the microstructure at the particle-matrix interface. In the following paper, the expansion behaviour of five Duralcan particle reinforced composite materials (A359/SiC/10, 20 and 40p, A360/SiC/30p and 6061/Al₂O₃/40p) will be discussed. Knowing that particle interactions are likely to be more important for high reinforcement volume fractions, the composites containing 40% v/o of ceramic particles were first studied. Significant CTE changes were observed in both composites after 20 complete temperature reversals between 25 and 350°C. However, the 40% Al₂O₃ composite showed a greater CTE change than the 40% SiC composite. Composites containing between 10 and 30% SiC particles were subjected to the same thermal history. The 30% composite showed little CTE increase while the 10 and 20% composites showed no apparent CTE variation. Theoretical predictions of the CTE changes considerably underestimate the actual CTE increase of the composites. However, the expansion behavior can be best described using four characteristic temperatures which clearly mark transitions in plastic response during thermal cycling.

Chapter 6. Effect of Thermal Cycling on Thermal Expansion Behavior of Isotropic Duralcan Metal-Matrix Composites

S. LEMIEUX^{a,b}, S. ELOMARI^a, J. A. NEMES^b, M. D. SKIBO^c, S. SURESH^d and M. CHIBANI^e

^aSpacecraft Engineering, Canadian Space Agency, 6767 route de l'Aéroport, Saint-Hubert, J3Y 8Y9, Canada, Fax: 514-926-4695

^bDepartment of Mechanical Engineering, McGill University, Montreal, Canada

^cMC-21 Incorporated, San Diego, CA 92121, USA

^dDepartment of Materials Science and Engineering and Department of Mechanical Engineering, Massachusetts Institute of Technology, Cambridge, MA 02139, USA

^e2CI Technologies Inc., 2041 Sunland Drive, Orlean, Ontario, Canada, K4A 3K8

(To be submitted to the Journal of Composite Science and Technology)

Abstract

The thermal expansion response of five Duralcan particle reinforced composite materials under thermal cycling was investigated. This set of MMCs comprises four Al-Si alloy matrix composites containing SiC reinforcements ranging from 10 to 40% and a 6061 aluminum matrix composite having 40% Al₂O₃ reinforcement particles in volume. The effect of thermal cycling was determined by measuring the composite coefficients of thermal expansion between 25 and 350°C with a high-precision Thermomechanical Analyzer (TMA). The experimental results were compared with the theoretical predictions of an elastoplastic analysis of thermal cycling and two elastic CTE models. Al-Si and 6061 aluminum matrix composites containing 40% volume fraction SiC and Al₂O₃ particles respectively showed a significant change of the CTE after 20 complete temperature reversals. For reinforcement volume fractions below 40%, thermal cycling had little or no influence on the CTE. We interpret these results as being the effect of the

interaction between the particles and the matrix causing plastic strain accumulation near and at the interface which is more prevalent for higher reinforcement volume fractions. Furthermore, the SiC composites experimental mean CTE values were found to lie between the Kerner and Schapery models predictions and the Al₂O₃ composite CTE values between the Kerner and Rule of Mixtures models for thermal cycling between 25-350°C.

Keywords: Metal-Matrix Composite, Ceramic Particle, Thermal Cycling, Thermal Expansion.

6.1 INTRODUCTION

Particle reinforced metal-matrix composites are now seen as good alternatives to conventional materials due to their isotropic properties, low density, high specific strength, high specific modulus, good fatigue response, low thermal expansion and high abrasion and wear resistance [1]. Over the last few years, MMCs have received considerations from the aerospace [2,3], automotive, and electronic [4,5] industries. In addition, MMCs are being successfully used as diecast components such as pistons [6,7], connecting rods, engine blocks, and brake drums. Their high thermal stability, allowed by their low coefficient of thermal expansion as well as their high thermal conductivity, makes these composite materials very attractive for changing temperature environments. However, in several applications and secondary processing, these composites are subjected to severe and cycled thermal loading. Examples of MMC structures are disc frames and engine blocks for automotive, radiator panels for spacecraft, such as the space shuttle and hubble telescope [8], advanced cryogenic tanks, and electronic packaging structures [9]. Examples of secondary manufacturing processes include hot rolling, forging, diffusion bonding and welding of advanced MMC materials. Under severe thermal cycling, composite hardware will sometimes undergo large internal plastic deformation. Therefore, it is necessary to know the effect of thermal cycling on the mechanical and thermal properties of MMCs, such as CTE, to properly design a structure from conception to structural application.

Modeling the thermal cycling effect on the expansion behavior of particle reinforced metal matrix composites has not often been considered by material scientists. However, increasing CTEs and strain ratcheting behaviors have often been experimentally observed in fiber and whisker reinforced composites [10-13]. The accumulation of plastic strain at the interface is often accompanied by the development of interfacial damage such as porosity, cracking and debonding. It is believed that the thermal expansion mismatch between the reinforcement phase and matrix is the cause of the plastic strain accumulation. For large temperature changes, large internal stresses often exceeding the yield stress of the matrix induce local plastic flow within the matrix near or at the interface.

The purpose of our investigation is, on one hand, to observe the effect of the reinforcement volume fraction on the expansion behavior of SiC/Al composites under thermal cycling. This is achieved by examining the expansion response of four Al/SiC composites containing between 10 and 40% volume fraction of particles. On the other hand, the effect of the nature of the phases in the composite under thermal cycling is investigated by comparing the expansion behavior of 6061/Al₂O₃/40p and A359/SiC/40p composite materials. The coefficients of thermal expansion of the MMCs were measured between 25 and 350°C by a high-precision Thermomechanical Analyzer (TMA) and compared to the predictions of an elastoplastic model as well as with the standard Kerner and Schapery models.

6.2 EXPERIMENTAL PROCEDURES

6.2.1 Composite materials

Five different composite materials were tested: A359/SiC/10p, 20p and 40p, A360/SiC/30p and 6061/Al₂O₃/40p. The chemical composition of the aluminum alloy matrices used in this study are given in Table 1 and the important mechanical and physical properties of the reinforcement particles and the aluminum alloys are shown in Table 2 [14]. The composite materials were received in the form of ingots from Duralcan Canada and MC-21 Incorporated, San Diego, California. The MMC materials were produced by the Duralcan[™] (Trademark, Alcan Aluminum Ltd, San Diego, U.S.A.)

molten metal mixing process [11,12]. The composites were permanent mold cast and then heat treated to the T4 condition (solutionized at 550°C for 1 hour then quenched in water followed by room temperature aging for a minimum of 2 days). Figures 1 and 2 show SEM micrographs of polished sections of the SiC/Al and Al₂O₃/Al composites, respectively. All composites exhibit a uniform particle distribution which seems to be responsible for the isotropic nature of mechanical and physical properties. At low volume fraction, the reinforcing particles are very effective in nucleating new grains within the aluminum matrix, and stabilizing the resulting fine grain size. The aspect ratio distribution histogram of SiC particulate for all four material systems accumulated during image analysis is shown in Figure 3. The SiC particulate is irregular in shape having an average aspect ratio of 1.4-2.2 with the rare occurrence of larger shards of much greater convexity. The average SiC particle size in the 10 v/o composite is 9.3 micrometers (600 grit), and at 20, 30 and 40 v/o, 13 micrometers (500 grit). The Al₂O₃ particle size is about 20 μm in the 6061/Al₂O₃/40p composite. The aluminum alloy matrix has a fine uniform grain size of the order of the interparticle spacing (5-40 μm depending on volume fraction). Energy dispersive X-ray analysis in the SEM revealed no unusual second phases other than those associated with the aluminum matrices and the typical trace elements. No evidence of chemical reaction between the matrix and the SiC and Al₂O₃ particles was noted. No particle cracking is apparent and essentially no porosity is present in the composite material.

6.2.2 TMA Test

The average dimension of the specimens for TMA testing was 10 x 5 x 1.5 mm. Coupons were cut from the cast materials using a diamond saw and were polished using 1 μm diamond paste. More than 4 samples of each composite were tested to verify reproducibility of the experimental data. CTE measurements were performed from 25°C to 350°C at 10°C/min using a commercial thermomechanical analysis equipment (model TMA 2940, Dupont, USA). The samples were air-cooled and no CTE measurements were made during cooling. The total number of complete temperature reversals was 20. The thicknesses of the samples were measured with increased sensitivity (0.01 μm) using the standard expansion probe. The TMA apparatus measures linear or volumetric

changes in the dimensions of a specimen as a function of time, temperature and force. The dimensional change of the sample is measured with a LVDT (linear variable differential transformer) that has an output which is proportional to the linear displacement of the core caused by changes in sample dimensions. The samples were placed in a chamber where atmosphere quality can be controlled. An inert gas, helium, was blown into the chamber at a rate of 40 ml/min. A thermocouple adjacent to the sample assures accurate measurements of the sample temperature. The final output is a plot of PLC (percent linear change) versus time, temperature or force. TMA standard data analysis software was used to evaluate instantaneous and average CTEs of the composites tested. In this study, average CTEs were determined at intervals of 50°C based on the calculated slope fit between two selected temperatures using PLC versus temperature curves.

6.3 RESULTS

6.3.1 Al/SiC composites

The experimental curves of the dimensional change with temperature for the first ($N = 1$) and last ($N = 20$) temperature changes of the four Al/SiC composites are shown in Figure 4. All SiC composites exhibit similar non-linear expansion behaviors over the 25-350°C interval. However, it is evident that the dimensional change decreases as the reinforcement volume fraction increases for any given temperature. The coefficients of thermal expansion of A359/SiC/10 and 20p composites are essentially unchanged after 20 repeated temperature cycles. However, while the A360/SiC/30p composite visibly shows little increase of its dimensional change under cycling, the A359/SiC/40p composite demonstrates a significant change of its dimensional change with temperature. This behavior is clearly established by looking at the CTE with the number of cycle curves shown in Figure 5. As expected from Figure 4, the A359/SiC/10 and 20p composite CTEs are relatively insensitive to the number of complete temperature reversals and stay constant between the 1st and 20th cycles. In addition, depending on the temperature interval, the A360/SiC/30p composite shows little or no increase of the CTE with cycling. On the average, this composite shows no significant increase of the CTE.

For the A359/SiC/40p composite, however, a significant increase in the CTE for all temperature intervals between 25 and 350°C is observed. Indeed, CTE measurements showed a 9.5% and 3.8% increase for the 25-50°C and 300-350°C temperature intervals respectively.

6.3.2 Al/Al₂O₃ composite

The experimental results of the dimensional change with temperature of the 6061/Al₂O₃/40p composite for the 1st and 20th cycles are shown in Figure 6. This composite shows an expansion behavior similar to its homologous A359/SiC/40p composite material. Again, the dimensional change with temperature curves are non-linear. As expected from the expansion behavior of the 40% SiC reinforced composite, the Al₂O₃ composite CTE is largely affected by thermal cycling. This behavior is even more evident by looking at the change of the CTE with the number of cycles in Figure 7. The experimental plot clearly indicates an increasing CTE with the number of cycles. Numerical CTE values give a 9% and 5.5% increase at low and high temperature respectively which is somewhat similar to the observations made on the A359/SiC/40p composite.

6.4 DISCUSSION

The CTE of metal-matrix composites is generally difficult to predict as it is influenced by several factors such as reinforcement volume fraction, fabrication process and nature of the composite constituents. It is even more difficult to predict the effect of thermal cycling with variable thermal amplitudes and number of cycles. In this study, the fabrication process variable parameter was eliminated since all the composites studied were processed with the Duralcan[™] molten metal mixing process. It will therefore be easier to explain the expansion behavior during thermal cycling with respect to the reinforcement volume fraction and the nature of the composite constituents.

6.4.1 CTE theoretical models

6.4.1.1 Kerner's model

The Kerner model [4,15,16] for predicting particle reinforced composite CTEs is often referred to as an upper bound since it is close to the rule of mixtures. The model assumes that the reinforcement is spherical and wetted by a uniform layer of matrix; thus the CTE of the composite is stated to be identical with that of a volume element composed of a spherical reinforcement particle surrounded by a shell of matrix, both phases having the volume fractions present in the composite. This model gives the composite CTE as:

$$\alpha_c = \bar{\alpha} + V_p (1 - V_p) (\alpha_p - \alpha_m) \frac{K_p - K_m}{(1 - V_p) K_m + V_p K_p + (3K_p K_m / 4G_m)} \quad (1)$$

Where the rule of mixtures is given by $\bar{\alpha} = (1 - V_p)\alpha_m + V_p\alpha_p$. K and G are the bulk and shear moduli, V is the volume fraction, α is the coefficient of thermal expansion and the subscripts c, p and m denote the composite, particle and matrix respectively. The bulk modulus is calculated using the standard relationship :

$$K = \frac{E}{3(3 - E/G)} \quad (2)$$

6.4.1.2 Schapery's model

Among the several formulae that have been suggested for the calculation of the thermal expansion coefficient of composite materials taking into account the stress interaction between components is that of Schapery who has derived the effective CTE of isotropic composites, by employing extremum principles of thermoelasticity [15]. The CTE value can be written as:

$$\alpha_c = \alpha_p + (\alpha_m - \alpha_p) \frac{(1/K_c) - (1/K_p)}{(1/K_m) - (1/K_p)} \quad (3)$$

Note that α_c depends on the volume fraction and phase geometry only through their effect on bulk modulus. This equation states an exact relation between the composite CTE and the bulk modulus. Since only upper and lower bounds of K_c can be determined

in a given case (Hashin's bounds [17]), this expression provides only bounds on CTE. The lower bound on bulk modulus is:

$$K_C = K_m + \frac{V_p}{\frac{1}{K_p - K_m} + \frac{V_m}{K_m + \frac{4}{3}G_m}} \quad (4)$$

The upper bound is obtained by interchanging indices m and p everywhere. The lower bound on K_c yields the upper bound on the composite CTE shown in Equation 3 (and vice-versa). Note that this upper bound of the composite CTE was shown by Schapery to coincide with the CTE value determined using the Kerner's model. This is not surprising since Hashin's lower bound for bulk modulus is stated to be an exact result for an elastic composite, in which the reinforcement is a sphere coated with a uniform layer of the matrix.

6.4.1.3 Elastoplastic theoretical analysis of thermal cycling

Most of the models for predicting CTEs under thermal cycling only apply for fully elastic composite constituents. In rare cases, attempts at modeling plastic deformation caused by thermal loads in the composites were made [18]. However it has often been demonstrated that large internal stresses often exceeding the yield stress of the matrix are generated due to the CTE mismatch between the composite constituents which lead to local plastic flow at the interface within the matrix. Olsson et al [19] developed a theoretical analysis of the elastoplastic deformation due to thermal cycling of a ceramic particle reinforced metal matrix composite. No comparison of the analysis results with experimental data has been reported in the literature and one of the goals of this study is to determine the validity of the analysis. In this model, the composite microstructure is represented by two concentric spheres having the composite constituents volume fractions. The particle and matrix, represented by the inner and outer sphere respectively, are shown in Figure 8. The interface is assumed to be mechanically bonded, i.e. free of any cracks or porosity. Heating and cooling rates are not considered in the analysis but are assumed to be slow enough to avoid thermal shock and fast enough to avoid creep

and diffusion. Finally, it is assumed that there is a uniform and constant temperature distribution throughout the representative volume element.

Considering that the particle is in a hydrostatic stress state and assuming continuity of traction and tangential deformation at the particle-matrix interface, the particle-matrix interface pressure as a function of the temperature change can be readily obtained:

$$p = \frac{\frac{2E_m}{3(1-\nu_m)}(\alpha_p - \alpha_m)(1-c)\Delta T}{\left[1 - \frac{2m}{3}(1-c)\right]} \quad c = \left(\frac{a}{b}\right)^3 \quad (5)$$

where p , is the interface pressure, ν , the Poisson's ratio, c , the reinforcement volume fraction and E , the elastic modulus. The elastic mismatch parameter, m , is given by [19]:

$$m = \frac{E_m}{(1-\nu_m)} \left[\frac{(1-2\nu_m)}{E_m} - \frac{(1-2\nu_p)}{E_p} \right] \quad (6)$$

The stresses in the matrix as a function of the position within the representative volume element can be written as:

$$\sigma_{rm} = \frac{cp}{(1-c)} \left[1 - \left(\frac{b}{r}\right)^3 \right] \quad \sigma_{\theta m} = \frac{cp}{(1-c)} \left[1 + \frac{1}{2} \left(\frac{b}{r}\right)^3 \right] \quad (7)$$

where r represents the radial position within the matrix constituent. In addition, the effective stress in the matrix can be written as:

$$\sigma_{em} = |\sigma_{\theta m} - \sigma_{rm}| = \frac{3}{2} \frac{c}{(1-c)} p \left(\frac{b}{r}\right)^3 \quad (8)$$

which is maximum at $r = a$. During the first temperature change, plastic deformation will occur when σ_{em} will exceed the matrix yield stress at the interface. Therefore, the expression of the temperature change at initiation of plastic deformation, ΔT_1 , is:

$$\left| (\alpha_p - \alpha_m) \Delta T_1 \right| = \frac{\sigma_y (1-\nu_m)}{E_m} \left[1 - \frac{2m}{3}(1-c) \right] \quad (9)$$

where σ_y is the yield stress of the matrix. A more general form of the previous equation gives the radius of plasticity, r_p , as a function of the first temperature change:

$$|(\alpha_p - \alpha_m)\Delta T| = \frac{\sigma_y(1-\nu_m)}{E_m} \left[\left(\frac{r_p}{a}\right)^3 - m \left(2 \ln\left(\frac{r_p}{a}\right) + \frac{2}{3} \left(1 - \left(\frac{r_p}{b}\right)^3 \right) \right) \right] \quad (10)$$

Letting $r_p = b$, the temperature change at which full plasticity of the matrix is reached during the first temperature change, ΔT_3 , can be readily found:

$$|(\alpha_p - \alpha_m)\Delta T_3| = \frac{\sigma_y(1-\nu_m)}{E_m} \left[\frac{1}{c} + \frac{2m}{3} \ln(c) \right] \quad (11)$$

For thermal cycling, we consider a typical temperature history as shown in Figure 9. The above equations are valid for the first temperature change only, i.e. from an initially stress free state at the origin to the first temperature peak at point A. Point A will then be taken as the starting point for thermal unloading. Knowing that the material response is incrementally linear elastic for the initial unloading and that the yield stress in tension and compression are equal, it can be found that:

$$\Delta T_2 = 2\Delta T_1 \quad (12)$$

is the lowest temperature change resulting in the onset of reversed plasticity at the interface in the matrix material. Similarly, ΔT_4 is the temperature change for full reversed plasticity to appear:

$$\Delta T_4 = 2\Delta T_3 \quad (13)$$

Table 3 provides the characteristic temperatures of the five composite materials tested in this study. Average material properties between 25 and 350°C from Table 4 were used for the numerical analysis. Analytical expressions now need to be determined for the overall thermal strain and coefficient of expansion. From the above analysis, equations for the total macroscopic thermal straining can be found depending on the severity of the first temperature change:

$$\varepsilon_T = \left[\alpha_m + \frac{(\alpha_p - \alpha_m)c}{\left(1 - \frac{2m}{3}(1-c)\right)} \right] \Delta T \quad \text{for } \Delta T < \Delta T_1 \quad (14)$$

$$\varepsilon_T = \alpha_m \Delta T + c \left(\frac{r_p}{a} \right)^3 \frac{\sigma_y (1 - \nu_m)}{E_m} \Phi, \quad \Phi = \text{Sign}\{(\alpha_p - \alpha_m) \Delta T\}$$

for $\Delta T_1 < \Delta T < \Delta T_3$ (15)

$$\varepsilon_T = [c \alpha_p + (1 - c) \alpha_m] \Delta T - \frac{2}{3} \sigma_y c \ln(c) \left[\frac{(1 - 2\nu_m)}{E_m} - \frac{(1 - 2\nu_p)}{E_p} \right] \Phi$$

for $\Delta T > \Delta T_3$ (16)

For repeated temperature changes, the thermal strains and the temperature are no longer proportional. Since the exact solution is complicated, it is more convenient to use an approximate relationship that gives the average thermal strain as a function of the thermal history. A sketch of the thermal strains as a function of the temperature change is shown in Figure 10. During the first thermal load, the strain with temperature curves follow the path described by equations 14, 15 and 16 up to point B. Unloading is taken from that point for which $\Delta T = \Delta T_a$. At first, the strain follows the linear elastic solution given by equation 14. However, as $\Delta T = \Delta T_a - \Delta T_2$ is reached, a reversed plastic zone starts to develop. Further decrease in the temperature will lead to residual strains in the composite at point D. Repeated temperature changes will result in the hysteresis loop DEBCD shown in Figure 10. Passing a line through point B and D will result in the following approximate relationship between the strain and the temperature during thermal cycling:

$$\varepsilon_T = \frac{(1 - \nu_m) \sigma_y c}{E_m} \Phi \left[\left(\frac{r_p}{a} \right)^3 - 2 \left(\frac{r_p}{a} \right)^3 \right] + \left[\alpha_m + \frac{2(1 - \nu_m) \sigma_y c}{E_m \Delta T_a} \Phi \left(\frac{r_p}{a} \right)^3 \right] \Delta T \quad (17)$$

6.4.2 Comparison between the experimental and theoretical results

6.4.2.1 Al/SiC composites

Comparison of the mean CTE over the 25-350°C temperature interval with the upper and lower elastic CTE bounds for the 10-40% volume fraction range is shown in Figure 11. The composite mean CTE values follow very closely the Schapery model predictions during the first thermal load. Variations of the experimental CTE with temperature and

reinforcement volume fraction was previously discussed in greater details elsewhere [20]. For the 20th temperature reversal, the experimental mean CTE values follow the Schapery model at low volume fraction but deviate towards the Kerner model as the reinforcement volume fraction increases. However, a very interesting observation is that the CTE values during thermal cycling are bounded by these two theoretical elastic CTE bounds. The normalized mean CTE values as a function of reinforcement volume fraction are presented in Figure 12. Experimental values were obtained by calculating the percent change in the mean CTE during thermal cycling after 20 complete temperature reversals compared to the initial mean CTE value for the first cycle:

$$\text{Normalized mean CTE} = \frac{(\bar{\alpha}_{20} - \bar{\alpha}_1)}{\bar{\alpha}_1} \times 100 \quad (18)$$

Theoretical normalized mean CTE values were obtained by computing the percent change of the CTE determined by the slope of the strain with temperature curves during thermal cycling given by Equation 17, as compared to the purely elastic CTE values found using Equation 14. In Figure 12, the observed 4.5% experimental CTE increase in the 40% SiC composite significantly exceeds the 1.04% elastoplastic model predictions. As theoretical calculations lead to a linear increase of the normalized CTE with volume fraction, experimental values show an exponential relationship which explains this large difference in the CTE change at high SiC concentrations. As reinforcement volume fraction increases in the composite material, interactions between the particles become more prominent. Possibly, this interaction has the effect of increasing the stresses at the particle-matrix interface which results in additional plastic deformation of the matrix. This additional plasticity is believed to be responsible for the large CTE change at high reinforcement volume fraction. Since the model predictions are based on an assumed dispersive morphology of the microstructure, it is not valid for high reinforcement volume fractions or interconnected phases which can appear in the 40 v/o composite materials. For low SiC concentrations, i.e. between 10 and 25% volume fraction, experimental normalized mean CTE values are below the theoretical predictions. No apparent CTE change was actually observed in the 10 and 20% SiC composite materials after 20 complete temperature reversals. As the major CTE changes for the 40% SiC and Al₂O₃ composites were observed during the first stage of thermal cycling, it would be

doubtful that the 10 and 20% SiC composites undergo any CTE change under additional temperature reversals.

The comparison of the experimental mean CTE values with the elastoplastic model predictions is shown in Figure 13 for reinforcement volume fractions between 10 and 40%. The elastoplastic model considerably overestimates the mean CTE values of the composite materials. It is interesting to note that the predictions of the elastoplastic model lie close to the Kerner model predictions, which also overestimates CTE values as shown in Figure 11. However, for both experimental and theoretical results, the increase in the CTE under thermal cycling is more important at high reinforcement volume fractions. These observations suggest the following explanation for the expansion behavior of these composites. It is known that upon initial cool down from its fabrication or heat treatment temperature, internal stresses form in the composite materials which, although complex on a microscopic level, are, on the average, tensile in the matrix and compressive in the reinforcement since the latter has a lower CTE. Upon heating of the composite, this compressive stress is reduced but the reinforcement phase stays, overall, in compression and is capable of transmitting stress from one particle to another across particle contact points. We therefore expect the composite to behave roughly as a material in which both, the ceramic and the metal phases are connected. As the composite is heated further, thermal stresses induced after initial cool-down of the composite are canceled by differential expansion of the matrix and reinforcement, the average reinforcement stress reaching zero to become tensile, on average, upon further heating. At that point, interparticle spacing increases and stresses cannot be transmitted from one particle to another. In other words, the ceramic particles behave like isolated particles in a continuous metal phase, causing a rise in the CTE of the composite. This feature is predicted by Shen *et al* [5], in their finite-element analyses of composite CTEs. Using models for a continuous ductile phase composite, analogous to the high temperature region of the particle composite strain curves, and for a continuous brittle phase, analogous to the low temperature region, Shen *et al* incorporated the effects of the thermal residual stresses on the derived CTE values. It was found that thermal residual stresses increased the CTE of the composite upon thermal cycling. Therefore, an

increase in CTE is to be expected when the composite is reinforced with high volume fraction of ceramic particles.

Although CTE predictions using equations 14 to 17 appear to be inaccurate, the observed experimental CTE changes might possibly be related to the four characteristic temperatures defined by Equations 9 through 13. Based on these four theoretical characteristic temperatures, a thermal amplitude of 325 degrees representing thermal cycling from 25 to 350°C, would induce plastic deformation representing between 19 and 86% of the matrix volume from 10 to 30% reinforcement volume fractions during the first thermal load. More importantly, it would induce full plastic deformation of the matrix in the 40% SiC composite. Thermal cycling with the same thermal amplitude would cause increased reversed plasticity with increasing reinforcement volume fraction. Since the characteristic temperature, ΔT_2 , given in Table 3, is approximately the same as the thermal amplitude, reversed plasticity extent is limited to 22% of the matrix volume in the 40% SiC composite material. This expansion behavior, described by the extent of the plastic deformations within the matrix, is similar to the observed expansion behavior, i.e. no CTE change in the 10 and 20% SiC composites due to large ΔT_1 and ΔT_2 values, a slight CTE change in the 30% SiC composite and a significant 9 and 5.5% CTE increase in the 40% SiC composite at low and high temperatures respectively due to full plasticity of the matrix during the first cycle.

Globally, according to the experimental observations on the SiC particle reinforced A359/A360 aluminum matrix composites, the elastoplastic model gives conservative estimates of the mean CTE change for reinforcement volume fractions below 25% but strongly underestimates CTE changes above that value for thermal cycling between 25 and 350°C for 20 cycles. In addition, in contrast to the elastoplastic model, which does not accurately predict mean CTE values, the Schapery model seems to be in good agreement with the experimental data.

6.4.2.2 *Al/Al₂O₃ composite*

Measured mean CTE values during thermal cycling over the 25-350°C temperature interval compared to theoretical predictions for the 6061/Al₂O₃/40p and A359/SiC/40p composite materials are given in Table 5. As expected from the CTE of the individual

constituents, the 6061/Al₂O₃/40p composite possesses a higher mean CTE than the A359/SiC/40p composite. However, unlike the SiC composite, which has a mean CTE value during the first cycle which lying close to the Schapery model prediction, the Al₂O₃ composite mean CTE value is closer to the Kerner model prediction. Nevertheless, both composites show a significant increase in their CTE under thermal cycling. Indeed, the Al₂O₃ composite experimental mean CTE value lies just above the Rule of Mixtures prediction after 20 complete temperature reversals. As was the case for the SiC reinforced composites, the elastoplastic model mean CTE predictions are inaccurate. However, in this case, contrary to the SiC composite mean CTE predictions that were higher than the experimental data, the elastoplastic analysis underestimates the mean CTE of the Al₂O₃ composite. In addition, the model also considerably underestimates the normalized mean CTE as shown in Table 6. Indeed, a significant 8.8% increase in the 6061/Al₂O₃/40p composite mean CTE was observed after 20 complete temperature reversals compared to 0.44% predicted by the analysis. Surprisingly, the experimental normalized mean CTE of the Al₂O₃ composite is higher than that of the SiC composite as the theoretical predictions give the opposite. By looking at the CTE mismatch ratios, being 3.6 and 5.2 for Al₂O₃ and SiC composites respectively, more severe plastic deformation and CTE change would be expected to appear in the SiC composite. Therefore, according to the experimental results, the CTE mismatch between the particles and the matrix is not the only parameter affecting the expansion behavior of the composites. It is believed that the ductility and bonding of the particle-matrix interface may also have a direct influence on the thermal response under thermal cycling.

6.5 CONCLUSIONS

The reinforcement volume fraction and nature of the composite constituents appear to have a direct influence on the expansion behavior of Duralcan MMCs subjected to repeated thermal loads. The reinforcement volume fraction effect was investigated using four Duralcan MMCs containing between 10 and 40% SiC particles. The composites mean CTE values follow the Schapery elastic CTE predictions during the first cycle but deviate towards the Kerner model at high SiC concentration during thermal cycling due to plastic strain accumulation at the particle-matrix interface. Nevertheless, the

composite experimental CTE values were bounded by the Schapery and Kerner theoretical models during the thermal cycling duration. Since the elastoplastic analysis of thermal cycling does not take into account particle interactions, it considerably underestimates CTE changes at high SiC concentrations. However, the experimental expansion behavior of these composites was best described using the four characteristic temperatures derived in the elastoplastic analysis.

In addition, the effect of the nature of the constituents was investigated by comparing the expansion behaviors of 6061/Al₂O₃/40p and A359/SiC/40p composites. The Al₂O₃ composite showed a higher normalized mean CTE than the SiC composite. Moreover, its mean experimental CTE values seem to lie between the Kerner and the Rule of Mixtures models. The CTE mismatch between the composite constituents does not appear to be the only factor influencing the expansion behavior. Ductility and bonding of the particle-matrix interface may also play an important role.

According to the experimental results of this study, Duralcan composites containing reinforcement volume fractions less than 30% exhibit a high CTE stability under thermal cycling between 25 and 350°C. However, for higher reinforcement concentrations, a significant CTE change was observed, which should be accounted for in design with such materials. Despite, experimental CTE values still lie within the standard theoretical bounds.

References

1. S. Elomari, R. Boukhili, M. D. Skibo and J. Masounave, Dynamic mechanical analysis of prestrained Al₂O₃/Al metal-matrix composites, *Journal of Materials Science*, **30** (1995) pp. 3037-44.
2. D. J. Lloyd, Particle reinforced aluminum and magnesium matrix composites, *International Materials Reviews*, **39** (1994) pp. 1-23.
3. S. Elomari, H. Richards, C. San Marchi, M. D. Skibo and G. Vukovich, Advanced composite materials in space structures, In *Proc. of the 37th Israel Annual Conference on Aerospace Sciences*, ed. Kenes Tel Aviv, Omanuth Press Ltd., Haifa (1997) pp. 287-97.
4. S. Elomari, R. Boukhili and D. J. Lloyd, Thermal expansion studies of prestrained Al₂O₃/Al metal matrix composite, *Acta Materialia*, **44** (1996) pp. 1873-82.
5. Y. -L Shen, A. Needleman and S. Suresh, Coefficients of Thermal Expansion of Metal-Matrix Composites for Electronic Packaging, *Metals and Materials Transactions A*, **25A** (1994) pp. 839-50.
6. H. E. Deve and C. McCullough, Continuous fiber reinforced aluminum composites : a new generation, *Journal of Metals*, **47** (1995) pp. 33-7.
7. T. Donomoto, K. Funatani, N. Miura and N. Miyaki, Ceramic fiber reinforced piston for high performance diesel engines, *SAE Technical Paper 830252*, Detroit, MI (1983)
8. M. Miller and A. Robertson, Boron/Aluminum and Borsic/Aluminum Metal-Matrix Composite Analysis, Design, Application and Fabrication, In *Hybrid and Select Metal Matrix Composites : A State-of-the-Art Review*, ed. W. J. Renton. American Institute of Aeronautics and Astronautics, New York, 1977, pp. 99-153.
9. M. K. Premkumar, W. H. Hunt and R. R. Sawtell, Aluminum Composite Materials for Multichip Modules, *Journal of Metals*, **44** (1992) pp. 24-8.
10. G. S. Daehn and G. Gonzalez-Doncel, Deformation of whisker-reinforced metal-matrix composites under changing temperature conditions, *Metallurgical Transactions A*, **20A** (1989) pp. 2355-68.

11. M. L. Dunn and M. Taya, Modeling of Thermal Cycling Creep Damage of Short Fiber Metal Matrix Composites, *Materials Science and Engineering A*, **176A** (1994) p. 349-55.
12. L. Boniface, S. L. Ogin and P. A. Smith, The change in thermal expansion coefficient as a damage parameter during thermal cycling of crossply laminates, *Composite Materials : Fatigue and Fracture* (1993) pp. 139-60.
13. M. Taya, W. D. Armstrong and M. Dunn, Analytical study on dimensional changes in thermally cycled metal matrix composites, *Materials Science and Engineering*, **143A** (1991) pp. 143-54.
14. P. K. Mallick, *Fiber-reinforced composites : Materials, manufacturing and design*, ed. Dekker, New York (1993)
15. R. A. Schapery, Thermal Expansion Coefficients of Composite Materials Based on Energy Principles, *Journal of Composite Materials*, **2** (1968) pp. 380-405.
16. E. H. Kerner, The Elastic and Thermo-Elastic Properties of Composite Media, *Proceedings Physics Society*, **69B** (1956) pp. 808-13
17. Z. Hashin and S. Shtrikman, A Variational Approach to the Theory of the Elastic Behavior of Multiphase Materials, *Journal of the Mechanics and Physics of Solids*, **11** (1963) pp. 127-40
18. T. A. Hahn and R. W. Armstrong, Thermal Expansion Properties of 6061 Al alloy Reinforced with SiC Particles or Short Fibers, *International Journal of Thermophysics*, **9** (1988) pp. 861-71.
19. M. Olsson, A. E. Giannakopoulos and S. Suresh, Elastoplastic Analysis of Thermal Cycling: Ceramic Particles in a Metallic Matrix, *Journal of mechanics and physics of solids*, **43** (1995) pp. 1639-71.
20. S. Lemieux, S. Elomari, J. A. Nemes and M. D. Skibo, Thermal Expansion of Isotropic Duralcan Metal-Matrix Composites, *Journal of Materials Science* (1997) Submitted.

	Si	Fe	Cu	Mn	Mg	Ti	Zn	Cr	All Other elements	Al
6061	0.40-0.80	0.70 max.	0.15-0.40	0.15 max.	0.80-1.20	0.15 max.	0.25 max.	0.04-0.35	0.05 max. 0.15 total	Rem
A359	8.50-9.50	0.20 max.	0.20 max.	0.45-0.65	0.45-0.65	0.20 max.	-	-	0.03 max. 0.10 total	Rem
A360	9.50-10.5	0.80-1.20	0.20 max.	0.50-0.80	0.50-0.70	0.20 max.	0.03 max.	-	0.03 max. 0.10 total	Rem

Table 1. Chemical composition of aluminum alloy matrices.

	Density (g/cm ³)	Ultimate tensile stress (Mpa)	Ultimate strain (%)	Thermal conductivity (W/mK)
Ceramics				
SiC	3.0-3.2	3000-4000	0.84	80-200
Al ₂ O ₃	3.4-4.0	1000-2000	0.4	30-50
Aluminum alloys				
6061	2.70	276	17	180
A359	2.685	207-262	3-5	138
A360	2.63	170	3.5	113

Table 2. Properties of reinforcement particles and aluminum matrices [14].

Characteristic Temperatures (°C)	ΔT_1	ΔT_2	ΔT_3	ΔT_4
A359/SiC/10p	98	196	1178	2355
A359/SiC/20p	101	202	575	1150
A360/SiC/30p	104	208	380	759
A359/SiC/40p	107	214	284	568
6061/Al ₂ O ₃ /40p	129	258	344	389

Table 3. Characteristic temperatures of five composite materials.

T°C	6061				A359				A360			
	E (GPa)	G (GPa)	K (GPa)	CTE ($\mu^\circ\text{C}$)	E (GPa)	G (GPa)	K (GPa)	CTE ($\mu^\circ\text{C}$)	E (GPa)	G (GPa)	K (GPa)	CTE ($\mu^\circ\text{C}$)
25	71.3	26.5	77.8	22.3	70.4	26.9	68.4	21.1	71.4	27.2	69.4	21.2
50	71.5	26.5	78.4	22.3	70.3	26.8	68.3	21.8	71.2	26.9	69.1	21.6
100	71.3	26.5	78.4	22.7	69.4	25.5	68.1	22.3	70.2	26.2	68.6	22.4
150	71.3	26.4	78.4	23.9	68.7	25.2	67.5	22.7	69.4	25.4	68.2	22.9
200	70.5	26.1	76.5	24.5	68.2	24.7	66.3	23.6	68.4	25.1	67.2	23.2
250	69.3	25.8	74.3	24.8	66.4	23.9	63.2	24.5	67.1	24.2	63.8	24.3
300	67.4	25.4	71.1	25.1	65.9	23.1	59.2	25.3	66.4	23.6	60.4	25.4
350	65.4	24.5	66.3	25.4	65.3	22.1	61.6	26.2	65.9	22.9	60.7	25.9

Table 4. Temperature-dependence of the properties of the matrix constituents.

Mean CTE values (ppm/°C)	Exp. N=1	Exp. N=20	Elastoplastic model, N=1	Elastoplastic model N=20	Kerner model	Schapery model	Rule of mixtures
6061/Al ₂ O ₃ /40p	16.20	17.63	15.0	15.07	16.24	13.88	17.20
A359/SiC/40p	12.88	13.45	14.7	14.85	14.88	12.53	15.95

Table 5. Comparison between experimental and theoretical mean CTE values.

(%)	Normalized experimental mean CTE	Normalized theoretical mean CTE
6061/Al ₂ O ₃ /40p	8.83	0.44
A359/SiC/40p	4.5	1.04

Table 6. Comparison between experimental and theoretical normalized mean CTE values.



Figure 2. Microstructure of Duralcan 6061/Al₂O₃/40p metal-matrix composite

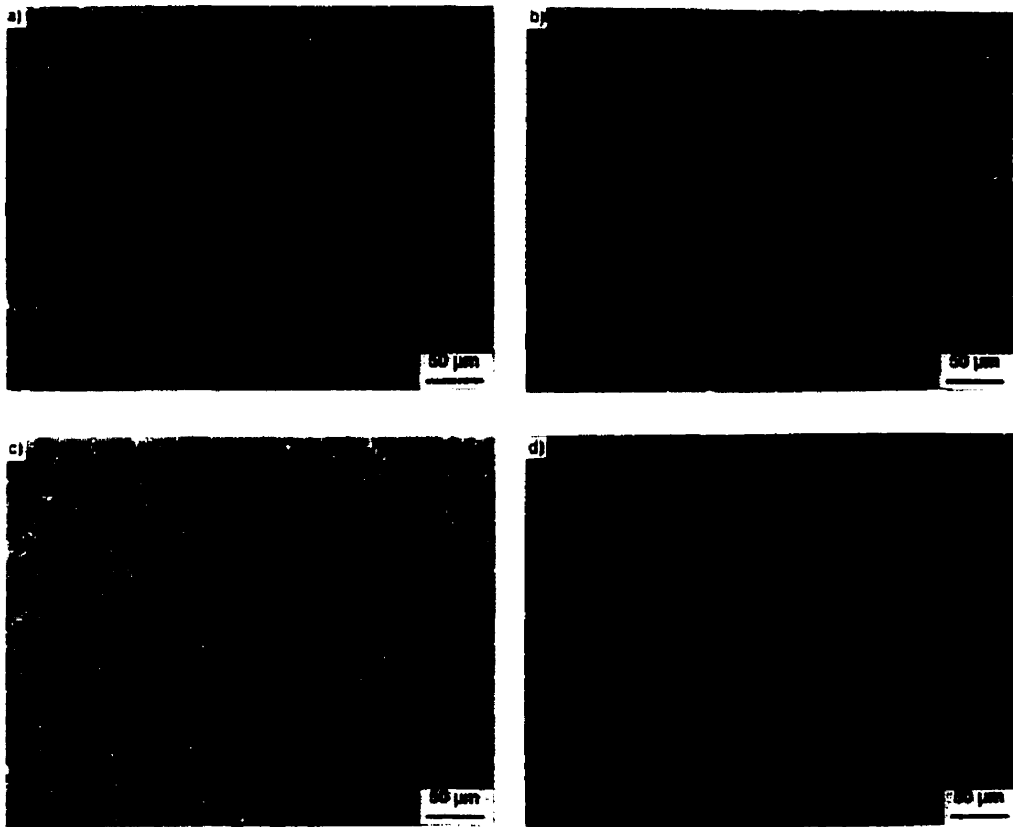


Figure 1. Microstructures of Duralcan SiC/Al metal-matrix composites: (a) 10% SiC, (b) 20% SiC, (c) 30% SiC, and (d) 40% SiC

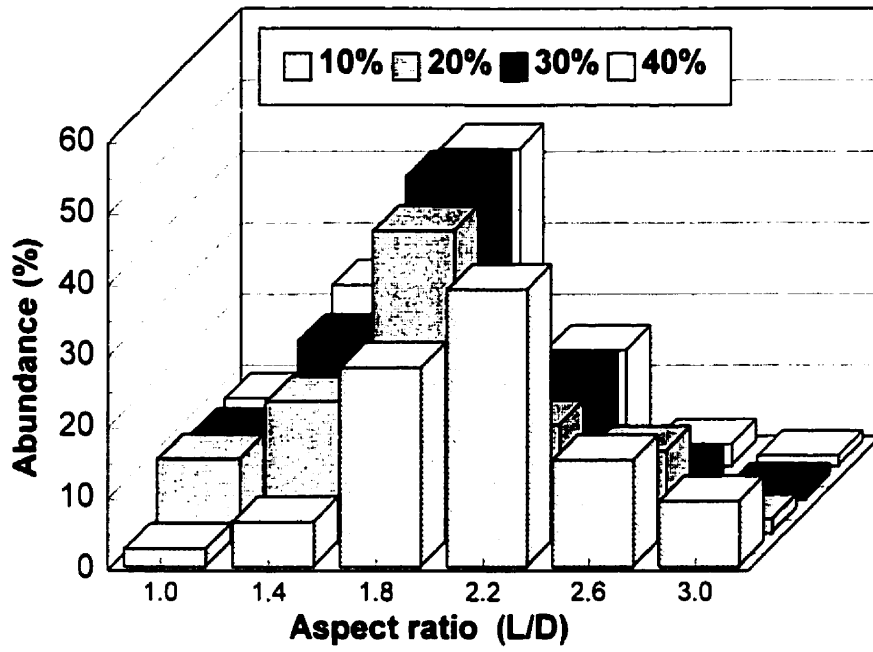


Figure 3. Aspect ratio histograms of SiC particles for Duralcan composites.

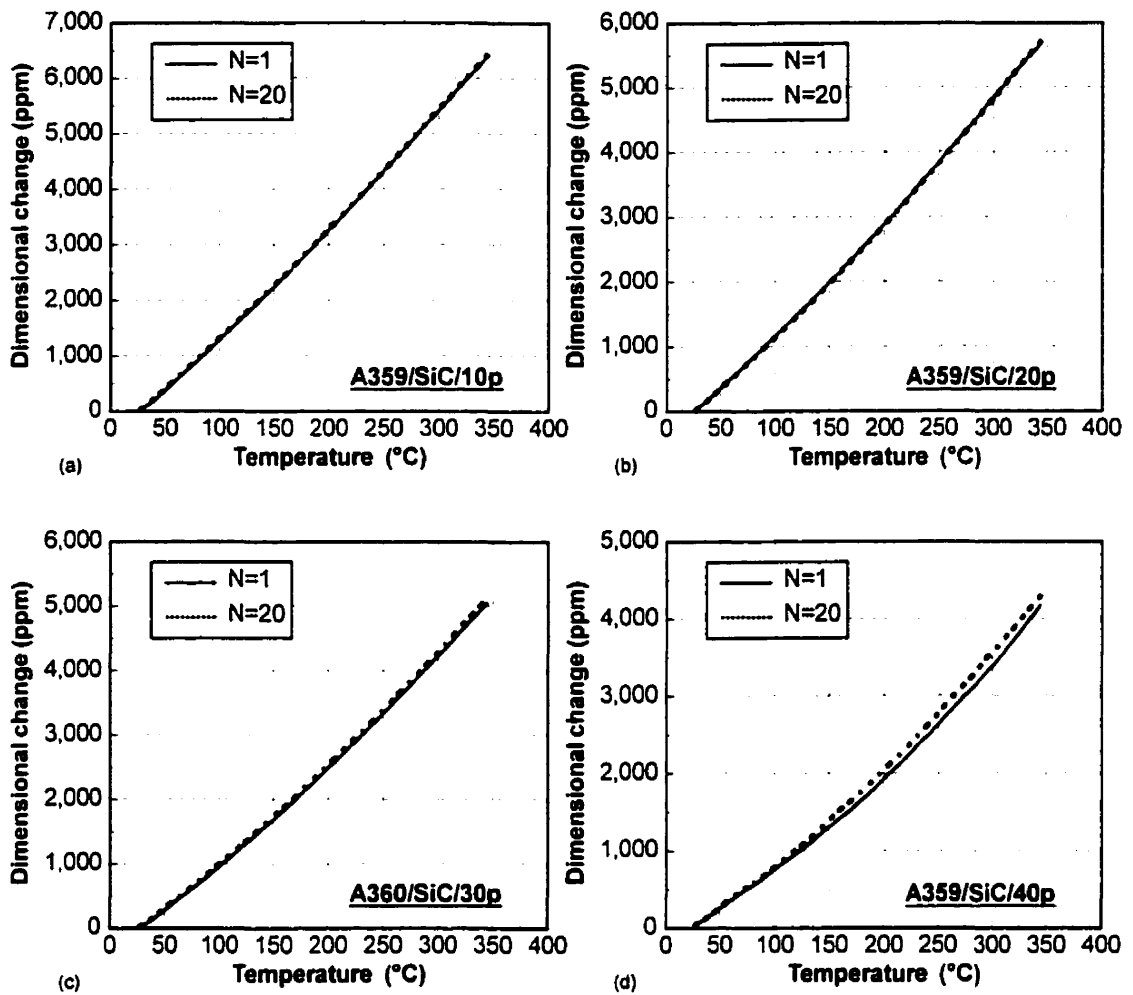


Figure 4. Comparison of the initial and last dimensional change with temperature curves for 20 complete temperature reversals between 25 and 350°C for SiC/Al Duralcan composites: (a) 10% SiC, (b) 20% SiC, (c) 30% SiC, and (d) 40% SiC.

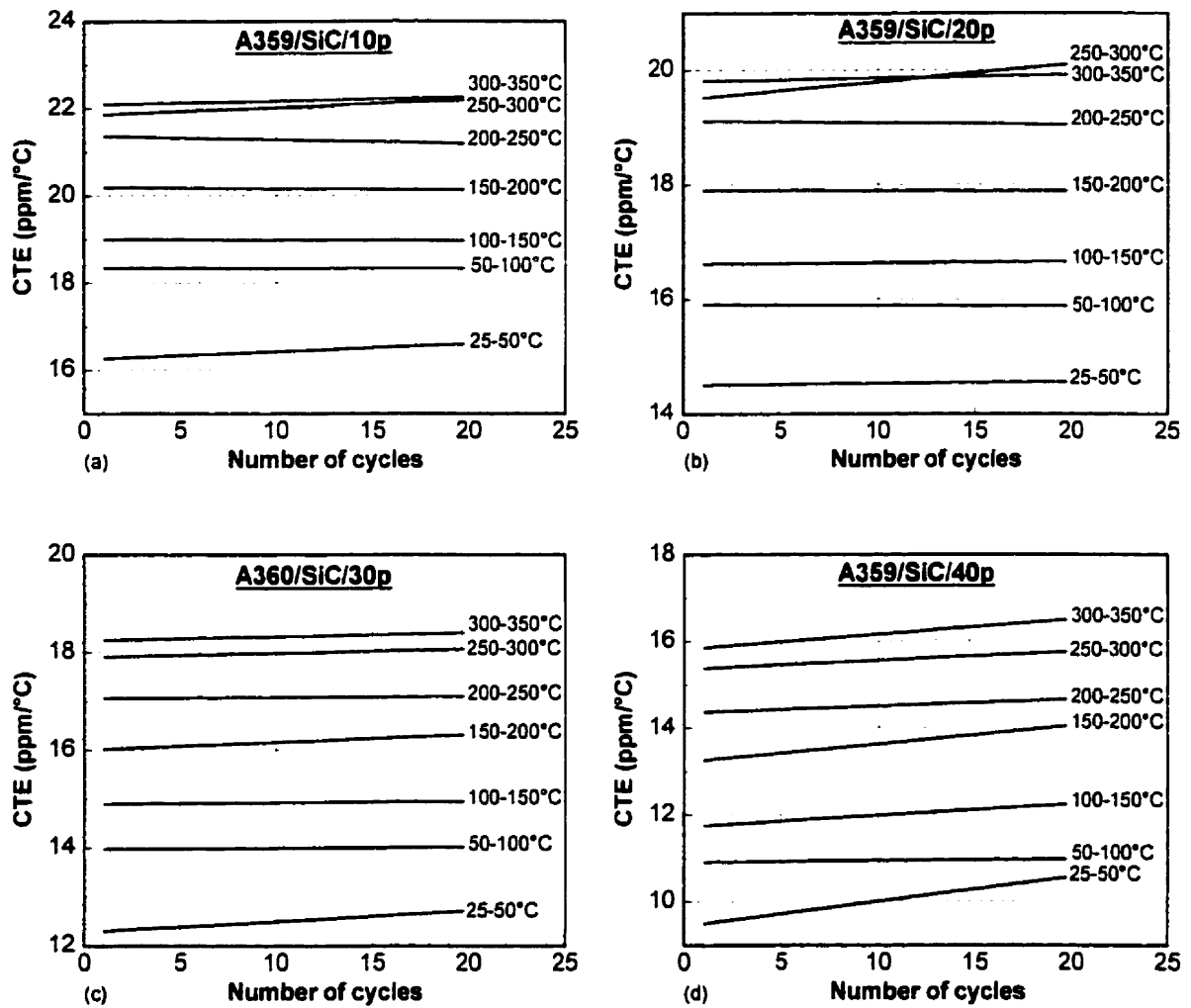


Figure 5. CTE variation with the number of complete temperature reversals for SiC/Al Duralcan composites: (a) 10% SiC, (b) 20% SiC, (c) 30% SiC, and (d) 40% SiC.

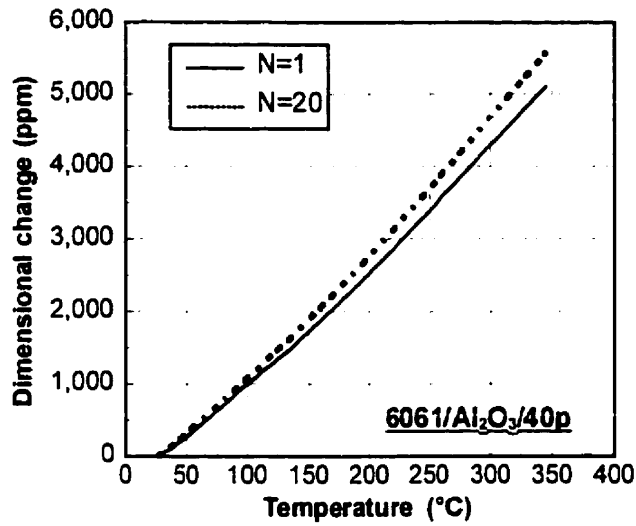


Figure 6. Comparison of the initial and last dimensional change with temperature curves for 20 complete temperature reversals between 25 and 350°C for 6061/Al₂O₃/40p Duralcan composite material.

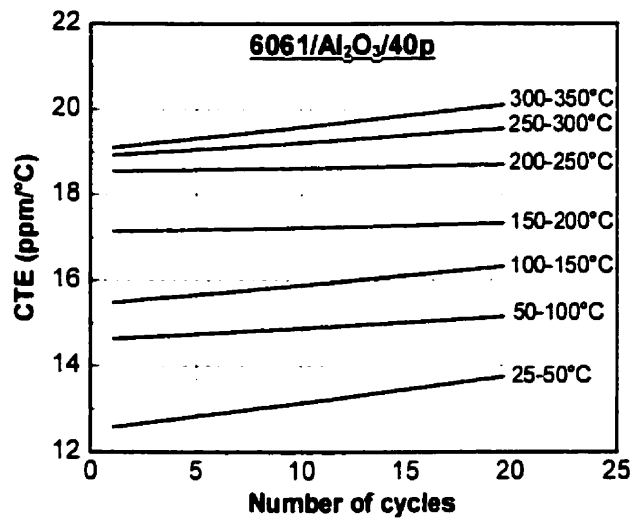


Figure 7. CTE variation with the number of complete temperature reversals for 6061/Al₂O₃/40p Duralcan composite material.

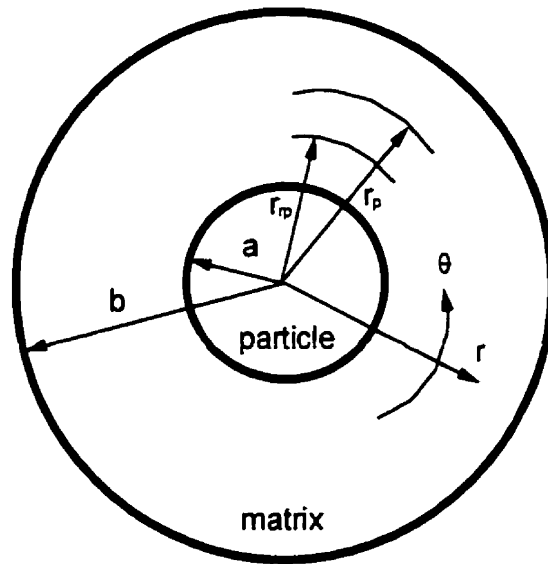


Figure 8. Geometry of the representative volume element for the elastoplastic model.

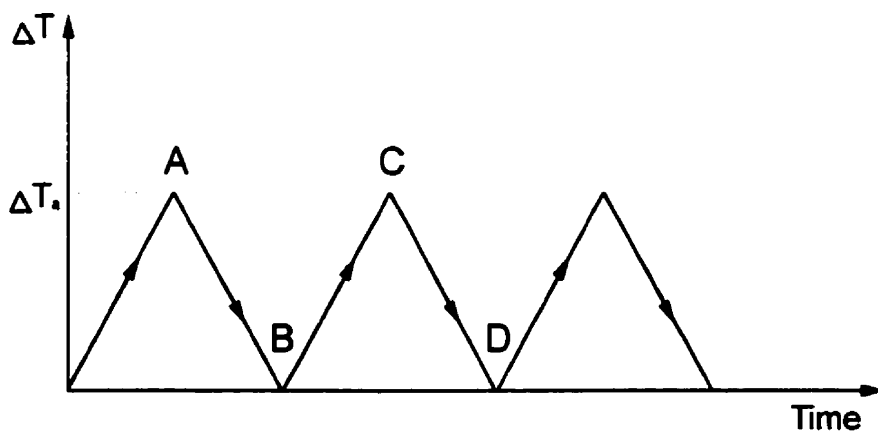


Figure 9. Typical thermal load history during thermal cycling.

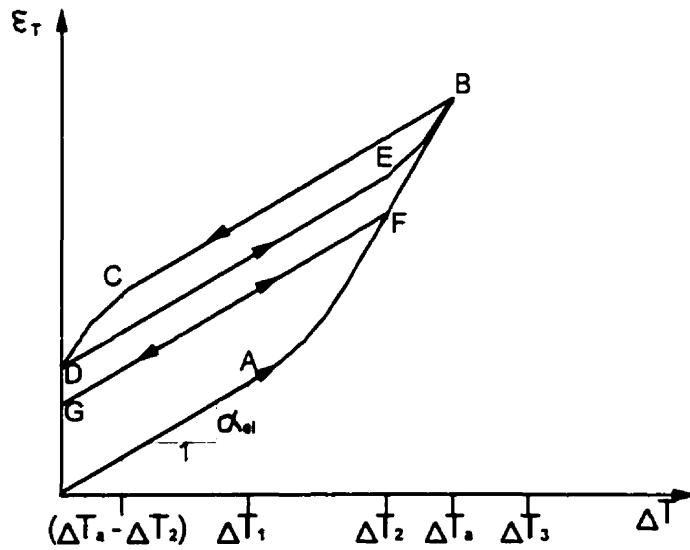


Figure 10. Typical thermal strain with temperature change curve during thermal cycling of a particle reinforced composite.

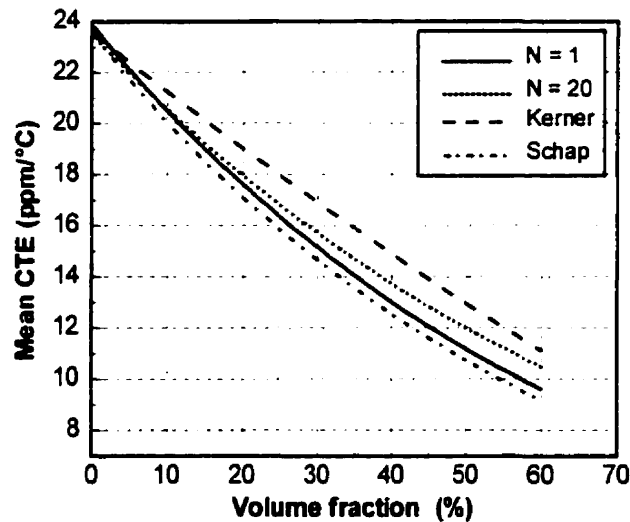


Figure 11. Comparison of the measured mean CTE during thermal cycling of Duralcan SiC/Al composites with theory for the 25-350°C temperature range.

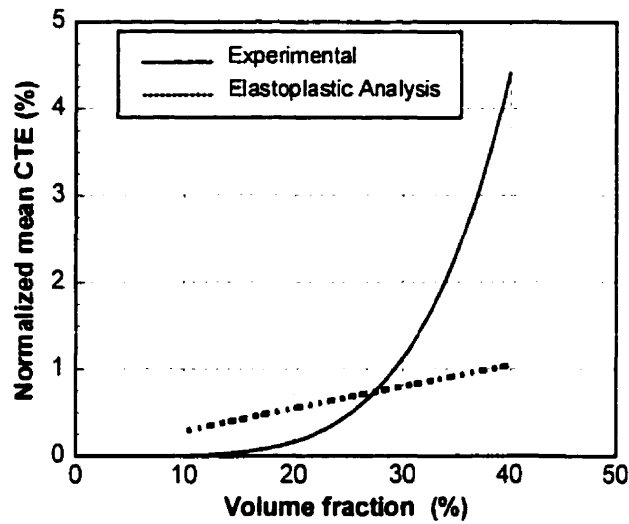


Figure 12. Comparison of the experimental normalized mean CTE values of SiC/Al composites with the theoretical predictions.

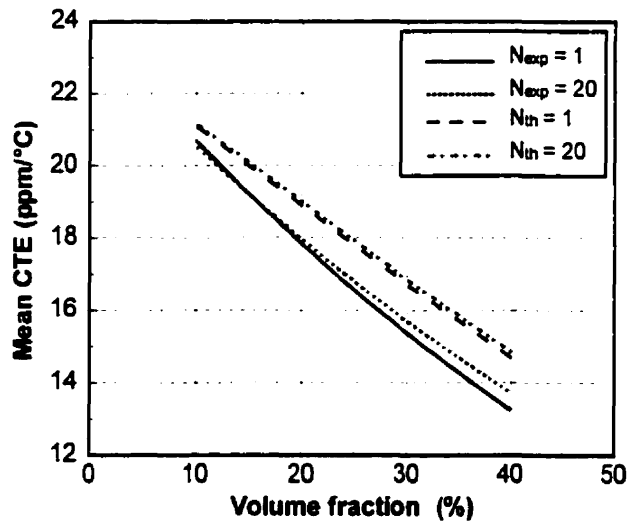


Figure 13. Comparison of the experimental and theoretical CTE change with reinforcement volume fraction during thermal cycling.

General conclusion

In the research described above, the thermal expansion behavior of particle reinforced metal-matrix composite materials has been studied. This thesis is divided into two sections. In the first section, the effect of reinforcement volume fraction and temperature on the coefficient of thermal expansion of Al/SiC Duralcan composites was investigated. Accurate CTE measurements with a high-precision thermomechanical analyzer showed that CTE values increase with temperature and decrease with increasing reinforcement volume fraction. The CTE mismatch between the particles and the matrix results in the generation of residual stresses at the particle-matrix interfaces. These stresses are possibly responsible for the very low CTE values found at low temperatures. In addition, a plot of the average CTE values between 25 and 350°C with reinforcement volume fraction between 0 and 60% was established incorporating other authors' experimental data.

In the second section of this thesis, the issue of thermal cycling was investigated. Thermal cycling is a relatively new research topic in materials science. It is known to have no influence on the expansion behavior of pure unreinforced aluminum alloys. However, this is not the case for particle reinforced MMCs. Numerical data obtained from a theoretical analysis of thermal cycling showed that subjecting the composites to identical thermal histories leads to an increasing CTE change with reinforcement volume fraction. This behavior was confirmed by experimentally measuring CTE changes during cycling. Indeed, experimental curves showed that 20 complete temperature reversals between 25 and 350°C on Al/SiC Duralcan composite materials had an increasing effect on the CTE with increasing reinforcement volume fraction. Moreover, thermal cycling of a Al/Al₂O₃ Duralcan composite showed that the composite's CTE mismatch is not the only factor influencing CTE variations under thermal cycling; the nature of the composite constituents also play an important role. The elastoplastic model of thermal cycling considerably underestimates CTE changes for all the composites studied. However, the experimental expansion behavior can accurately be described using four characteristic temperatures, which mark transitions in plastic response during thermal cycling. Although large CTE increases were observed in the 40 v/o composites, mean CTE values

still lie between the upper and lower elastic CTE bounds derived from the Schapery model.

The experimental results found in this thesis are an important finding in the field of composite materials science. Duralcan particle reinforced metal-matrix composites represent the high performance materials of the future. Their low and stable CTE combined with their high thermal conductivity and excellent mechanical properties when compared to unreinforced alloys make these composites an excellent choice for electronic and space applications in varying temperature environments.

Recommendations

This thesis represents an initial study of the effects of temperature and thermal cycling on the coefficient of thermal expansion. The following recommendations consist of unique and original research topics for scientists interested in working on the expansion behavior of particle reinforced metal-matrix composite materials.

- Theoretical models accuracy for thermal cycling need to be improved. An interesting research topic would be to describe the ductility of the particle-matrix interface in terms of temperature, processing technique and nature of the composite constituents. Further work should also consist of experimentally determining the effect of linear strain hardening in the matrix.
- Another interesting option would be to experimentally determine the effect of the heating and cooling rates as well as dwelling periods at high temperature on the CTE change during thermal cycling.
- Significant CTE changes were observed in Duralcan composites containing 40% reinforcement in volume. It would be interesting to experimentally determine if the same trend is observed for different composite materials.

Appendix 1

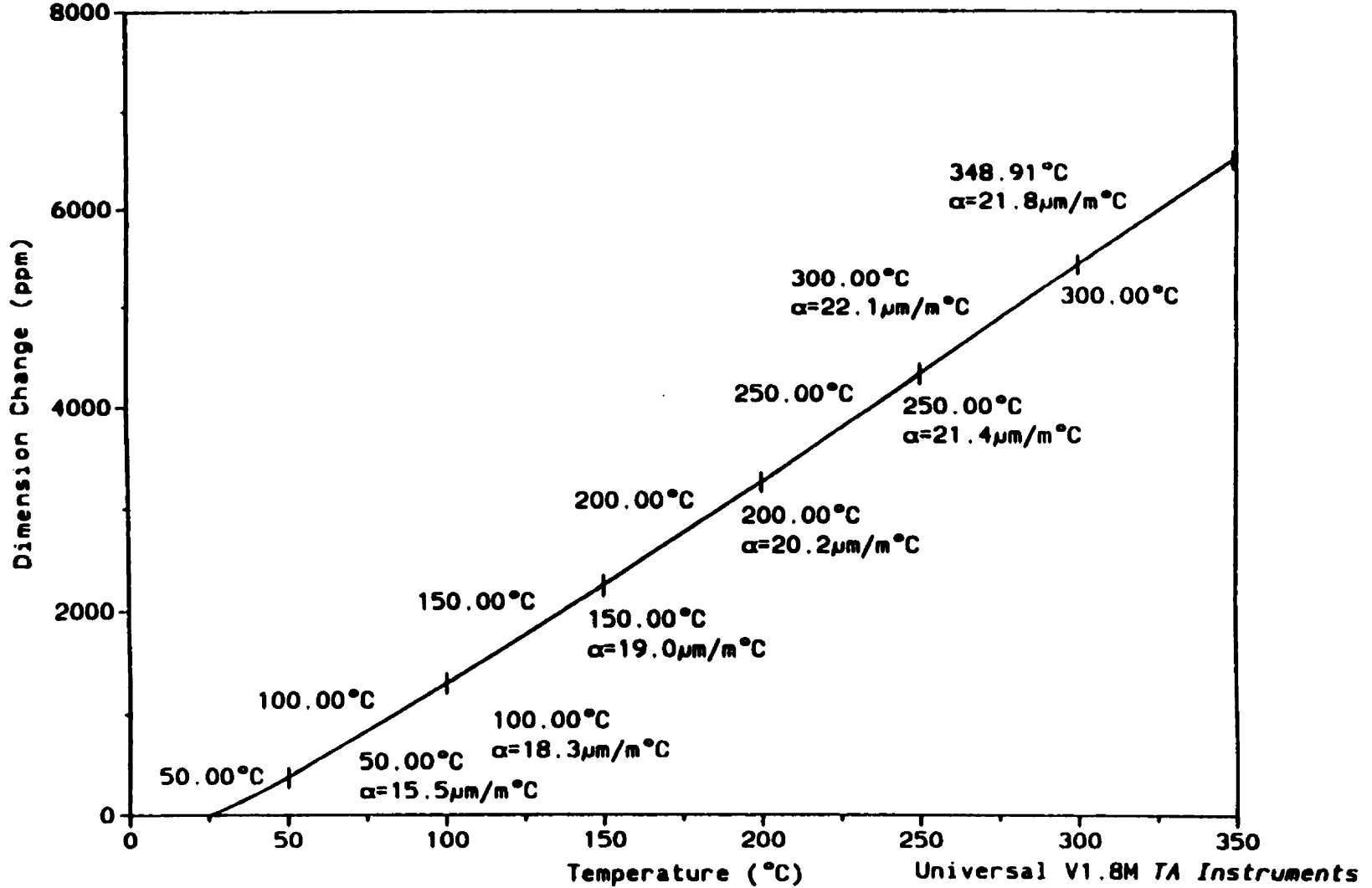
Typical Dimensional change versus temperature plot from the Thermomechanical Analyzer

Figure 1. Typical dimensional change versus temperature curve for A359/SiC/10p

Sample: A359-SiC-10p
Size: 13.0318 mm
Method: Stephane
Comment: Transverse

TMA

File: D:\SIC10\SIC10_N4.002
Operator: Stephane
Run Date: 23-Jun-97 12:40

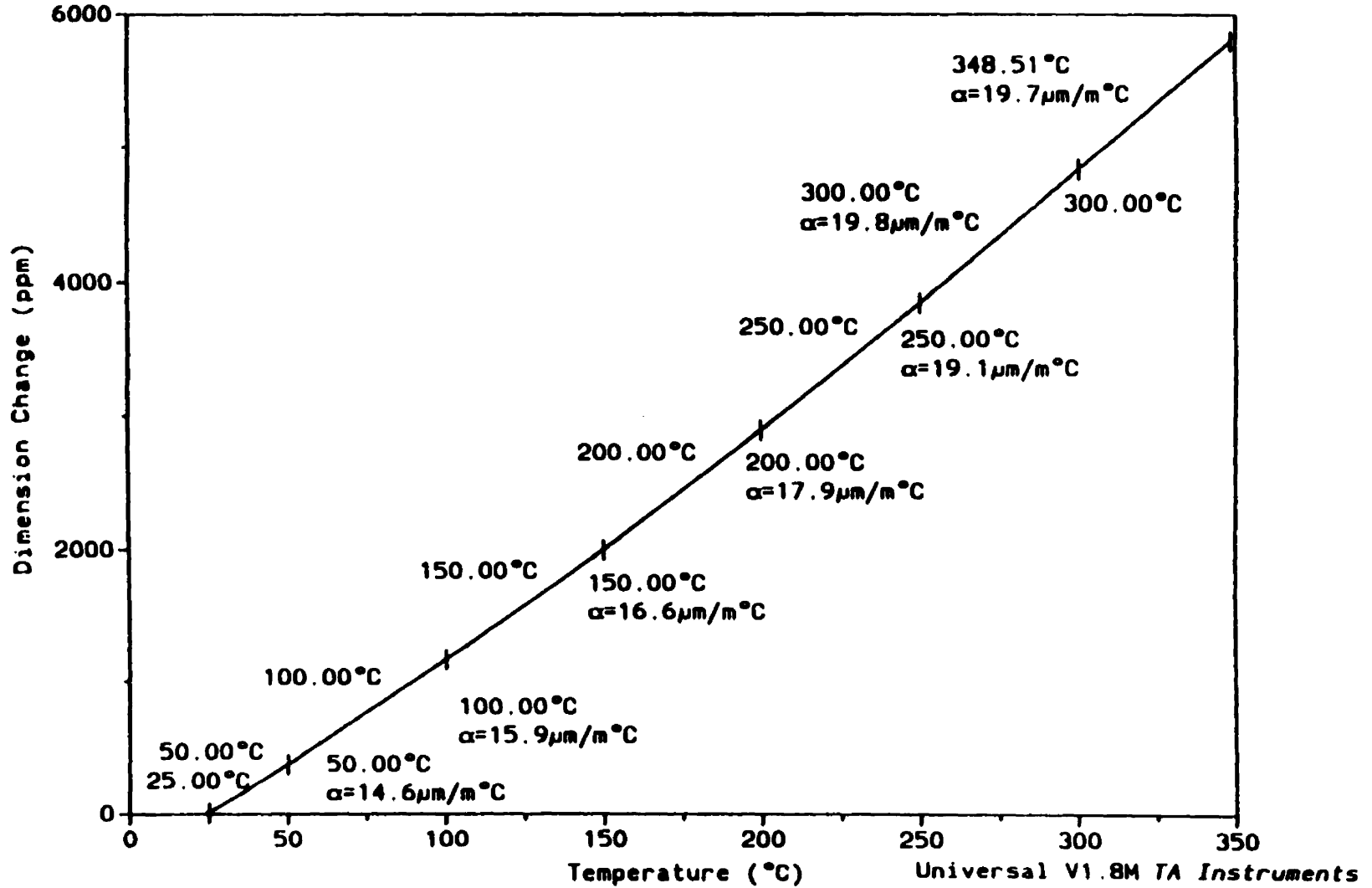


Sample: A359-SiC-20p
Size: 12.8480 mm
Method: Stephane

TMA

File: D:\SIC20\SIC20_N1.011
Operator: Stephane
Run Date: 27-Jun-97 14:06

Figure 2. Typical dimensional change versus temperature curve for A359/SiC/20p

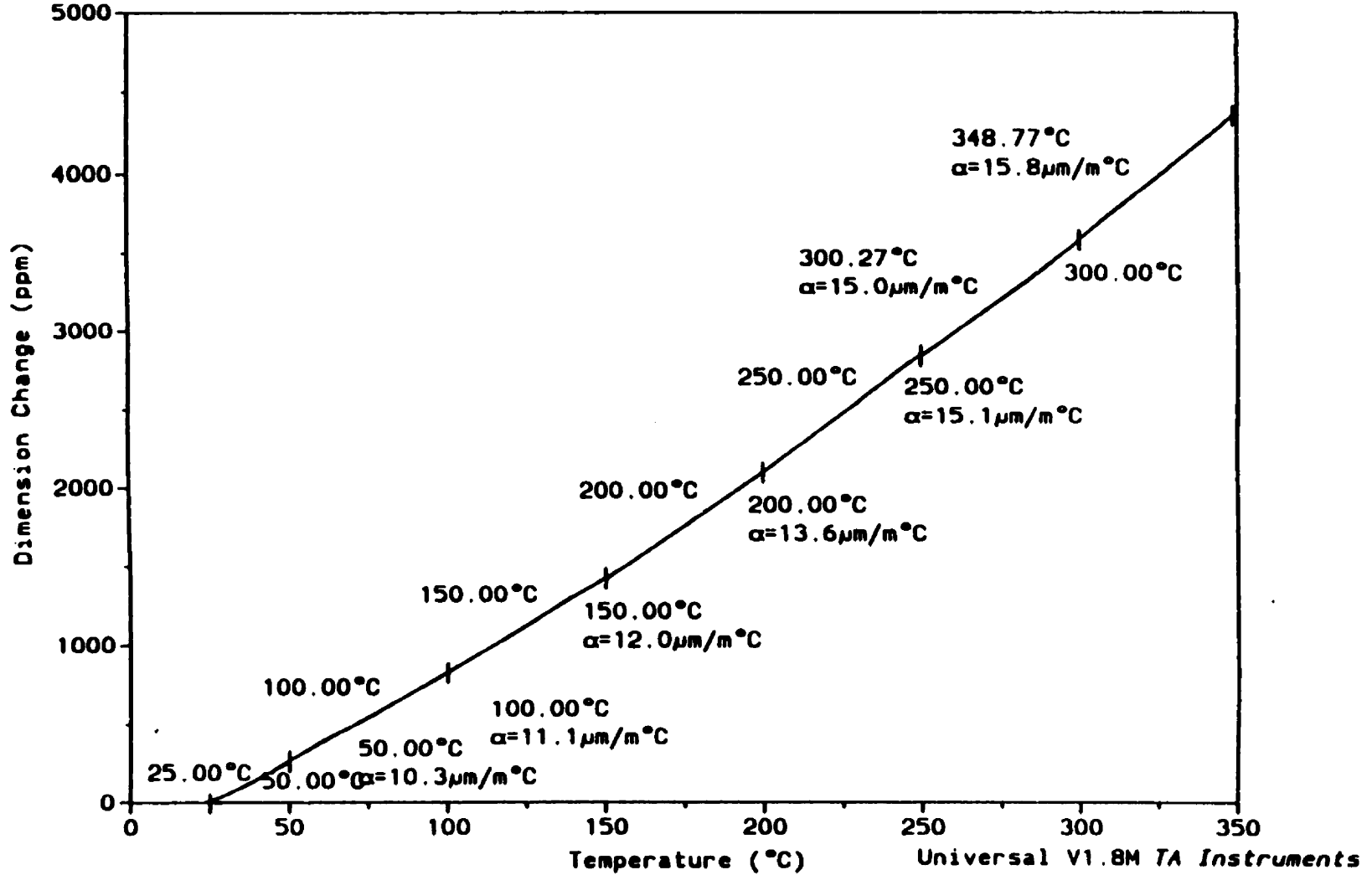


Sample: A359-SiC-40%p
Size: 1.3926 mm
Method: Stephane
Comment: CTE

TMA

File: D:\...\SIC\SIC_N5.010
Operator: Stephane
Run Date: 12-Jun-97 13:56

Figure 3. Typical dimensional change versus temperature curve for A359/SiC/40p



Appendix 2

Program listing of the Maple V mathematical sheet

Elastoplastic Analysis of Thermal Cycling

Software: MAPLE V release 4

Date: May 1997

This Maple sheet summarizes the equations used by Olsson et al for predicting the effect of thermal cycling on strains, stresses and CTE of a particulate reinforced metal matrix composite.

MATERIAL SELECTION

Choose materials for particles and matrix:

MATRIX:

1 - A359

2 - 6061

PARTICLES:

1 - Silicon carbide (SiC)

2 - Alumina (Al₂O₃)

> restart :

> Material_matrix := 1 :

> Material_particles := 1 :

> Matrices_list := ['Matrix is aluminum alloy A359', 'Matrix is aluminum alloy 6061'] :

> Particles_list := ['with silicon carbide particles (SiC)', 'with alumina particles (Al₂O₃)'] :

> Data_particles := readdata
(`c:/lemieux/maple/projet/pardata.dat`, 2) :

> Data_matrix := readdata (`c:/lemieux/maple/projet/matdata.dat`,
2) :

Choose volume fraction of reinforcement particles:

> Volume_fraction_of_particles := 0.20 ;

Volume_fraction_of_particles := .20

Choose average particle diameter (meters):

> Average_particle_diameter := 10e-6 ;

Average_particle_diameter := .000010

MATERIAL PROPERTIES

Type of composite material:

> Matrices_list [Material_matrix] ;

> Particles_list [Material_particles] ;

Matrix is aluminum alloy A359

with silicon carbide particles (SiC)

Particles:

> nu_[2] := Data_particles[2,Material_particles] ;

> alpha_[2] := Data_particles[3,Material_particles] ;

> E_[2] := Data_particles[1,Material_particles] ;

Elastic modulus (Pa):

> E[2] = E_[2] ;

$$E_2 = .450 \cdot 10^{12}$$

Poisson's ratio:

> nu[2] = nu_[2] ;

$$\nu_2 = .17$$

Coefficient of thermal expansion (1/C):

> alpha[2] = alpha_[2] ;

$$\alpha_2 = .47 \cdot 10^{-5}$$

Matrix:

> H_ := Data_matrix[6,Material_matrix] ;

> D_ := Data_matrix[5,Material_matrix] ;

> nu_[1] := Data_matrix[2,Material_matrix] ;

> alpha_[1] := Data_matrix[3,Material_matrix] ;

> sigma_[Y] := Data_matrix[4,Material_matrix] ;

> E_[1] := Data_matrix[1,Material_matrix] ;

Elastic modulus (Pa):

> E[1] = E_[1] ;

$$E_1 = .724 \cdot 10^{11}$$

Poisson's ratio:

> nu[1] = nu_[1] ;

$$\nu_1 = .33$$

Coefficient of thermal expansion (1/C):

> alpha[1] = alpha_[1] ;

$$\alpha_1 = .0000209$$

Yield stress (Pa):

> sigma[Y] = sigma_[Y] ;

$$\sigma_Y = .241 \cdot 10^9$$

Maximum ductility of the interface:

> D = D_ ;

$$D = .20$$

Linear strain hardening parameter (Pa):

> H = H_ ;

> beta_ := 2*H_*(1-nu_[1])/E_[1] ;

$$H = .241 \cdot 10^8$$

Volume fraction of reinforcement particles:

> c = (a/b)^3 ;

> c_ := Volume_fraction_of_particles ;

> c = c_ ;

$$c = \frac{a^3}{b^3}$$

$$c = .20$$

Average particle radius (meters):

```
> a_ := Average_particle_diameter/2 ;
> a = evalf (a_ ) ;
```

$$a = .5000000000 \cdot 10^{-5}$$

Average matrix sphere radius (meters):

```
> b_ := (a_^3/c_)^(1/3) ;
> b = b_ ;
```

$$b = .8549879733 \cdot 10^{-5}$$

STRESS STATE MODEL

Mismatch parameters:

```
> q_ := E_[1]/E_[2]*(1-nu_[2])/(1-nu_[1])-1 ;
> m_ := E_[1]/(1-nu_[1])*((1-2*nu_[1])/E_[1]-(1-2*nu_[2])/E_[2])
:
> s_ := E_[1]/E_[2]*(1+nu_[2])/(1+nu_[1])-1 ;
> s = E[1]/E[2]*(1+nu[2])/(1+nu[1])-1 ;
> q = E[1]/E[2]*(1-nu[2])/(1-nu[1])-1 ;
> m = E[1]/(1-nu[1])*((1-2*nu[1])/E[1]-(1-2*nu[2])/E[2]) ;
```

$$s = \frac{E_1(1+\nu_2)}{E_2(1+\nu_1)} - 1$$

$$q = \frac{E_1(1-\nu_2)}{E_2(1-\nu_1)} - 1$$

$$m = \frac{E_1 \left(\frac{1-2\nu_1}{E_1} - \frac{1-2\nu_2}{E_2} \right)}{1-\nu_1}$$

Interface hydrostatic pressure:

```
> p_ :=
  2/3*E_[1]*(alpha_[2]-alpha_[1])*(1-c_)*Delta_(T)/((1-nu_[1]))/(
  1-2*m_/3*(1-c_)) ;
> p =
  2/3*E[1]*(alpha[2]-alpha[1])*(1-c)*Delta(T)/((1-nu[1]))/(1-2*m/
  3*(1-c)) ;
```

$$p = \frac{2 E_1 (\alpha_2 - \alpha_1) (1 - c) \Delta(T)}{3 (1 - \nu_1) \left(1 - \frac{2}{3} m (1 - c) \right)}$$

Stresses in the spherical particle:

```

> sigma_[r.2] := -p :
> sigma_[theta.2] := -p :
> sigma[r.2] = sigma_[r.2] ;
> sigma[theta.2] = sigma_[theta.2] ;

```

$$\sigma_{r2} = -p$$

$$\sigma_{\theta2} = -p$$

Stresses in the matrix:

```

> sigma_[r.1] := c_*p_/(1-c_)*(1-(b_/r_)^3) :
> sigma_[theta.1] := c_*p_/(1-c_)*(1+1/2*(b_/r_)^3) :
> sigma[r.1] = c*p/(1-c)*(1-(b/r)^3) ;
> sigma[theta.1] = c*p/(1-c)*(1+1/2*(b/r)^3) ;

```

$$\sigma_{r1} = \frac{c p \left(1 - \frac{b^3}{r^3} \right)}{1 - c}$$

$$\sigma_{\theta1} = \frac{c p \left(1 + \frac{1}{2} \frac{b^3}{r^3} \right)}{1 - c}$$

Effective stress in the matrix:

```

> sigma_[e.1] := abs(sigma_[theta.1]-sigma_[r.1]) :
> sigma[e.1] = abs(sigma[theta.1]-sigma[r.1]) ;
> sigma[e.1] = 3/2*c/(1-c)*abs(p)*(b/r)^3 ;

```

$$\sigma_{e1} = |\sigma_{\theta1} - \sigma_{r1}|$$

$$\sigma_{e1} = \frac{3}{2} \frac{c |p| b^3}{(1-c) r^3}$$

CHARACTERISTIC TEMPERATURES

First thermal load (forward plastic zone, half of the first cycle):

Temperature change for plasticity to appear on first load:

```

> (Delta_)(T.1) := abs
  (sigma_[Y]*(1-nu_[1])/(E_[1]*(alpha_[2]-alpha_[1]))*(1-2/3*m_*(
  1-c_)) :
> eq10 := (Delta)(T.1) =
  sigma[Y]*(1-nu[1])/(E[1]*(alpha[2]-alpha[1]))*(1-2/3*m*(1-c)) :
> eq10 ;

```

$$\Delta(T1) = \frac{\sigma_Y (1 - \nu_1) \left(1 - \frac{2}{3} m (1 - c) \right)}{E_1 (\alpha_2 - \alpha_1)}$$

Full plasticity:

```

> (Delta_)(T.3) := abs (evalf
  (-sigma_[Y]*(1-nu_[1])/(E_[1]*(alpha_[2]-alpha_[1]))*(1/c_+2/3*

```

```

    m_*log(c_))) :
> eq12 := (Delta)(T.3) =
    sigma[Y]*(1-nu[1])/(E[1]*(alpha[2]-alpha[1]))*(1/c+2/3*m*log(c)
    ) :
> eq12 ;

```

$$\Delta(T3) = \frac{\sigma_Y(1-\nu_1) \left(\frac{1}{c} + \frac{2}{3} m \ln(c) \right)}{E_1(\alpha_2 - \alpha_1)}$$

For thermal cycling (reversed plastic zone):

Temperature change for reversed plasticity to appear:

```

> (Delta_)(T.2) := 2*(Delta_)(T.1) :
> eq13 := (Delta)(T.2) = 2*(Delta)(T.1) :
> eq13 ;

```

$$\Delta(T2) = 2 \Delta(T1)$$

Full reversed plasticity:

```

> (Delta_)(T.4) := evalf (2*(Delta_)(T.3)) :
> eq15 := (Delta)(T.4) = 2*(Delta)(T.3) :
> eq15 ;

```

$$\Delta(T4) = 2 \Delta(T3)$$

CHARACTERISTIC VOLUME FRACTION

The characteristic volume fraction of reinforcement is found when the rise in temperature for the first cycle gives full plasticity in the matrix and that there is no reversed plasticity upon cooling, i.e. $\Delta(T2) = \Delta(T3)$.

```

> eq1 := 1-2*cc_+2*m_/3*cc_*(log(cc_)+2*(1-cc_))=0 :
> eq16 := 1-2*c+2*m/3*c*(log(c)+2*(1-c))=0 :
> 1-2*c+2*m/3*c*(log(c)+2*(1-c))=0 :

```

Solving for c, we get:

```

> Characteristic_volume_fraction = solve (eq1, cc_) :
> cc_ := solve (eq1, cc_) :

```

TEMPERATURE HISTORY

Thermal amplitude (Assuming that the material is in a stress-free state at room temperature):

```

> Thermal_amplitude_ := 325 :
> Thermal_amplitude = Thermal_amplitude_ ;
    Thermal_amplitude = 325

```

Number of cycles:

```

> Number_cycles_ := 20 :
> n = Number_cycles_ ;

```

$$n = 20$$

STRAIN ON FIRST THERMAL LOADING

For the first thermal load:

```

> Phi_ := sign((alpha_[2]-alpha_[1])*Thermal_amplitude_) :
> Phi = Sign ((alpha[2]-alpha[1])*(Delta)(T[a])) :
>
> if Thermal_amplitude_ < (Delta_)(T.1) then #Elastic behavior
only
>   epsilon_eq19[T] := (alpha_[1] + (alpha_[2] -
alpha_[1])*c_/(1-2/3*m_*(1-c_)))*Delta.T:
>   eq19 :=
epsilon[T]=(alpha[1]+(alpha[2]-alpha[1])*c/(1-2/3*m*(1-c)))*The
rmal_amplitude;
>   PlotA := plot (epsilon_eq19[T],
Delta.T=0..Thermal_amplitude_, color=BLUE) :
>
>   First_cycle_plot := {PlotA} ;
>
> elif (Delta_)(T.3) > Thermal_amplitude_ then #Plastic behavior
> #Elastic behavior at beginning of first cycle
>   epsilon_eq19[T] := (alpha_[1] + (alpha_[2] -
alpha_[1])*c_/(1-2/3*m_*(1-c_)))*Delta.T:
>   eq19 :=
epsilon[T]=(alpha[1]+(alpha[2]-alpha[1])*c/(1-2/3*m*(1-c)))*(De
lta)(T);
>   PlotA := plot (epsilon_eq19[T], Delta.T=0..(Delta_)(T.1),
color=BLUE) :
>
>   #Plastic behavior described by eq.20
>   eq11a := abs((alpha_[2]-alpha_[1])*Delta.T) =
sigma_[Y]*(1-nu_[1])/E_[1]*((r_[p]/a_)^3-m_*(2*(r_[p]/a_-1-(r_[
p]/a_-1)^2/2+(r_[p]/a_-1)^3/3)+2/3*(1-(r_[p]/b_)^3))) ;
>   eq11 := abs((alpha[2]-alpha[1])*(Delta)(T)) =
sigma[Y]*(1-nu[1])/E[1]*((r[p]/a)^3-m*(2*(r[p]/a-1-(r[p]/a-1)^2
/2+(r[p]/a-1)^3/3)+2/3*(1-(r[p]/b)^3))) ;
>
>   #Find the radius of plasticity during the first cycle
>   roots_ := solve (eq11a, r_[p]) :
>   r_[p] := Re (roots_[1]) ; #Only first root is valid.
>
>   epsilon_eq20[T] := alpha_[1]*Delta.T +
c_*(r_[p]/a_)^3*(1-nu_[1])*sigma_[Y]/E_[1]*sign((alpha_[2]-alph
a_[1])*Delta.T) :
>   eq20 := epsilon[T] = alpha[1]*(Delta)(T) +
c*(r[p]/a)^3*(1-nu[1])*sigma[Y]/E[1]*Sign((alpha[2]-alpha[1])*(
Delta)(T)) ;
>   PlotB := plot (epsilon_eq20[T],
Delta.T=(Delta_)(T.1)..Thermal_amplitude_, color=BLUE) :
>
>   r_[p] := evalf (subs(Delta.T=Thermal_amplitude_, r_[p])) ;

```

```

>
>   First_cycle_plot := (PlotA, PlotB) ;
Full plasticity during the first cycle.
> else #Full plasticity during the first cycle
>   #Elastic behavior at beginning of first cycle
>   epsilon_eq19[T] := (alpha_[1] + (alpha_[2] -
alpha_[1])*c_/(1-2/3*m_*(1-c_)))*Delta.T:
>   eq19 :=
epsilon[T]=(alpha[1]+(alpha[2]-alpha[1])*c/(1-2/3*m*(1-c)))*(De
lta)(T);
>   PlotA := plot (epsilon_eq19[T], Delta.T=0..(Delta_)(T.1),
color=BLUE) :
>
>   #Plastic behavior described by eq.20
>   eq11a := abs((alpha_[2]-alpha_[1])*Delta.T) =
sigma_[Y]*(1-nu_[1])/E_[1]*((r_[p]/a_)^3-m_*(2*(r_[p]/a_-1-(r_[
p]/a_-1)^2/2+(r_[p]/a_-1)^3/3)+2/3*(1-(r_[p]/b_)^3))) ;
>   eq11 := abs((alpha[2]-alpha[1])*(Delta)(T)) =
sigma[Y]*(1-nu[1])/E[1]*((r[p]/a)^3-m*(2*(r[p]/a-1-(r[p]/a-1)^2
/2+(r[p]/a-1)^3/3)+2/3*(1-(r[p]/b)^3))) ;
>
>   #Find the radius of plasticity during the first cycle
>   roots_ := solve (eq11a, r_[p]) :
>   r_[p] := Re (roots_[1]) ; #Only first root is valid.
>   test1 := subs (Delta.T=Thermal_amplitude_, roots_[1]) ;
>   test2 := subs (Delta.T=Thermal_amplitude_, roots_[2]) ;
>   test3 := subs (Delta.T=Thermal_amplitude_, roots_[3]) ;
>   epsilon_eq20[T] := alpha_[1]*Delta.T +
c_*(r_[p]/a_)^3*(1-nu_[1])*sigma_[Y]/E_[1]*sign((alpha_[2]-alph
a_[1])*Delta.T);
>   eq20 := epsilon[T] = alpha[1]*(Delta)(T) +
c*(r[p]/a)^3*(1-nu[1])*sigma[Y]/E[1]*Sign((alpha[2]-alpha[1])*(
Delta)(T)) ;
>   PlotB := plot (epsilon_eq20[T],
Delta.T=(Delta_)(T.1)..(Delta_)(T.3), color=BLUE) :
>
>   epsilon_eq21[T] := (c_*alpha_[2]+(1-c_)*alpha_[1])*Delta.T -
2/3*sigma_[Y]*c_*log(c_)*((1-2*nu_[1])/E_[1]-(1-2*nu_[2])/E_[2]
)*sign((alpha_[2]-alpha_[1])*Delta.T) ;
>   eq21 := epsilon[T] = (c*alpha[2]+(1-c)*alpha[1])*(Delta)(T)
-
2/3*sigma[Y]*c*log(c)*((1-2*nu[1])/E[1]-(1-2*nu[2])/E[2])*Sign(
(alpha[2]-alpha[1])*(Delta)(T)) ;
>   PlotC := plot (epsilon_eq21[T],
Delta.T=(Delta_)(T.3)..Thermal_amplitude_, color=BLUE) :
>   r_[p] := evalf (subs (Delta.T=Thermal_amplitude_, r_[p])) :#
Full plasticity (matrix completely plastic)
>   # r_[p] := b_ ;

```

```

> First_cycle_plot := (PlotA, PlotB, PlotC) ;
>
> fi :

For thermal cycling:
> Delta_.T := 0 : #Need to find radius of reversed plasticity for
Delta T = 0.
> eq14 :=
abs((alpha_[2]-alpha_[1])*(Thermal_amplitude_-Delta_.T)) =
2*sigma_[Y]*(1-nu_[1])/E_[1]*((r_[rp]/a_)^3-m*(2*log(r_[rp]/a_)
)+2/3*(1-(r_[rp]/b_)^3))) :
> roots_ := solve (eq14, r_[rp]) :
> if roots_[1] < a_ then
>   r_[rp] := roots_[2] ;
> else
>   r_[rp] := roots_[1] ;
> fi :
> eq14a := abs((alpha[2]-alpha[1])*((Delta)(T[a])-(Delta)(T))) =
2*sigma[Y]*(1-nu[1])/E[1]*((r[rp]/a)^3-m*(2*log(r[rp]/a)+2/3*(1
-(r[rp]/b)^3))) :
> if Thermal_amplitude_ < (Delta_)(T.2) then
>   alpha_[EL] := (alpha_[1] + (alpha_[2] -
alpha_[1])*c_/(1-2/3*m*(1-c_))) :
>   epsilon_[T,tc] := (alpha_[1]-alpha_[EL])*Thermal_amplitude_
+
c*(r_[p]/a_)^3*sigma_[Y]*(1-nu_[1])/E_[1]*sign((alpha_[2]-alph
a_[1])*Thermal_amplitude_) + alpha_[EL]*Delta.T;
>   PlotE := plot (epsilon_[T,tc],
Delta.T=0..Thermal_amplitude_, color=BLUE) :
>   First_cycle_plot := First_cycle_plot union {PlotE} :
> else
>   epsilon_[T,tc] :=
(1-nu_[1])*sigma_[Y]*c_/E_[1]*sign((alpha_[2]-alpha_[1])*Therma
l_amplitude_)*((r_[p]/a_)^3-2*(r_[rp]/a_)^3) +
(alpha_[1]+2*(1-nu_[1])*sigma_[Y]*c_*sign((alpha_[2]-alpha_[1])
*Thermal_amplitude_)/E_[1]/Thermal_amplitude_*(r_[rp]/a_)^3)*De
lta.T ;
>   PlotD := plot (epsilon_[T,tc],
Delta.T=0..Thermal_amplitude_, color=BLUE) :
>   First_cycle_plot := First_cycle_plot union {PlotD} ;
> fi :

> if Thermal_amplitude_ < (Delta_)(T.2) then
> eq24 := epsilon[T,tc] = (alpha[1]-alpha[EL])*(Delta)(T[a]) +
c*(r[p]/a)^3*sigma[Y]*(1-nu[1])/E[1]*Sign((alpha[2]-alpha[1])*(
Delta)(T[a])) + alpha[EL]*(Delta)(T):
> else

```

```

> eq25 := epsilon[T,tc] =
(1-nu[1])*sigma[Y]*c/E[1]*Phi*((r[p]/a)^3-2*(r[rp]/a)^3) +
(alpha[1]+2*(1-nu[1])*sigma[Y]*c*Phi/E[1]/(Delta)(T[a])*(r[rp]/
a)^3)*(Delta)(T) :
> fi :

```

■ PLASTIC STRAIN ACCUMULATION DURING CYCLING

```

> Strain_accumulation_plot := {} :
> if (Thermal_amplitude_ > (Delta_)(T.3)) and (Thermal_amplitude_
< (Delta_)(T.4)) then
>   epsilon_[eff_acc] :=
2*sigma_[Y]*(1-nu_[1])/E_[1]*(((b_/r_)^3*(1+c_*E_[1]*abs(alpha_
[2]-alpha_[1]))*(abs(Thermal_amplitude_)-(Delta_)(T.3))/(sigma_[
Y]*(1-nu_[1])))-1)+2*(n_-1)*((r_[rp]/r_)^3-1)) :
>   eq31 := epsilon[eff_acc] =
2*sigma[Y]*(1-nu[1])/E[1]*(((b/r)^3*(1+c*E[1]*abs(alpha[2]-alph
a[1]))*(abs(Thermal_amplitude)-(Delta)(T.3))/(sigma[Y]*(1-nu[1]
))-1)+2*(n-1)*((r[rp]/r)^3-1)) :
>   Strain_accumulation_plot := {} ;
>   for i from 2 to Number_cycles_ do
>     PlotI.i := plot (subs(n_=i, epsilon_[eff_acc]),
r_=a_..r_[rp], color=BLUE) :
>     Strain_accumulation_plot := Strain_accumulation_plot
union {PlotI.i} :
>   od :
> elif (Thermal_amplitude_ > (Delta_)(T.2)) and
(Thermal_amplitude_ < (Delta_)(T.4)) then
>   epsilon_[eff_acc] :=
2*sigma_[Y]*(1-nu_[1])/E_[1]*(((r_[p]/r_)^3-1)+2*(n_-1)*((r_[rp
]/r_)^3-1)) ;
>   for i from 2 to Number_cycles_ do
>     PlotI.i := plot (subs(n_=i, epsilon_[eff_acc]),
r_=a_..r_[rp], color=BLUE) :
>     Strain_accumulation_plot := Strain_accumulation_plot
union {PlotI.i} :
>   od :
> fi :
> if Thermal_amplitude_ > (Delta_)(T.1) then
>   epsilon_[eff_first] :=
2*sigma_[Y]*(1-nu_[1])/E_[1]*((r_[p]/r_)^3-1) :
>   eq29 := epsilon[eff_first] =
2*sigma[Y]*(1-nu[1])/E[1]*((r[p]/r)^3-1) :
>   PlotJ := plot (epsilon_[eff_first], r_=a_..r_[p],
color=BLUE) :
> else
>   PlotJ := plot (0,0,WHITE) ;
> fi :

```

```
[ > Strain_accumulation_plot := Strain_accumulation_plot union
  {PlotJ} :
```

■ COEFFICIENT OF THERMAL EXPANSION

Calculation the slopes of the curves from page 35.

For the first thermal load:

```
[ > Phi_ := sign((alpha_[2]-alpha_[1])*Thermal_amplitude_) :
> Phi = Sign ((alpha[2]-alpha[1])*(Delta)(T[a])) :
> CTE_eq19_ := (alpha_[1] + (alpha_[2] -
  alpha_[1])*c_/(1-2/3*m_*(1-c_))):
> CTE_eq19 :=
  CTE[T]=(alpha[1]+(alpha[2]-alpha[1])*c/(1-2/3*m*(1-c)))*Thermal
  _amplitude:
> Plot_CTEA := plot (CTE_eq19_[T], Delta.T=0..Thermal_amplitude_,
  color=BLUE) :
>
> First_cycle_CTE_plot := {Plot_CTEA} :
>
>
```

For thermal cycling:

```
[ > if Thermal_amplitude_ < (Delta_)(T.2) then
>   alpha_[EL] := (alpha_[1] + (alpha_[2] -
  alpha_[1])*c_/(1-2/3*m_*(1-c_))) :
>   CTE_eq24_[T,tc] := alpha_[EL]:
>   Plot_CTEE := plot (CTE_eq24_[T,tc],
  Delta.T=0..Thermal_amplitude_, color=BLUE) :
>   First_cycle_CTE_plot := First_cycle_CTE_plot union
  {Plot_CTEE} :
>   d_ := (CTE_eq24_ - CTE_eq19_)/CTE_eq19_ :
> else
>   CTE_eq25_ :=
  (alpha_[1]+2*(1-nu_[1])*sigma_[Y]*c_*sign((alpha_[2]-alpha_[1])
  * Thermal_amplitude_)/E_[1]/Thermal_amplitude_*(r_[rp]/a_)^3) :
>   Plot_CTED := plot (CTE_eq25_, Delta.T=0..Thermal_amplitude_,
  color=BLUE) :
>   First_cycle_CTE_plot := First_cycle_CTE_plot union
  {Plot_CTED} :
>   d_ := (CTE_eq25_ - CTE_eq19_)/CTE_eq19_ :
> fi :
```

■ NUMBER OF CYCLES TO DECOHESION

No strain hardening:

```
[ > N_[f] := E_[1]*D_/(4*sigma_[Y]*(1-nu_[1])*((r_[rp]/a_)^3-1)) :
> eq43 := N[f] = E[1]*D/(4*sigma[y]*(1-nu[1])*((r[rp]/a)^3-1)) :
```

Linear strain hardening:

```

> N_ss[f] :=
  ln(1-H_/sigma_[Y]*D_/((r_[rp]/a_)^3-1))/ln((1-beta_)/(1+beta_))
:
> eq44 := N[f] =
  ln(1-H/sigma[y]*D/((r[rp]/a)^3-1))/ln((1-beta)/(1+beta)) :

```

■ NUMERICAL RESULTS

Appendix 3

Typical Maple V mathematical sheet numerical results output

Elastoplastic Analysis of Thermal Cycling

Software: MAPLE V release 4

Date: May 1997

This Maple sheet summarizes the equations used by Olsson et al for predicting the effect of thermal cycling on strains, stresses and CTE of a particulate reinforced metal matrix composite.

☐ MATERIAL SELECTION

☐ MATERIAL PROPERTIES

☐ STRESS STATE MODEL

☐ CHARACTERISTIC TEMPERATURES

☐ CHARACTERISTIC VOLUME FRACTION

☐ TEMPERATURE HISTORY

☐ STRAIN ON FIRST THERMAL LOADING

☐ PLASTIC STRAIN ACCUMULATION DURING CYCLING

☐ COEFFICIENT OF THERMAL EXPANSION

☐ NUMBER OF CYCLES TO DECOHESION

☐ NUMERICAL RESULTS

Date: August 13th, 1997

Time: 14:15 PM

Subject: Results of the theoretical analysis on thermal cycling developed by Olsson et Al [M. Olsson, A. E. Giannakopoulos and S. Suresh, Journal of the Mechanics and Physics of Solids, March, 1995] applied to specific particle reinforced metallic matrix composites.

Type of composite material:

*Matrix is aluminum alloy A359
with silicon carbide particles (SiC)
Volume_fraction_of_particle = .40*

Temperature history:

Amplitude of the temperature change (°C):

$$\Delta(T) = 325$$

Number of complete cycles:

$$n = 20$$

Characteristic temperatures:

Temperature change for plasticity to appear at the interface (°C):

$$\Delta(T1) = \frac{\sigma_Y (1 - \nu_1) \left(1 - \frac{2}{3} m (1 - c) \right)}{E_1 (\alpha_2 - \alpha_1)}$$

$$\Delta(T1) = 118.4523520$$

Temperature change for reversed plasticity to appear at the interface (°C):

$$\Delta(T2) = 2 \Delta(T1)$$

$$\Delta(T2) = 236.9047040$$

Temperature change for full plasticity of the matrix on the first thermal load (°C):

$$\Delta(T3) = \frac{\sigma_Y (1 - \nu_1) \left(\frac{1}{c} + \frac{2}{3} m \ln(c) \right)}{E_1 (\alpha_2 - \alpha_1)}$$

$$\Delta(T3) = 314.8264222$$

Temperature change for full reversed plasticity of the matrix with thermal cycling (°C):

$$\Delta(T4) = 2 \Delta(T3)$$

$$\Delta(T4) = 629.6528444$$

Characteristic volume fraction:

$$1 - 2c + \frac{2}{3} m c (\ln(c) + 2 - 2c) = 0$$

$$c = .5184663362$$

Determination of the extent of plasticity in the matrix:

Radius of plasticity determined by the following equation (meters):

$$|(\alpha_2 - \alpha_1) \Delta(T)| = \frac{\sigma_Y (1 - \nu_1) \left(\frac{r_p^3}{a^3} - m \left(2 \frac{r_p}{a} - \frac{4}{3} - \left(\frac{r_p}{a} - 1 \right)^2 \right) + \frac{2}{3} \left(\frac{r_p}{a} - 1 \right)^3 - \frac{2}{3} \frac{r_p^3}{b^3} \right)}{E_1}$$

$$.6854429243 \cdot 10^{-5}$$

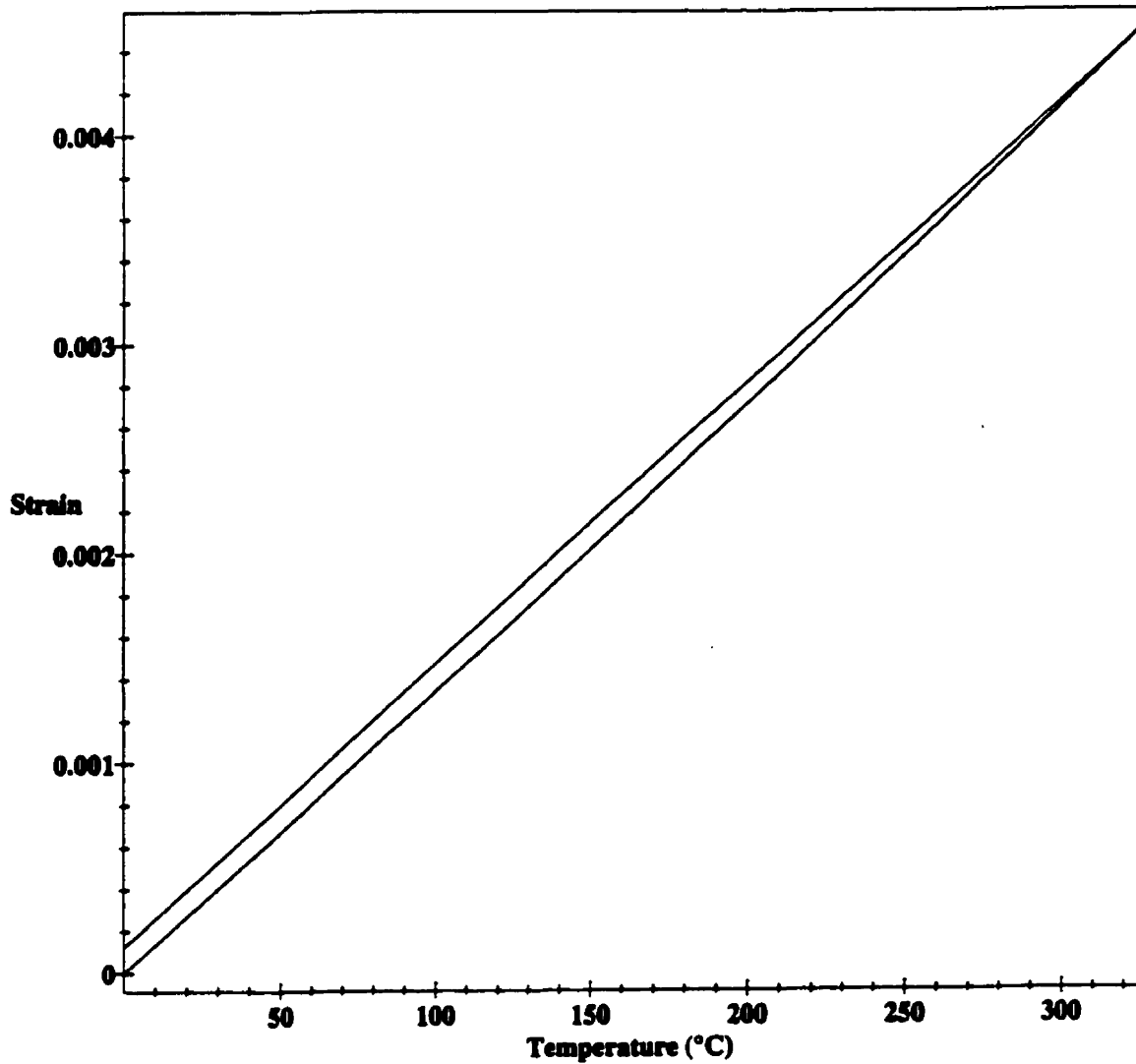
Radius of reversed plasticity after a complete cycle, i.e. Delta(T)=0 (meters):

$$|(\alpha_2 - \alpha_1)(\Delta(T_a) - \Delta(T))| = 2 \frac{\sigma_y(1 - \nu_1) \left(\frac{r_p^3}{a^3} - m \left(2 \ln \left(\frac{r_p}{a} \right) + \frac{2}{3} - \frac{2}{3} \frac{r_p^3}{b^3} \right) \right)}{E_1}$$

$$r_p = .5536691012 \cdot 10^{-5}$$

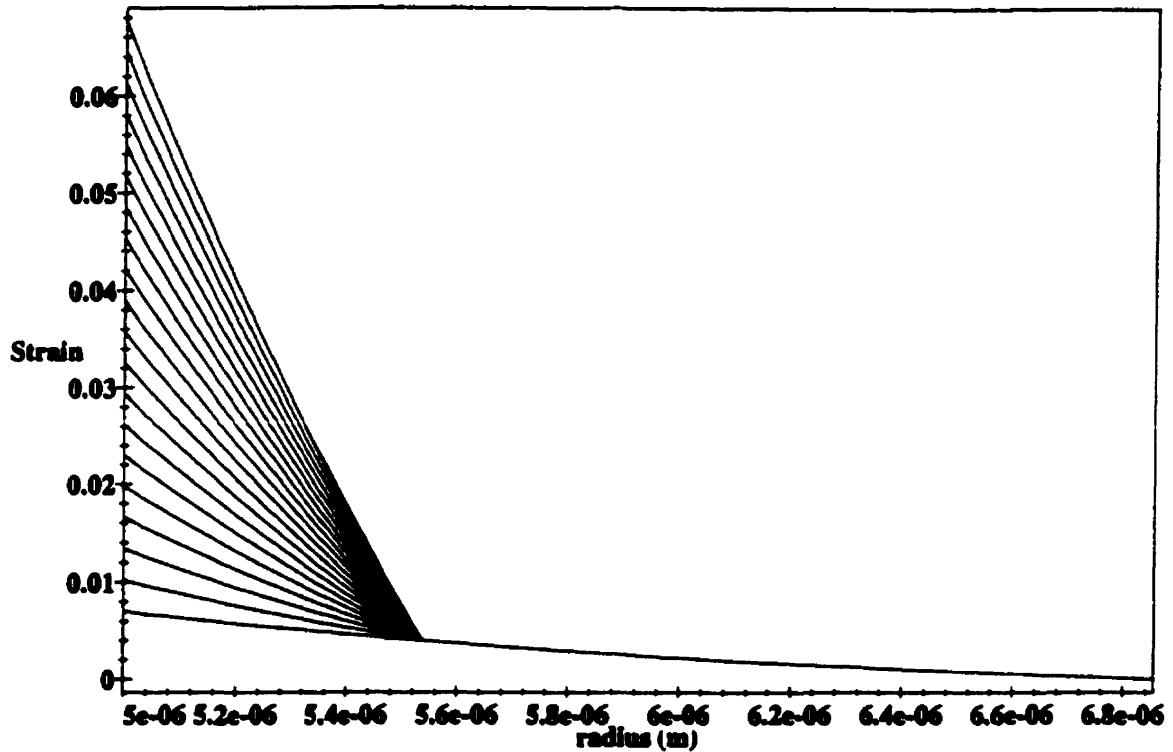
Plot of the thermal straining versus the temperature change:

Strain vs temperature change for the first and subsequent cycles



Plot of the effective plastic strain accumulation throughout the matrix during thermal cycling:

Strain accumulation within the matrix during thermal cycling



CTE predictions:

Elastic CTE (1/°C):

.00001336870634

Damage parameter (in %) (relative to the elastic CTE of the composite):

$d = .5767093542$

Decohesion of the interface:

Number of cycles to decohesion of the interface without taking into account linear strain hardening:

$$N_f = \frac{1}{4} \frac{E_1 D}{\sigma (1 - \nu_1) \left(\frac{r_p^3}{a^3} - 1 \right)}$$

62.65521803

Number of cycles to decohesion of the interface with linear strain hardening of the matrix:

$$N_f = \frac{\ln \left(1 - \frac{HD}{\sigma_y \left(\frac{r_p^3}{a^3} - 1 \right)} \right)}{\ln \left(\frac{1-\beta}{1+\beta} \right)}$$

64.47435232